NAVAL POSTGRADUATE SCHOOL

MONTEREY, CALIFORNIA

THESIS

SAFER SKI JUMPS: DESIGN OF LANDING SURFACES AND CLOTHOIDAL IN-RUN TRANSITIONS

by

Andrew Davis Swedberg

June 2010

Thesis Advisor:	Mont Hubbard
Co-Advisor:	Arthur Krener

Approved for public release; distribution is unlimited

THIS PAGE INTENTIONALLY LEFT BLANK

REPORT DOCUMENTATION PAGE			Form Approved OMB No. 0704-0188
Public reporting burden for this collection of information is estimated to average 1 hour per response, including the time for reviewing instruction, searching existing data sources, gathering and maintaining the data needed, and completing and reviewing the collection of information. Send comments regarding this burden estimate or any other aspect of this collection of information, including suggestions for reducing this burden, to Washington headquarters Services, Directorate for Information Operations and Reports, 1215 Jefferson Davis Highway, Suite 1204, Arlington, VA 22202-4302, and to the Office of Management and Budget, Paperwork Reduction Project (0704-0188) Washington DC 20503.			
1. AGENCY USE ONLY ***(Leave blank)***	**2. REPORT DATE** June 2010	**3. REPORT TYPE AND DATES COVERED** Master's Thesis	
4. TITLE AND SUBTITLE: Safer Ski Jumps: Design of Landing Surfaces and Clothoidal In-Run Transitions		**5. FUNDING NUMBERS**	
6. AUTHOR(S) Andrew Davis Swedberg			
7. PERFORMING ORGANIZATION NAME(S) AND ADDRESS(ES) Naval Postgraduate School Monterey, CA 93943-5000		**8. PERFORMING ORGANIZATION REPORT NUMBER**	
9. SPONSORING /MONITORING AGENCY NAME(S) AND ADDRESS(ES) N/A		**10. SPONSORING/MONITORING AGENCY REPORT NUMBER**	
11. SUPPLEMENTARY NOTES The views expressed in this thesis are those of the author and do not reflect the official policy or position of the Department of Defense or the U.S. Government.			
12a. DISTRIBUTION / AVAILABILITY STATEMENT Approved for public release; distribution is unlimited		**12b. DISTRIBUTION CODE**	

13. ABSTRACT (maximum 200 words)

This thesis explores the recent rise of skiing and snowboarding injuries from jumps fabricated with no scientific design process. It summarizes a previous method to develop a first order ordinary differential equation (ODE) for the landing surface shape, based on kinematics and dynamics, which limits the equivalent fall height (EFH) on landing. These are compared with theoretical expressions for EFH in tabletop jumps, which are shown to have linearly increasing and possibly large EFH values near the ends of the tabletop and linear landing surface portions. Finding solutions to the ODE is explored, with a large emphasis on determining the singular point where the ODE numerical integration can begin. Analysis is conducted to determine a good way to design a curved in-run transition portion of the jump that limits the additional centripetal acceleration on a particle undergoing the required velocity change of direction of a given amount. This turn can be accomplished using a unique curve known as a clothoid, which minimizes jerk along the path. The final topics include a plan for providing maintenance for safe terrain park ski jumps, and an algorithm that will assist a manager in planning where and how to build a jump.

14. SUBJECT TERMS Skiing, Snowboarding, Terrain Park, Injuries, Singular Point, Clothoid			**15. NUMBER OF PAGES** 142
			16. PRICE CODE
17. SECURITY CLASSIFICATION OF REPORT Unclassified	**18. SECURITY CLASSIFICATION OF THIS PAGE** Unclassified	**19. SECURITY CLASSIFICATION OF ABSTRACT** Unclassified	**20. LIMITATION OF ABSTRACT** UU

NSN 7540-01-280-5500 Standard Form 298 (Rev. 2-89)
Prescribed by ANSI Std. 239-18

THIS PAGE INTENTIONALLY LEFT BLANK

Approved for public release; distribution is unlimited

SAFER SKI JUMPS: DESIGN OF LANDING SURFACES AND CLOTHOIDAL IN-RUN TRANSITIONS

Andrew D. Swedberg
Major, United States Army
B.S., United States Military Academy, 2000

Submitted in partial fulfillment of the
requirements for the degree of

MASTER OF SCIENCE IN APPLIED MATHEMATICS

from the

NAVAL POSTGRADUATE SCHOOL
June 2010

Author: Andrew Davis Swedberg

Approved by: Mont Hubbard, University of California - Davis
Thesis Advisor

Arthur Krener
Co-Advisor

Carlos Borges
Chairman, Department of Applied Mathematics

THIS PAGE INTENTIONALLY LEFT BLANK

ABSTRACT

This thesis explores the recent rise of skiing and snowboarding injuries from jumps fabricated with no scientific design process. It summarizes a previous method to develop a first order ordinary differential equation (ODE) for the landing surface shape, based on kinematics and dynamics, which limits the equivalent fall height (EFH) on landing. These are compared with theoretical expressions for EFH in tabletop jumps, which are shown to have linearly increasing and possibly large EFH values near the ends of the tabletop and linear landing surface portions. Finding solutions to the ODE is explored, with a large emphasis on determining the singular point where the ODE numerical integration can begin. Analysis is conducted to determine a good way to design a curved in-run transition portion of the jump that limits the additional centripetal acceleration on a particle undergoing the required velocity change of direction of a given amount. This turn can be accomplished using a unique curve known as a clothoid, which minimizes jerk along the path. The final topics include a plan for providing maintenance for safe terrain park ski jumps, and an algorithm that will assist a manager in planning where and how to build a jump.

THIS PAGE INTENTIONALLY LEFT BLANK

TABLE OF CONTENTS

LIST OF FIGURES

LIST OF TABLES

THIS PAGE INTENTIONALLY LEFT BLANK

EXECUTIVE SUMMARY

This thesis explores the rise of skiing and snowboarding injuries from jumps fabricated with no scientific design process, and presents a method to design a much safer jump. Recent skiing progression has resulted in a much more aggressive and acrobatic style of skiing. Current tabletop terrain park jumps are not designed with any scientific process that mitigates injuries. Furthermore, a skier's equivalent fall height (EFH) increases as the jump size increases. Clearly, there is a need for a safe jump transition, ramp, and landing surface.

A safe jump landing surface can be designed through exploring the kinematic requirements for a safe landing scenario, where the flight path angle is equal to the landing surface angle. On a tabletop jump, angle equality like this rarely occurs. By choosing a reasonable and low EFH, it is possible to limit the perpendicular velocity upon landing. As a result, a low impulse on landing occurs, which results in a softer landing. Exploring these requirements leads to a first order ordinary differential equation (ODE) for the landing surface shape. The EFH in tabletop jumps have linearly increasing and possibly large EFH values near the ends of the tabletop and linear landing slope portions. Conversely, the EFH in a safe jump design remains constant at the desired level.

The ODE has an infinite family of solutions for given values of the EFH, takeoff angle θ_0 and initial velocity v_0. A skier flight path intersects these ODE solutions at points that have values of EFH of a desired quantity. The ODE has a "singular point," or starting point, where the ODE numerical integration can begin. This unique singular point is shown to lie along a rotated ellipse, which is generated for a set of parameters θ_0 and EFH. Without knowing the singular point, the only method to integrate the ODE is through estimating a conservative integration starting point. With the singular point location, numerical integration becomes much more exact. Physically, the singular point exists where the skier flight path is perpendicular to the landing surface.

Further analysis is conducted to determine a good way to design a curved in-run transition portion of the jump that limits the additional centripetal acceleration on a skier undergoing the required velocity change of direction of a given amount. A circular transition, found on design for some Olympic ski jumps, does not limit the jerk that a skier feels upon entering and exiting the transition. A better shape, which limits jerk, can be accomplished using a unique shape known as a clothoid. A clothoid has a variable radius along its length, and it provides the smoothest link between a straight line and a circular curve. On a clothoid, the distance from the start of a transition and the radius at that point are inversely proportional to each other. For a given set of incoming and outgoing angles in a transition region, an exact clothoid shape can be found. Comparing the centripetal accelerations found in a circular transition versus a clothoidal transition shows that the clothoid shape is a better design.

Through careful sight designation and thoughtful analysis, a ski area manager can design a safe in-run, transition, takeoff ramp, and landing surface. Furthermore, safety and skier enjoyment can be continued by ensuring that jump maintenance is conducted daily.

LIST OF ACRONYMS AND ABBREVIATIONS

A	Flatness of a spiral curve (clothoid)
A_{cs}	Cross sectional area of a skier
C	Snowmelt coefficient
C_d	Drag coefficient
D	A set defined in a two dimensional vector space of real numbers
EFH, h	Equivalent Fall Height
F	Force
F_n	Force in normal direction
F_t	Force in tangential direction
I	Impulse
L	Lipschitz constant
L_c	Total clothoid length
L_R	Length of linear in-run
M	Snowmelt rate
MATLAB	Matrix Laboratory, the primary computer program used in this research
N	Normal Force
ODE	Ordinary Differential Equation
P	Parameter used in defining a quadratic curve
Q	Parameter used in defining a quadratic curve
R	Parameter used in defining a quadratic curve

T_a	Air temperature
T_b	Base air temperature
a	Acceleration
a_e	Length of semi-major axis of an ellipse
b_e	Length of semi-minor axis of an ellipse
$c_1, c_2, c_3, c_4, c_5, c_6$	Coefficients of a general ellipse equation
g	Gravitational acceleration
h_1	Height of skier from takeoff point, while airborne
h_2	Height of takeoff point from tabletop
m	Mass
r	Radius of a circle
r_{min}	Minimum radius required for a clothoid design
s	Arc distance from the start of the transition to any point along a clothoid
s_c	Circular arc length
t	Time
t_z	Time at zenith (maximum height of flight path)
v	Skier velocity
v_a	Velocity before landing impact
v_b	Velocity after landing impact
v_i	Initial takeoff velocity when skier glides off the jump
v_0	Initial takeoff velocity when skier boosts off the jump
v_x	Horizontal component of skier velocity
v_{tr}	Skier velocity at the beginning of the transition region

v_y	Vertical component of skier velocity
$\dot{v}$	Derivative of velocity (acceleration)
$\dot{v}_N$	Acceleration in normal direction
$\dot{v}_T$	Acceleration in tangential direction
v_{x0}	Initial horizontal skier velocity
v_{y0}	Initial vertical skier velocity
$v_\perp$	Component of landing velocity normal to landing surface
Δv	Increase in perpendicular takeoff velocity induced by skier boost
x	Horizontal position of skier
x_e	Ellipse center *x* coordinate
x_L	Horizontal landing surface limit
x_{sp}	Singular point *x* coordinate
x_t	Tabletop length; also *x* coordinate of the knuckle
y	Vertical position of skier
y_1	Variable referring to Lipschitz continuity
y_2	Variable referring to Lipschitz continuity
y_e	Ellipse center *y* coordinate
y_L	Vertical landing surface limit
y_s	Safe surface landing shape, a function of *x*
y_{sp}	Singular point *y* coordinate
y_t	Height of takeoff ramp from tabletop; also *x* coordinate of the knuckle
α	Counterclockwise angle of rotation from horizontal

β	Linear slope upon exit from a clothoidal transition
β_0	Jump takeoff angle (ramp only)
γ	Additional percent of normal acceleration over $1g$
ε	Interior angle that a skier rotates in a circular transition
$\dot{\varepsilon}$	Rate of change of interior angle
ζ	Turning angle at any point along the clothoid, measured from the tangent line to the curve at the transition point
$\dot{\zeta}$	Rate of change of turning angle
θ	Skier trajectory angle, measured from horizontal
θ_0	Angle of velocity vector from horizontal to takeoff
Θ	Angle of a skier from horizontal, while in a transition, prior to jumping
κ	Vertical height that a skier can jump from horizontal, while wearing skis boots and skis or a snowboard
λ	Existing linear hill slope angle
μ	Coefficient of friction
ρ	Air density
φ	Landing slope angle, measured from horizontal
ω	Angular velocity
$\mathbb{R}^2$	Two dimensional vector space of real numbers

ACKNOWLEDGMENTS

This thesis is dedicated to skiers and snowboarders worldwide who have suffered injuries on conventional terrain park jumps. Hopefully the methods and analysis discussed in this thesis will prompt leaders in skiing and snowboarding to reconsider what a fun, yet safe, jump can look like. I would like to thank Professor Mont Hubbard for allowing me to work with him on this exciting topic, as well as his patience and excellent discussions. I also thank Professor Carlos Borges for allowing me to work at the Naval Postgraduate School while my advisor was at the University of California-Davis, and Professor Art Krener for his willingness to be my co-advisor and for helpful explanations of mathematical topics. I would also like to thank MAJ Joe Lindquist for his altruism and time he spent helping me with numerous MATLAB codes and Mathematica plots. Lastly, I thank the Victor Constant ski area at West Point, NY for giving me the opportunity to possibly build a safe ski jump. I sincerely hope that cadets, Soldiers and their families skiing at West Point will enjoy the thrill of skiing while knowing that their jump has been scientifically designed with safety in mind.

THIS PAGE INTENTIONALLY LEFT BLANK

I. BACKGROUND ON SKI JUMPING

A. AN ABBREVIATED HISTORY OF SKIING

Skiing is one of the oldest sports in human history. The earliest known accounts of skiing occurred over 4000 years ago, when people in Scandinavia skied for travelling and hunting [1]. Proof of early skiing as a method of travel and hunting is documented in Figure 1, which depicts a petroglyph of a skier discovered in Norway [2]. More recently, in the past 150 years, skiing has transitioned from a utilitarian sport into one of pleasure, adventure, and recreation. As skiing gained popularity, ski clubs and competitions began appearing in Europe around 1850, and later in the United States [3]. Skiing culture continued to grow as equipment improved, allowing skiers to perform better and enjoy themselves more than ever before [4].

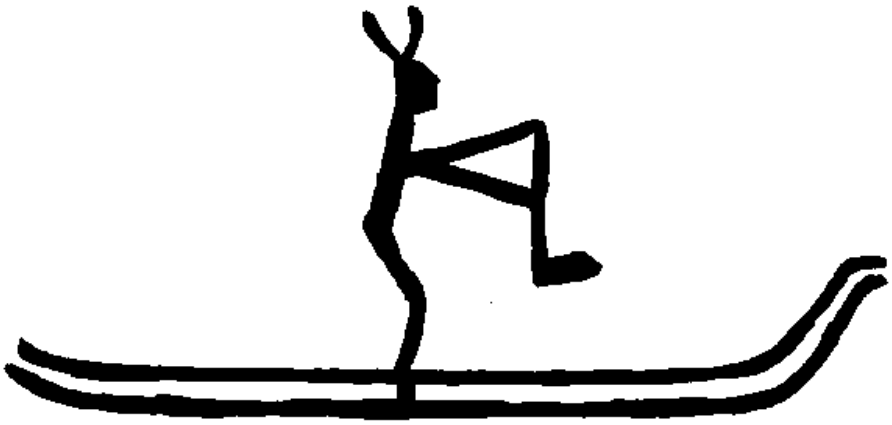

Figure 1. Earliest known ski drawing, from [2]

B. THE RISE OF FREESTYLE SKIING

The broader sport of skiing has many different aspects that have evolved throughout the past few hundred years. Some of these smaller niche styles include mogul skiing, racing, ski ballet, jibbing, powder skiing, aerials, ski jumping, skiercross, and others.

1. Olympic Jumps and Aerials

Ski jumping gained popularity in Norway in the mid 1800s, and has become a facet of the Winter Olympics and many other competitions. In this aspect of skiing, skiers slide down a path and glide off a jump. They fly through the air for as long as possible before landing. Skiers are rated for their style and how far they go before landing [5]. Figure 2 shows a ski jump in Einsiedeln, Switzerland.

Figure 2. Ski jump in Einsiedeln, Switzerland, from [5]

Aerial ski jumping is another kind of skiing. In this sport, skiers launch from a nearly vertical jump and perform many flips and twists before landing on a steep landing slope. Judges grade each jump on the complexity of the aerial maneuvers that skiers perform in the air, and how good the landing is [6]. Figure 3 shows a skier performing an aerial trick off a jump.

Figure 3. A skier performing an aerial trick, from [7]

2. Steep Skiing

Since the mid-1990s, skiing has progressed in a highly acrobatic and aggressive direction. Along with the growth in popularity of the action sports industry, such as motor bike racing, skateboarding, surfing, wakeboarding and other sports, skiers and snowboarders quickly learned to ride on steeper terrain and launch off bigger jumps than ever before. Rather than being confined to a set of rules on how to ski, the "freeskiing" movement continues to grow every year. Today, skiers are pushing the boundaries of where it is possible to ski. Skiing in locations and conditions that were once considered unthinkable and impossible just a few years ago is now quite attainable. In Figure 4, a skier (in the circle) is contemplating his next turn down an extremely steep mountain in Alaska [8].

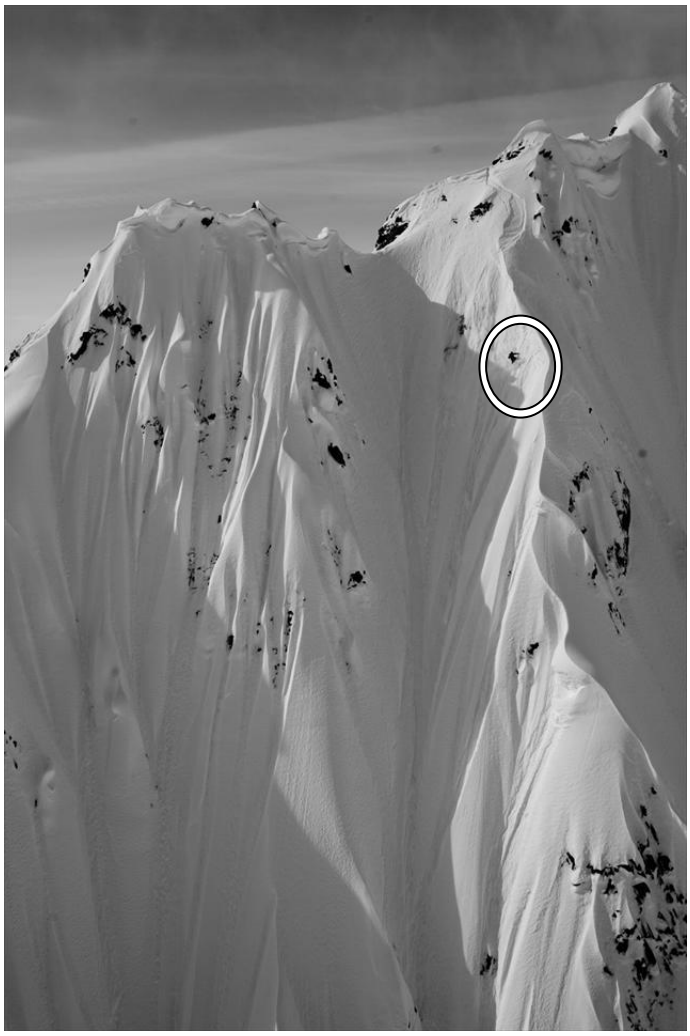

Figure 4. Steep skiing in Alaska, from [8]

3. Terrain Parks

Within the past 15 years, man-made terrain parks grew from simple jumps to a series of obstacles, including features such as large jumps, halfpipes, quarterpipes, and rails to slide on [9]. This unprecedented change in a ski area's terrain led to a new way to think of what is possible while riding on skis or a snowboard.

a. Components of a Current Terrain Park Jump

The current industry standard for a terrain park jump consists of shaping snow into a "tabletop" jump [10]. Figure 5 presents the five main components to a

conventional tabletop terrain park jump: the in-run, the transition, the takeoff ramp, the tabletop, and the landing slope where skiers exit the jump area. There is also a location known as the "knuckle," which is single spot where the tabletop changes to the landing surface.

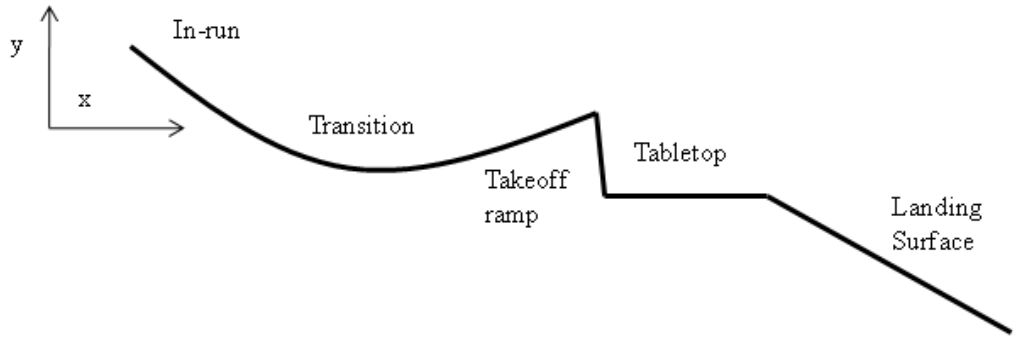

Figure 5. Profile for a typical terrain park jump

b. Non-existent "Design" of a Table-Top Jump

Recently, two journals provided analysis of terrain park jumps and methodologies for improvement. Hubbard [10] and McNeil and McNeil [11] discussed the fabrication of today's tabletop jumps and provided guidelines to make them safer. Despite these publications, most ski areas do not use any engineering methods in the design and construction of terrain park ski jumps. Currently, ski areas privately envision and control the construction of tabletop jumps. This process varies by ski area, and is managed solely based on the experience of the ski area staff. Most often, the jump shape and dimensions are based on past jumps that the staff has seen, built, or imagined. As a result, there is an ad-hoc method in building a jump ostensibly to limit injury while still providing a fun feature for skiers to jump off [10]. Most often, after construction of the jump with a snow cat and shovels, a few brave skiers test its suitability by skiing off it. Depending on the landing and experience of the skier, the jump builder might slightly adjust the jump to make it better. This process may continue, as the skiers provide feedback to the jump builder, who in turn adjusts the shape of the jump, including the

takeoff angle, length of the flat tabletop, and length and slope of the landing area. The end result is a tabletop jump that is then opened to the public for any skier to enjoy, while accepting the risks involved.

On a tabletop jump, a skier hopefully approaches the jump at a fast enough speed so that he will fly through the air past the flat/horizontal tabletop portion, and land on his skis somewhere along the linear landing area. The experienced skier often knows how fast to be skiing for a given jump, but an inexperienced skier may find himself out of place. Too little speed at the beginning of the jump may result in a landing on the flat tabletop. Conversely, too much speed at the beginning of the jump may result in landing deep into the ending of the landing surface, which typically becomes flatter as the feature ends. The severity of impact (which can result in injuries) depends on the velocity of the skier [10]. These facts are the risks that accompany current terrain park ski jumps. Figure 6 shows a typical tabletop ski jump found at most major ski areas, and Figure 7 shows a skier performing an aerial trick after leaving the takeoff ramp. Notice the horizontal tabletop and the linear landing slope.

Figure 6. Current tabletop ski jump, from [12]

Figure 7. A skier jumping off of a terrain park jump, from [13]

c. Severe Injuries on Table-Top Jumps

As terrain park ski jumps have become more popular for skiers to perform tricks off, serious spinal injuries have become more prevalent. The progression also led to an increase in skiing injuries, especially to the neck and head [14]. Although there are highly successful ski safety programs and equipment, the injuries continue. The fabrication of these terrain park features themselves may have contributed to the injuries sustained by the skiers and snowboarders [11].

d. Scientific Method Needed to Design Terrain Park Jumps

The severity of the injuries that some have sustained while on terrain park jumps motivates a need for a scientific method to build terrain park jumps. Although there are many terrain park features, such as rails, boxes, and halfpipes, this thesis will focus solely on man-made terrain park jumps. It will explain a procedure to design safer ski jumps to minimize skier injuries, and will explain the mathematical conditions that lead to the design of both an in-run transition and a landing surface.

For continuity, consider a reference system with the skier travelling from left to right. A skier will ski down an initially linear surface, enter a curved transition region and then jump or glide off a takeoff ramp. The origin of the (x,y) coordinate system is at the jump take off point, which is the last point of contact with the takeoff ramp's snow surface. The x axis is horizontal. All measurements of distance will be in meters, angles will be in both degrees (in written explanations), and radians (in calculations). Additionally, all references in this paper to a skier are to men, such as "he/his/him." This is for simplicity; it does not imply that all skiers are men. Anywhere that "he/his/him" is mentioned, it can certainly be replaced with "she/hers/her". Also, all references to "ski/skier/skiing" can certainly be replaced with "snowboard/snowboarder/snowboarding". This analysis applies for all jumping winter sports athletes, men and women, skiers and snowboarders.

In keeping with previous research, and for simplicity in modeling the flight, this thesis will ignore rotations and tricks of the skier while in the air, and follow the motion of the skier center of mass [10]. Additionally, the term "safe" is meant to be used in the context of a skier landing with his skis against the ground. This study assumes that a skier will be able to land properly; it is not a study concerning a faulty landing.

II. DESIGN METHOD FOR SAFE SKI JUMP LANDING SURFACES

A. SAFER JUMP LANDINGS THROUGH IMPULSE MINIMIZATION

As a skier leaves the takeoff ramp and flies through the air at a certain velocity and takeoff angle, there will be a unique point that he will impact the landing surface. After leaving the takeoff ramp, but prior to impact, when the skier is in the air, the velocity of the skier is most likely not parallel to the landing slope [10]. After landing impact, all of the velocity is in the tangent plane of the landing surface. As a result, the perpendicular velocity $v_\perp$ instantaneously changes from nonzero magnitude for flight velocity v_a, to zero, with sliding velocity v_b.

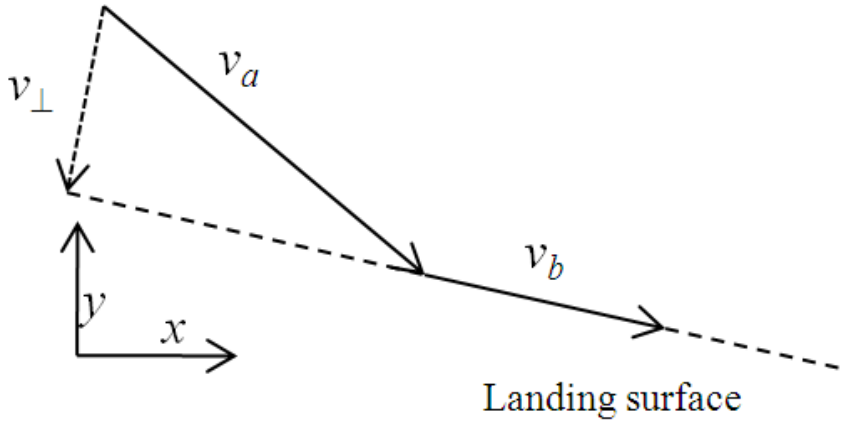

Figure 8. Perpendicular velocity changes upon landing impact

The concept of force is understood by Newton's Second Law as equivalent to the product of mass and acceleration [15]. Similarly, impulse is the integral of force with respect to time [16]. Upon landing, the skier will feel a force, and therefore an impulse, of the landing surface against his skis.

$$Force = F = ma \tag{2.1}$$

$$Impulse = I = \int F dt = \int ma\, dt = mv_b - mv_a \tag{2.2}$$

The skier velocity before impact v_a has a perpendicular component, while the velocity after impact v_b does not. As a result, the impulse is proportional to $v_\perp$ by a mass constant *m*.

$$I = mv_\perp \tag{2.3}$$

In order to make the impulse small, the perpendicular velocity must be small. By limiting $v_\perp$ on a jump landing, the impulse is limited, and the skier will experience a safer landing than if the impulse is large. Even if a skier flexes his legs to absorb the shock of landing, he will still be subjected to the same impulse.

A skier will have a lower chance of sustaining an injury if his velocity upon landing is nearly parallel to the landing surface. The more nearly parallel to the landing slope that a skier's landing velocity is, the less perpendicular the velocity will be against the landing surface. This ideal situation results in a small normal impulse, and the skier's chance of injury will be lower [10]. As the landing slope angle φ and skier trajectory angle θ become increasingly similar in magnitude, the skier will land more safely. As a result, the chance of injury will be less, especially if the skier fails to land on his skis.

Because limiting $v_\perp$ is not instinctively understood, an analogous quantity can be used, known as equivalent fall height (EFH). Equivalent fall height is the height that results in velocity $v_\perp$in a $1g$ environment. The measure of EFH is known through the energy equation $h = {v_\perp}^2/2g$. The essential requirement is that $v_\perp$ is made to correspond to a reasonable EFH [10]. Figure 9 shows a skier flight path with a safe landing surface. The perpendicular component of velocity is the sine of the difference of the safe landing slope angle and the skier flight path angle.

$$v_\perp = v\,sin(\varphi - \theta) \tag{2.4}$$

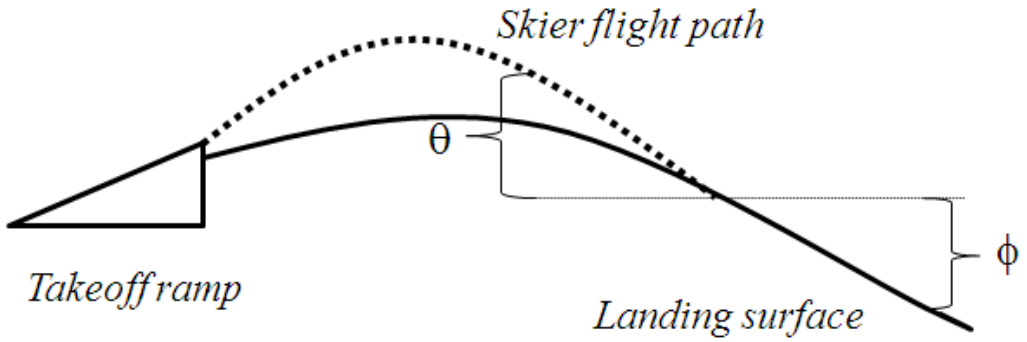

Figure 9. Skier flight path and safe surface design

When $\varphi = \theta$, the perpendicular component of velocity is zero. In this ideal situation, there is no perpendicular velocity; all velocity is parallel to the landing surface and no impulse is required on landing.

B. DETERMINATION OF SKIER VELOCITY AT TAKEOFF

Landing safely on a surface is related to the EFH and velocity upon landing. In the safest landing condition, the flight path angle and landing surface angle have the same value at impact ($\theta = \varphi$). This section will explore the velocity of a skier at the ramp takeoff point. Most explained concepts and equations in sections B and C of this chapter are a summary of Hubbard's work [10].

The angle of the flight path measured from horizontal θ is determined from the vertical *y* and horizontal *x* velocity components of the skier.

$$\theta = tan^{-1}\frac{v_y}{v_x} \tag{2.5}$$

The angle φ measured from horizontal is found by the inverse tangent of the rate of change of the landing surface *y* distance to its *x* distance.

$$\varphi = tan^{-1}\frac{dy_s}{dx} \tag{2.6}$$

A skier will leave the jump takeoff by either jumping off the top edge or by gliding smoothly from the takeoff point. If the skier simply glides off the jump, the

initial takeoff velocity v_o is parallel to the jump takeoff angle β_0, relative to the horizon. These horizontal and vertical components of initial velocity are given by:

$$v_{xo} = v_i \cos \beta_0 \tag{2.7}$$

$$v_{yo} = v_i \sin \beta_0 \tag{2.8}$$

However, not every skier will simply glide off the jump into the air. He may decide to increase the velocity at takeoff by popping off the top of the jump takeoff point. Nearly all of his change in velocity will be perpendicular to the velocity vector by an amount Δv. In modeling, this velocity increase Δv will have an upper limit $\sqrt{2g\kappa}$, where κ is the vertical height the skier can jump in meters. Typical recreational skiers, wearing boots and skis, will jump a maximum of approximately 0.25 meters. The corresponding Δv is therefore about 2.21 meters per second.

When the skier glides off of the jump, the initial velocity v_o is parallel to the ramp angle, β_0. As a result, the jump takeoff angle θ_0 is equal to β_0. In this scenario, $v_0 = v_i$. If the skier jumps with additional velocity Δv, the takeoff angle changes by an additional amount $\Delta\theta = tan^{-1}\frac{\Delta v}{v_i}$. The initial velocity then becomes $v_0 = \sqrt{v_i^2 + \Delta v^2}$.

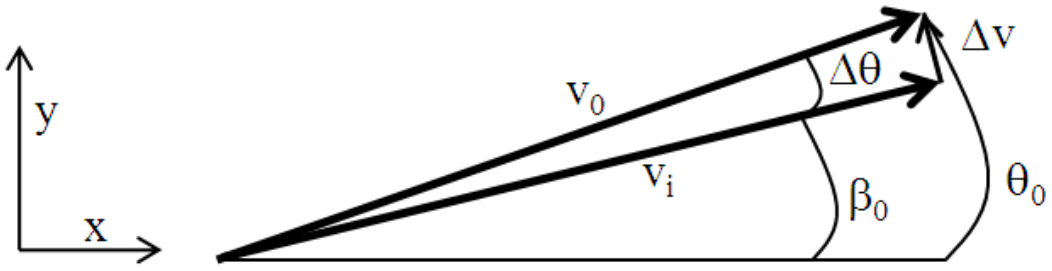

Figure 10. Diagram of a ski jump take-off ramp, after [10]

With the added boost from the skier, the new takeoff angle θ_0 is $\theta_0 = \beta_0 + \Delta\theta$. The faster a skier is moving, the higher he will be in the air after leaving the jump.

C. DEVELOPMENT OF AN ORDINARY DIFFERENTIAL EQUATION FOR A SAFE LANDING SURFACE

For a safe landing surface, the primary requirements are to have skier impulse from the surface both limited to a reasonable value, and to be reasonable no matter where a skier lands. The velocity components along the path as a function of time are known from basic physics projectile equations (neglecting aerodynamic forces).

$$v_x = v_{x0} = v_0 \cos\theta_0 \tag{2.9}$$

$$v_y = v_{y0} = v_0 \sin\theta_0 - gt \tag{2.10}$$

Integrating these expressions with respect to time allows us to find the (*x*,*y*) position of the skier at any desired time.

$$x = v_{x0}t \tag{2.11}$$

$$y = v_{y0}t - \frac{gt^2}{2} \tag{2.12}$$

Solving for time yields:

$$t = \frac{x}{v_0 \cos\theta_0} \tag{2.13}$$

By eliminating time, the parabolic vertical position *y* of a skier flight path can be written in terms of only the variable *x* and parameters v_0 and θ_0.

$$y = x \tan\theta_0 - \frac{gx^2}{2\,(v_0 \cos\theta_0)^2} \tag{2.14}$$

Solving for v_0 results in an expression for the initial velocity a skier needs in order to reach a certain point (*x*,*y*).

$$v_0 = \sqrt{\frac{x^2 g}{2\,(x\tan\theta_0 - y)\,(\cos\theta_0)^2}} \tag{2.15}$$

The total velocity has *x* and *y* components.

$$v = \sqrt{{v_x}^2 + {v_y}^2} \tag{2.16}$$

Substituting Equations 2.9 and 2.10 in Equation 2.16 results in an equation for skier velocity involving parameters, *t*, v_0 and θ_0.

$$v = \sqrt{(v_0 \cos\theta_0)^2 + (v_0 \sin\theta_0 - gt)^2} \tag{2.17}$$

Substituting for *t* yields the following equation for the skier velocity at an arbitrary (*x*,*y*) position in flight.

$$v = \sqrt{(v_0 \cos\theta_0)^2 + (v_0 \sin\theta_0 - \frac{gx}{v_0 \cos\theta_0})^2} \tag{2.18}$$

Using Equation 2.15, Equation 2.18 can be rewritten in terms of *x*, *y*, and θ_0. This gives the expression for the velocity at any (*x*,*y*) coordinate along the flight path.

$$v = \sqrt{\frac{x^2 g}{2(x\tan\theta_0 - y)\cos^2\theta_0} - 2gy} \tag{2.19}$$

The rate of change in vertical position is the derivative of Equation 2.14.

$$\frac{dy}{dx} = \frac{v_y}{v_x} = \tan\theta = \tan\theta_0 - \frac{gx}{(v_0 \cos\theta_0)^2} \tag{2.20}$$

With Equation 2.20, it is possible to solve for the flight path angle θ in terms of known parameters g, v_0, and θ_0, and variable *x*.

$$\theta = \tan^{-1}(\tan\theta_0 - \frac{gx}{(v_0 \cos\theta_0)^2}) \tag{2.21}$$

Further simplification (by substituting Equation 2.15 into 2.21) results in the flight path θ involving only terms of known variables x, y, and parameter θ_0.

$$\theta = \tan^{-1}(\frac{2y}{x} - \tan\theta_0) \tag{2.22}$$

Building upon these established formulas, it is possible to develop a differential equation that must be satisfied by a safe surface landing shape y_s. The safest place to land is where the landing slope and the skier flight path angles are equal, and there is no perpendicular velocity. From Equation 2.4 and knowing that $v_\perp = \sqrt{2gh}$, it is possible to solve for φ, the landing surface angle.

$$\varphi = sin^{-1}\left(\frac{\sqrt{2gh}}{v}\right) + \theta \tag{2.23}$$

Using Equation 2.21, the landing surface angle can be found in terms of known parameters *g*, *h*, and θ_0.

$$\varphi = sin^{-1}\left(\frac{\sqrt{2gh}}{v}\right) + tan^{-1}(tan\,\theta_0 - \frac{gx}{(v_0 cos\,\theta_0)^2}) \tag{2.24}$$

With Equation 2.6, the rate of change of the landing surface angle $\frac{dy_s}{dx}$ can be found.

$$tan\,\varphi = \frac{dy_s}{dx} = tan\left(tan^{-1}\left(tan\,\theta_0 - \frac{gx}{(v_0 cos\,\theta_0)^2}\right) + sin^{-1}\left(\frac{\sqrt{2gh}}{v}\right)\right) \tag{2.25}$$

Substituting the relationship for velocity (Equation 2.17) in Equation 2.25 yields a differential equation for the safe landing surface.

$$\frac{dy_s}{dx} = tan\left(tan^{-1}\left(tan\,\theta_0 - \frac{gx}{(v_0 cos\,\theta_0)^2}\right) + sin^{-1}\left(\sqrt{\frac{2gh}{(v_0 cos\,\theta_0)^2 + (v_0 sin\,\theta_0 - \frac{gx}{v_0 cos\,\theta_0})^2}}\right)\right) \tag{2.26}$$

This ordinary differential equation (ODE) for the safe landing surface is in terms of variables *x*, *y*, and parameters v_0 ,θ_0, *g*, and *h*. While *g*, *h*, and θ_0 are constant values (with θ_0 varying as desired), v_0 is known already in terms of *x* and *y*. With the known expression for v_0 (Equation 2.15), simplification results in an expression for the rate of change of the landing surface in terms of variables *x*,*y*, and parameters *h* and θ_0.

$$\frac{dy_s}{dx} = tan(tan^{-1}(\frac{2y}{x} - tan\,\theta_0) + sin^{-1}\sqrt{\frac{h}{\frac{x^2}{4\,(x\,tan\,\theta_0 - y)\,(cos\,\theta_0)^2} - y}}) \tag{2.27}$$

A safe landing surface solution is found when the skier flight path y crosses the landing surface y_s. This occurs when $y = y_s$.

$$\frac{dy_s}{dx} = \tan\left(\tan^{-1}\left(\frac{2y_s}{x} - \tan\theta_0\right) + \sin^{-1}\sqrt{\frac{h}{\frac{x^2}{4\,(x\tan\theta_0 - y_s)\,(\cos\theta_0)^2} - y_s}}\right) \qquad (2.28)$$

This first order ODE must be satisfied in order to allow for a safe landing slope for any given value of θ_0 and desired value of h. It is an ODE for the dependent variable y_s (the landing surface height) as a function of x (the dependent variable). Note that the gravity constant g no longer appears in Equation 2.28.

The EFH, also denoted as h in the equations, is a quantifiable measure of the acceptable distance that a person feels comfortable with falling to the ground. For example, most adults might be comfortable with an EFH of one meter, but anything over that is less acceptable. With this safe ski jump model, it is possible to design a safe landing surface for a given EFH (preferably at around one meter). As a result, a jump can be built so a skier will "fall" only the EFH value, unlike what happens today in existing tabletop ski jumps.

D. NUMERICAL SOLUTIONS OF SAFE LANDING SURFACE ODE

The solution to the ODE cannot be arrived at analytically. Rather, it must be solved numerically using a program such as MATLAB. Furthermore, integration must be completed backwards, from the terminal conditions. Because the ODE is not Lipschitz continuous (to be discussed in detail later), it is not possible to integrate forward from the origin. Figure 11 is a plot of five solutions, corresponding to y_L (vertical landing surface limit) of 1m, -1m, -3.5m, -7m, and -8.5m, and a 40 meter horizontal jump x_L. These five solutions are chosen from an infinite family of solutions.

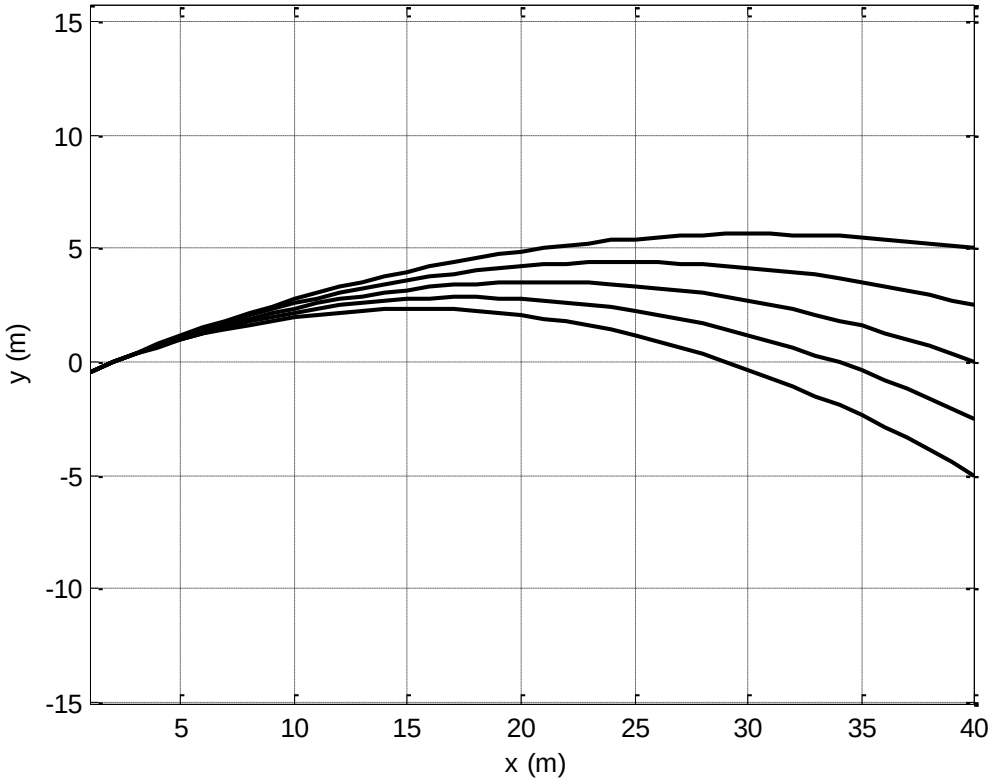

Figure 11. Plot of five safe landing surfaces for a 40m jump

The faster a skier is travelling at takeoff, the further horizontally he will fly. In order to limit the landing impulse, the value of φ must increase as the distance increases. As a result, all solutions have monotonically decreasing slope [10].

Overlaying skier flight paths (from Equation 2.14) for different takeoff velocities onto safe landing surfaces shows how these surfaces can result in the same EFH for all velocities. Figure 12 shows the same safe landing surfaces in figure 11, but also includes skier flight paths from velocities of 5 to 40 mph, in 5 mph increments. The intersection of every landing spot and the flight paths all have the same EFH, no matter which jumper path one is on. In this example, EFH is arbitrarily chosen to be 1m and the jump takeoff angle is 25 degrees.

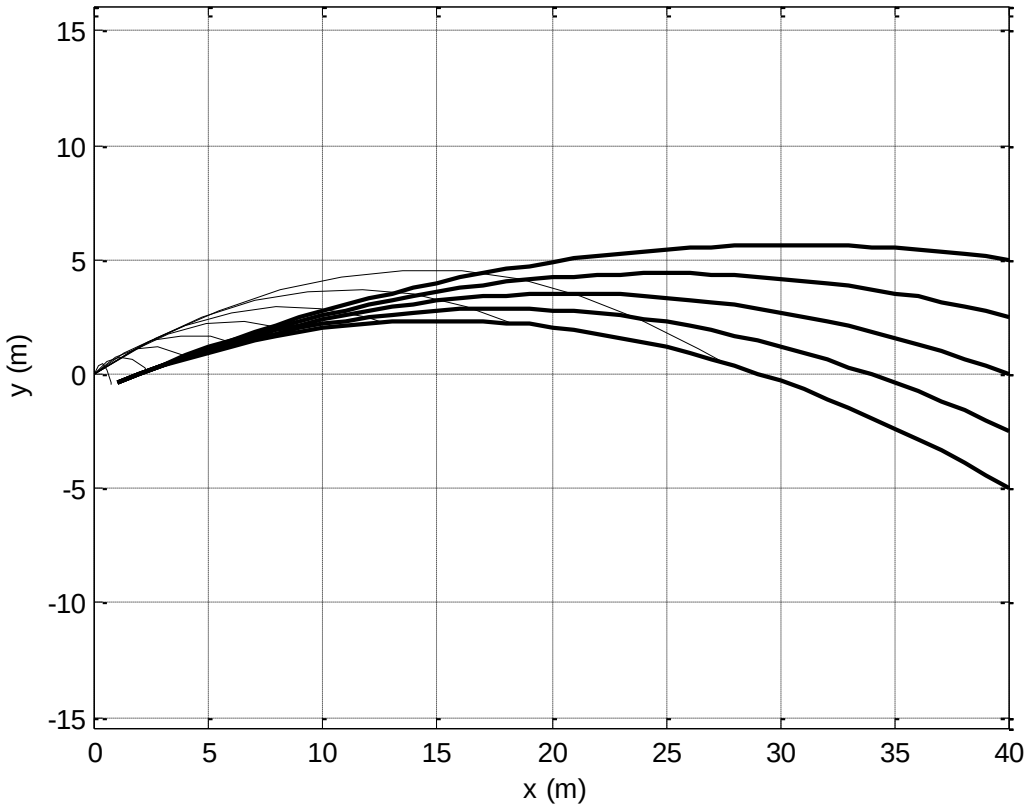

Figure 12. Plot of five illustrative safe landing surfaces (heavy lines) with eight jumper paths (light lines)

Superimposing a conventional table-top jump onto one safe landing surface (from an infinite family), it becomes apparent that safe ski jump design calls for a monotonically decreasing slope as a function of *x*, while a table-top jump maintains a generally linear landing slope. Figure 13 shows that depending on the tabletop dimensions, there is at most one or two landing points that these two different jump landing surfaces have in common. Clearly, safe landing surfaces differ from what is currently being built at ski areas.

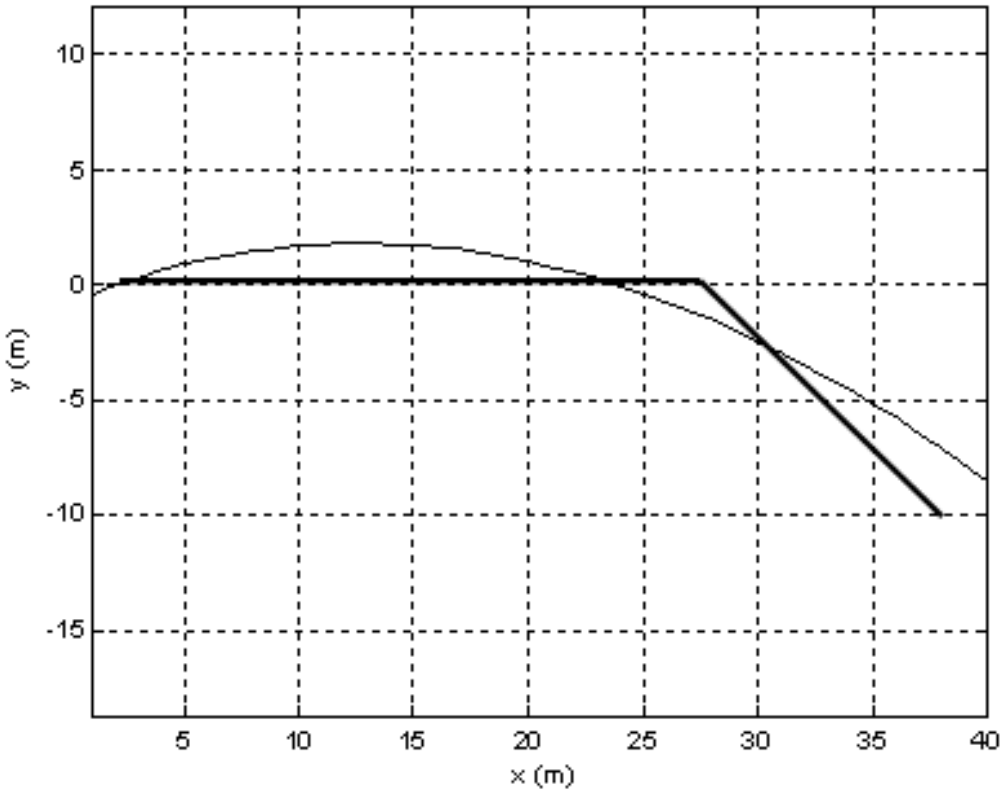

Figure 13. Tabletop jump (heavy line) with safe jump (light line)

In [10], Hubbard outlines an algorithm for safe landing surface design.

1. Decide what EFH is desired. A possible value is 1 meter, but this must be chosen by the designer based on safety considerations.

2. Decide on entire jump size, so it fits into a given area (x_L, y_L).

3. For a fixed take-off angle β_0, choose a safe surface that passes through (x_L, y_L). Overshoot may occur, and limiting v_i may be needed.

4. For a free take-off angle β_0, choose a safe surface that passes through (x_L, y_L), so that all maximum reasonable v_i's can be accommodated.

E. TABLE-TOP JUMPS DO NOT LIMIT EQUIVALENT FALL HEIGHT

As mentioned in Chapter I, table-top jumps are often associated with serious skiing injuries. This section will show that on a table top jump, the equivalent fall height generally increases as the horizontal flight path distance *x* increases. These results will be contrasted with a safe jump design, and the EFH values will be compared for similar size jumps.

1. Equivalent Fall Height as a Function of Distance

As previously stated, perpendicular velocity $v_\perp$ can be better understood by measuring the corresponding EFH, which is related to $v_\perp$ by $EFH = {v_\perp}^2/2g$. Equation 2.29 is formed by using Equation 2.4 as a substitute for $v_\perp$.

$$EFH = \frac{v^2\, sin^2(\varphi - \theta)}{2g} \tag{2.29}$$

This equation can be rewritten in terms of *x* by substituting the expressions for *v* (Equation 2.19) and θ (Equation 2.22). Equation 2.30 expresses EFH as a function of variables *x,y* along a flight path and jump design parameters θ_0 and φ.

$$EFH(x) = \left[\frac{x^2}{4\, cos^2\, \theta_0 (x\, tan\, \theta_0 - y)} - y\right] sin^2\left[\varphi - (tan^{-1}(\frac{2y}{x} - tan\, \theta_0))\right] \tag{2.30}$$

On a tabletop jump, a skier will have two general locations where he can land: before or after the knuckle, which has coordinates $(x_t, -y_t)$. Figures 14 and 15 show the two cases. The length of the tabletop is x_t, the height of the takeoff point above the tabletop is y_t, and the landing surface angle is $-\varphi$. The time at the zenith (top) of the skier flight path is denoted by t_z.

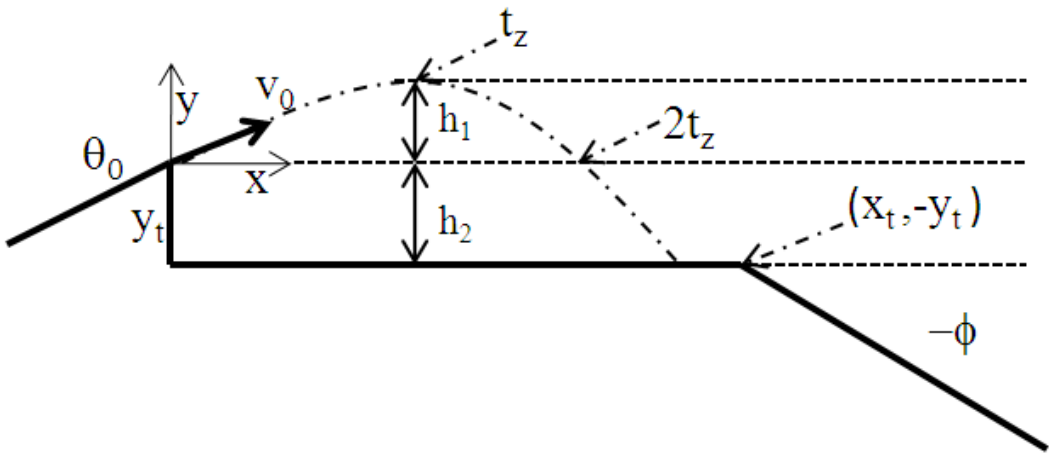

Figure 14. The flight path of a skier landing on a tabletop, after [10]

If a skier lands on the tabletop (Figure 14), a simple expression for EFH can be determined. At the zenith of the trajectory, the EFH has two portions, h_1 and h_2. In this case, h_2 is the height of the takeoff point above the tabletop, and h_1 is the height of the flight path zenith above the takeoff point.

$$h_1 = \frac{(v_{y0})^2}{2g} \tag{2.31}$$

The initial vertical velocity is related to the initial horizontal velocity by the tangent of the takeoff angle. Equation 2.32 is a rewritten version of Equation 2.5 with initial conditions $v_x = v_{x0,}$ $v_y = v_{y0}$, and $\theta = \theta_0$, which occurs when a skier boost off the jump.

$$v_{yo} = v_{xo}\, tan\, \theta_0 \tag{2.32}$$

Substituting v_{yo} from Equation 2.32 into 2.31 results in an expression for h_1.

$$h_1 = \frac{(v_{xo})^2\, tan^2\, \theta_0}{2g} \tag{2.33}$$

After substituting $v_{x0} = v_0 \cos\theta_0$ (Equation 2.9) and simplifying, h_1 can be expressed in terms of v_0, θ_0, and g.

$$h_1 = \frac{{v_0}^2 \sin^2 \theta_0}{2g} \tag{2.34}$$

Substituting the previously determined initial velocity v_0 (Equation 2.15) into Equation 2.34 results in an expression for h_1 in terms of x, θ_0, and y_t, so that $y_t = -y$.

$$h_1 = \frac{x^2 \tan^2 \theta_0}{4(x \tan \theta_0 + y_t)} \tag{2.35}$$

The final EFH is found by adding the additional constant h_2.

$$EFH = h_1 + h_2 = y_t + \frac{x^2 \tan^2 \theta_0}{4(x \tan \theta_0 + y_t)} \tag{2.36}$$

Equation 2.36 gives the EFH for a skier landing on a tabletop. The next case shows the EFH for a skier landing on a downward slope (Figure 15).

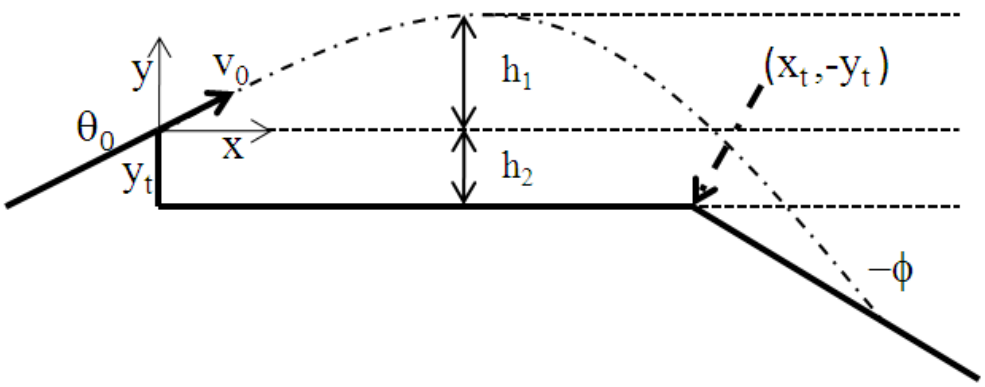

Figure 15. The flight path of a skier landing on a linear surface

When a skier lands on the downward sloping linear landing surface, the height y is given by:

$$y = -y_t + (x - x_t)\tan \varphi \tag{2.37}$$

Substituting for y (Equation 2.37) in Equation 2.30 gives an expression for EFH when landing after the knuckle in terms of x only, together with desired parameters θ_0, φ, x_t, and y_t.

$$EFH= \left[\frac{x^2}{4\cos^2\theta_0(x\tan\theta_0-(y_t+(x-x_t)\tan\varphi)}-y_t-(x-x_t)\tan\varphi\right]\sin^2\left[\varphi-(\tan^{-1}(\frac{2(y_t+(x-x_t)\tan\varphi}{x}-\tan\theta_0)\right] \quad (2.38)$$

The two general landing cases occur when the skier lands on the tabletop before the knuckle (governed by Equation 2.36) or on the downward sloping landing surface after the knuckle (Equation 2.38).

2. Analysis of Tabletop Equivalent Fall Height Plots

Equivalent fall height sensitivity can be determined by choosing a reasonable linear takeoff angle θ_0 and individually varying the parameters tabletop x_t, jump height y_t, and landing surface φ. Each tabletop jump landing scenario is researched individually.

a. Flat Landing Equivalent Fall Height Analysis

When a skier lands before the knuckle ($x < x_t$), his EFH is governed by Equation 2.36. Figure 16 shows that changing y_t to realistic values (0m, 1m, 2m, 3m) while keeping θ_0 constant at 25°, the EFH values are spaced fairly evenly and increase roughly linearly as the horizontal length of the jump increases. The value for φ in this case is zero, as the skier lands on the flat tabletop. For a large jump, the EFH values become quite dangerous.

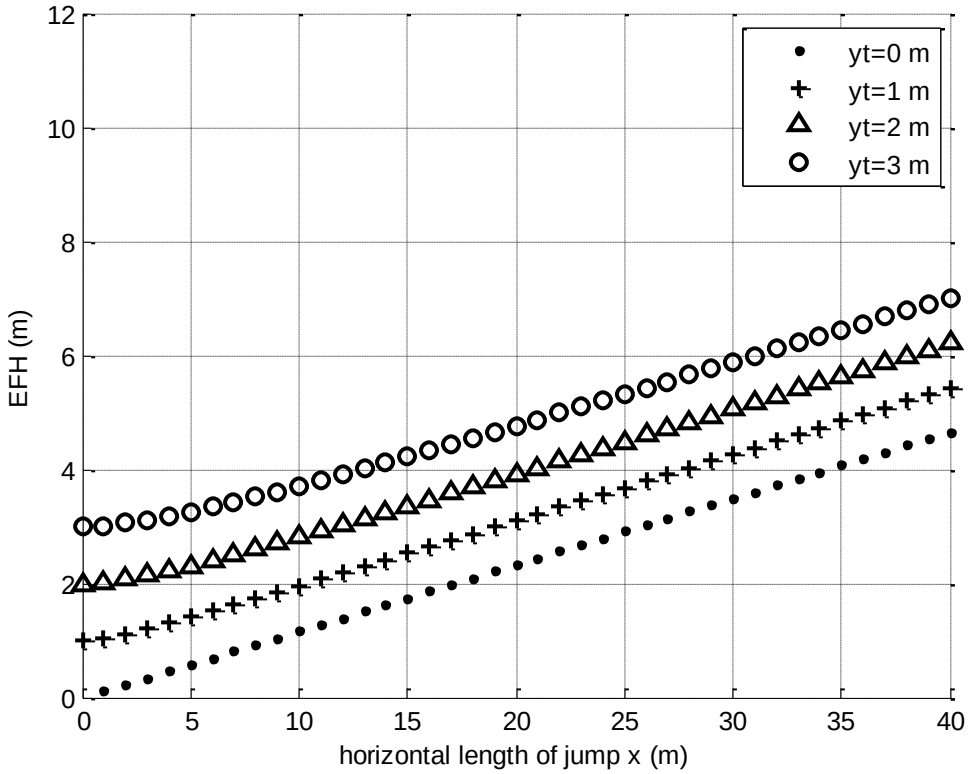

Figure 16. EFH of a flat tabletop landing as a function of jump distance *x* for several values of y_t and constant $\theta_0 = 25°$

Similarly, for several values of the takeoff angle θ_0 while holding y_t constant shows again that the EFH nearly increases linearly as the horizontal length of the jump increases. Figure 17 shows EFH vs. *x* for several $\theta_0$values and a constant y_t at one meter. The knuckle position x_t is arbitrarily large, since the landing will always be on the tabletop. Again, the EFH grows to dangerous levels as the jump size increases.

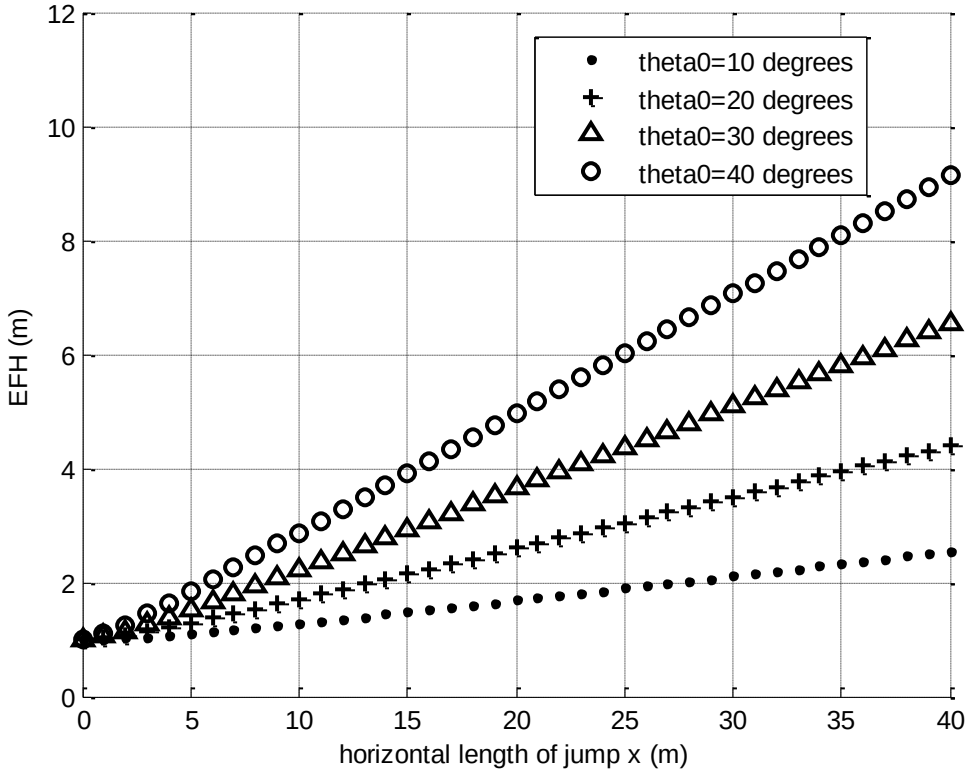

Figure 17. EFH of a flat tabletop landing as a function of jump distance *x* for several values of θ_0 and constant $y_t = 1\text{m}$

In both cases of individually varying the parameters y_t and θ_0, the EFH is shown to increase linearly with jump distance.

b. Angled Landing Surface Equivalent Fall Height Analysis

When a skier lands after the knuckle ($x > x_t$), his EFH is governed by Equation 2.38. Plots of EFH as a function of jump distance are shown in Figure 18. Here, y_t varies from 0 to 3 meters while all other parameters are held constant ($x_t = 10\text{m}, \theta_0 = 25^\circ, \varphi = -30°$).

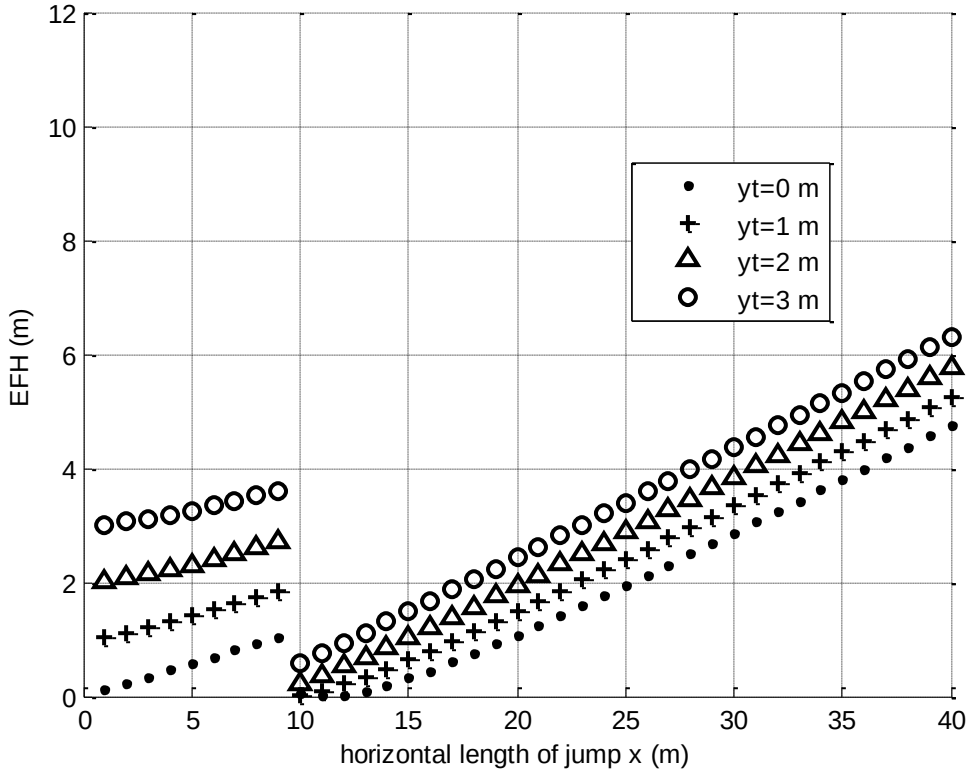

Figure 18. EFH of landing on a constant downward slope as a function of jump distance *x* for several values of $y_t$and constant parameters x_t=10m, θ_0=25°, and φ= -30°

Every graph in Figure 18 starts at its respective height above the tabletop and increases to the value of x_t. At the knuckle, the EFH dramatically decreases to a comfortable level. However, thereafter, the EFH again increases linearly without bound. Choosing larger values of x_t, while keeping other parameters constant, results in a very similar outcome of EFH behavior. Figures 19 ($x_t = 20\text{m}$) and 20 ($x_t = 30\text{m}$) show that moving the knuckle position does not change the overall behavior of the EFH on a tabletop jump. In each case, the EFH increases as the horizontal jump length increases to the knuckle position. Then, although the EFH drastically decreases at the knuckle, it immediately begins to increase again. Tabletop jumps today are built with generally constant linear landing surfaces. This type of landing cannot protect a skier from a large

EFH if he lands far out horizontally from the takeoff point. Clearly, the linear landing surface is not an ideal design, as EFH is never consistently limited.

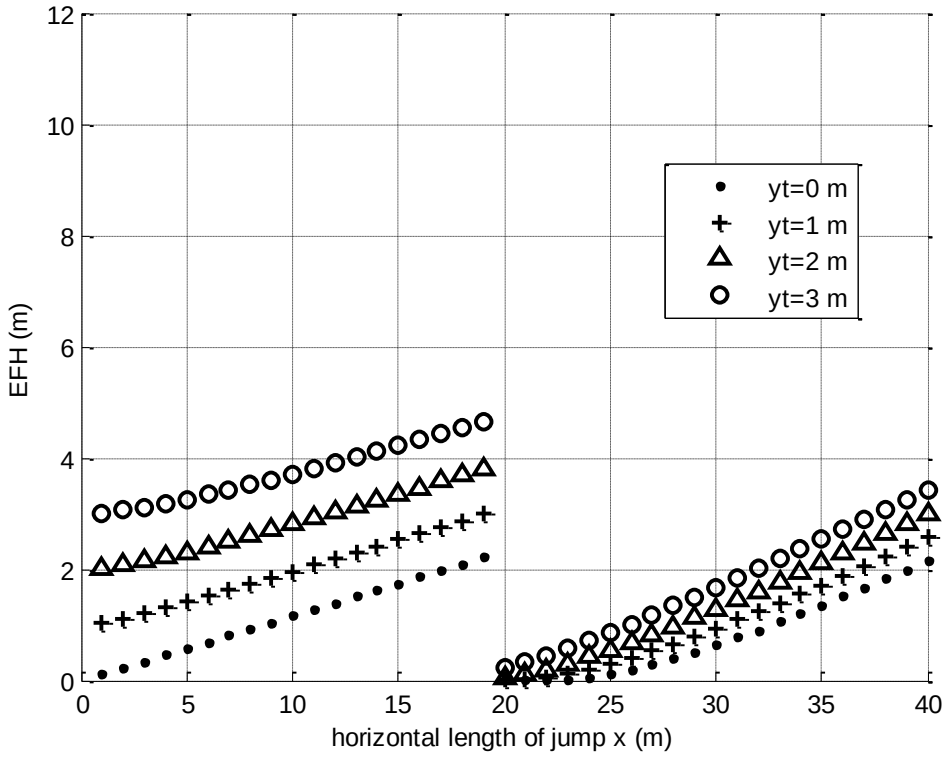

Figure 19. EFH of landing on a constant downward slope as a function of jump distance *x* for several values of $y_t$and constant parameters x_t=20m, θ_0=25°, and φ= -30°

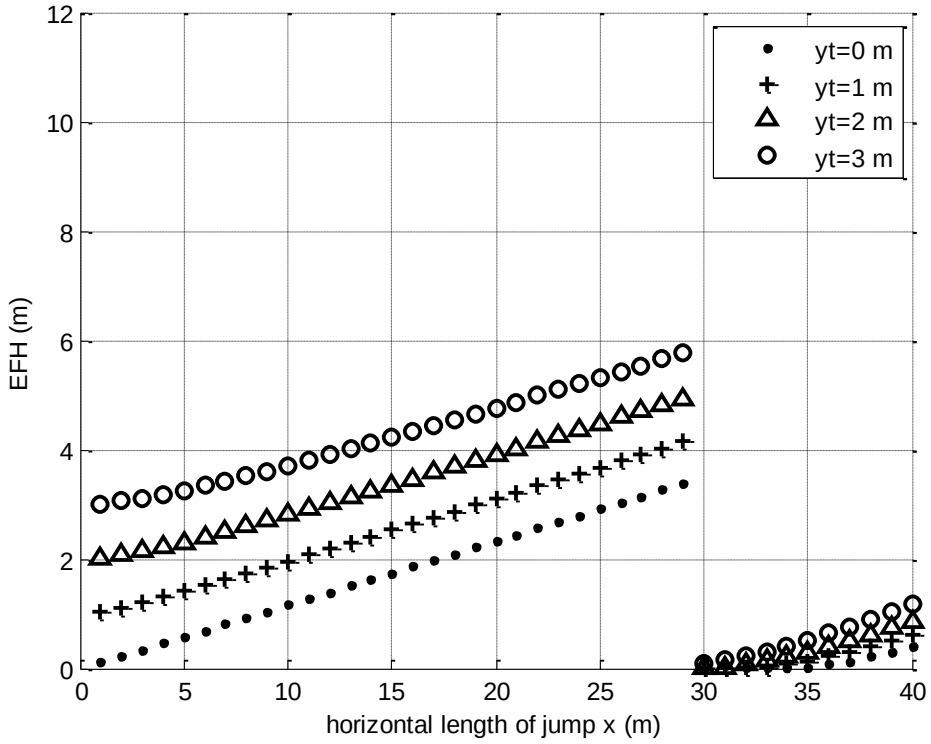

Figure 20. EFH of landing on a constant downward slope as a function of jump distance *x* for several values of y_t and constant parameters x_t=30m, θ_0=25°, and φ= -30°

Figures 18, 19, and 20 verify that varying the knuckle position x_t for different y_t and constant θ_0 and φ does not affect the roughly linear dependence of the EFH and horizontal length of the jump *x*. For jumps with no step-down to the tabletop ($y_t = 0$), the skier flight path is symmetric about the zenith of the trajectory. In this case, the landing angle will be equal in magnitude to the takeoff angle. If the magnitude of the flight path angle θ is greater than the magnitude of the landing surface angle φ, a skier will be able to land anywhere on the landing surface. The closer the landing is to the knuckle (but after it), the lower the EFH is. However, if the magnitude of the flight path angle θ is less than the magnitude of the landing surface angle φ, there is a physical region where landing becomes impossible. This region can be imagined by travelling through the landing surface and arriving at the top of it; an impossibility. Figures 18, 19, and 20 all show this impossibility for $y_t = 0$. In Figure 18, this region exists at approximately 10 to 12 meters. After about 12 meters, it is possible for a skier to land on

the downward slope, and the EFH continues to increase. In Figure 19, this region exists at approximately 20 to 23 meters, and in Figure 20 it is around 30 to 34 meters. Increasing y_t can make it possible to land anywhere on the downward slope.

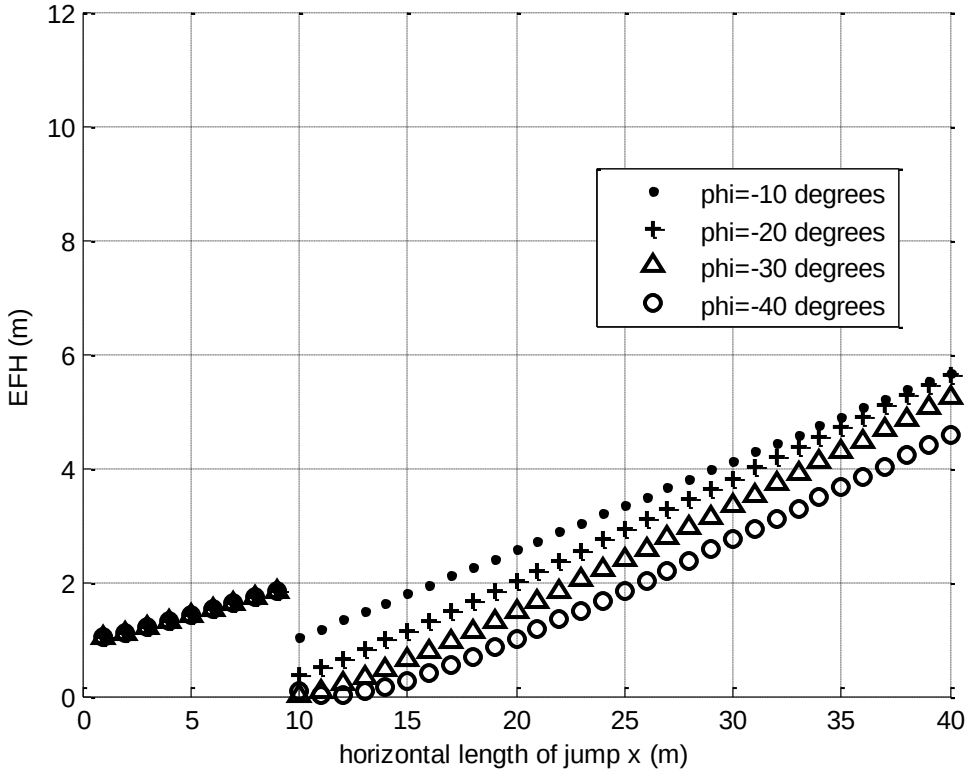

Figure 21. EFH of landing on a downward slope as a function of jump distance *x* for several values of φ with constant parameters x_t=10m, $y_t = 1$m, and θ_0=25°

Figure 21 shows that varying the landing surface angle φ while keeping other parameters constant also results in a generally increasing EFH. From the origin to the knuckle, all values of EFH are the same, as φ plays no part in landing in this region. For a symmetric flight path, where $y_t = 0$m, the takeoff angle θ_0 equals the landing angle φ. In this case ($\theta_0 = \varphi$), the EFH is zero. For cases where $\theta_0 > \varphi$, landing on the downward surface is possible, and the EFH is small, positive, and reasonable. For situations where $\theta_0 < \varphi$, the EFH becomes negative, which correlates to the impossible region previously described. A rule of thumb in terrain park jumps today states that the angle of the landing surface should equal the takeoff angle. This rule attempts to control

the EFH that a skier experiences upon landing. However, as the recent figures show, landing on the tabletop can result in large and unsafe EFH. Furthermore, although the EFH decreases when landing occurs beyond the knuckle, it immediately begins to increase and can be unsafe for large *x* values.

Comparing these EFH tabletop plots for the EFH from a similar sized safe jump (Figure 22) presents some astounding differences. Tabletop jumps have just a few instances where the EFH would be considered comfortable to a skier, while a safe jump is designed with the low EFH requirement first and foremost in mind. Any landing point along a safe landing surface has the same EFH as any other. Figure 22 shows that no matter where a skier lands on a safe surface, his EFH will be the same as any other.

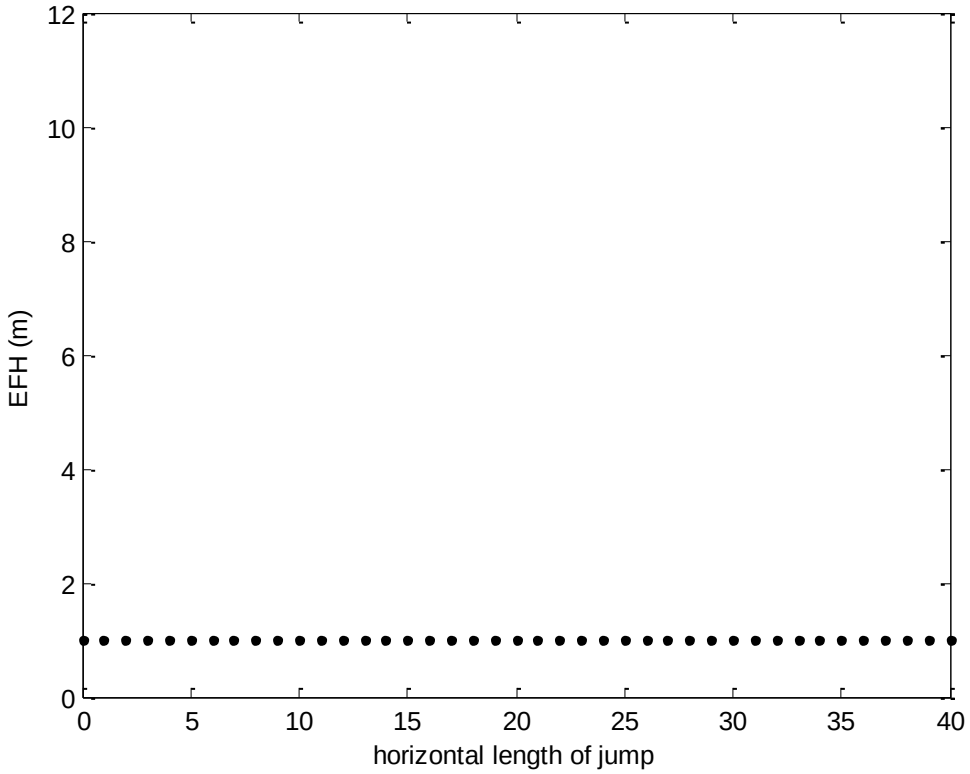

Figure 22. EFH of landing on a safe landing surface as a function of jump distance *x* with constant parameters θ_0=25° and y_t=1m

If a jump has consistent and reasonable EFH values, injuries can be minimized. Furthermore, skiers will know that the jumps they enjoy are built with safety

in mind. Equations 2.36 and 2.38 are analytic expressions for EFH in tabletop jumps. Equation 2.36 models the EFH felt by a skier landing on the flat tabletop, while Equation 2.38 models the EFH felt by a skier landing on the linear downward sloping landing surface. Figures 16 and 17 show the numerical implementations of Equation 2.36, and Figures 18-21 show the numerical implementations of Equation 2.38. An overarching and alarming consistency arises in all of the plots: the EFH increases roughly linearly with horizontal distance x no matter what the ramp height y_t is, no matter where the knuckle position x_t is, and no matter what the angled landing slope φ is. If the takeoff angle θ_0 is equal to φ, and $y_t = 0$, it is possible to have small EFH just past the knuckle. This is sometimes called the "sweet spot" [17]. However, for all landings past the knuckle, the EFH increases roughly linearly as the distance jumped increases. A tabletop jump landing is safe only if a skier lands in the "sweet spot" just past the knuckle. However, this critical requirement puts much constraint on the skier, who will not be able to greatly control his landing location after takeoff. Landing before or after the sweet spot is not ideal, as the EFH can be at a dangerous level.

Constant downward sloping landing surfaces are therefore not safe if the landing distance x is significantly larger than the knuckle position x_t, even if $\varphi = \theta_0$. As a result of this analysis, one can conclude that large tabletop jumps are not safe, despite what adjustments one makes to the knuckle position, takeoff ramp angle, and landing surface angle, if the tabletop is long, or if the landing position on the downward surface is large.

THIS PAGE INTENTIONALLY LEFT BLANK

III. SINGULAR POINT OF THE SAFE SLOPE ODE

A. MOTIVATION FOR THE EXISTENCE OF A SINGULAR POINT

In Figure 11, it is clear that the five safe surface solutions emanate from a common point, and all appear to have the same slope at that point. This "singular point" occurs only at one location along any safe landing surface. Physically, the singular point must be below and to the right of the origin (take off point). For a given EFH and takeoff angle θ_0, there is a unique jumper path that hits all of the safe surfaces perpendicular to the landing surface. This single skier jump path, with a specific initial velocity v_0, passes through the singular point. Furthermore, there is a different singular point for every value of v_0, as the skier's flight path change as v_0 varies.

Decreasing the initial velocity that a skier has upon takeoff decreases the horizontal distance at which he will impact the landing surface. Continuing to decrease the velocity increases the difference between the skier flight path angle θ and the landing surface angle φ. The difference between these two angles increases to a limit of $\pi/2$, which occurs when the skier velocity is perpendicular to the landing slope.

This singular point is the point where forward integration can begin in a MATLAB automated integration program. Rather than integrating backwards only, knowing the (*x*,*y*) coordinates for the singular point for a given EFH and θ_0 enable the ODE (Equations 2.26, 2.27, and 2.28) to be solved forward numerically from the singular point. Prior to knowing the singular point coordinates, the best method to integrate the ODE is by making a best estimate of where the singular point is, and integrating forwards from there, or backwards to there.

Rewriting Equation 2.23 results in Equation 3.1, which is an expression for the conditions required at the singular point. No velocity gets transmitted to a tangential slope component; rather all of the velocity is perpendicular to the safe landing surface.

$$\varphi - \theta = \frac{\pi}{2} = sin^{-1}\left(\frac{\sqrt{2gh}}{v}\right) \tag{3.1}$$

This is true when $\sin\frac{\pi}{2} = 1 = \frac{\sqrt{2gh}}{v}$. This is equivalent to stating that the numerator is equal to the denominator in the argument of the inverse sine function in Equation 3.1.

$$v = \sqrt{2gh} \tag{3.2}$$

Substituting the available expression for initial velocity v_0 (Equation 2.15) into that for velocity along the flight path v (Equation 2.18) results in a new expression for v in terms of *x*, *y*, and θ_0.

$$v = \sqrt{\frac{x^2 g + g(x\tan\theta_0 - 1)^2}{2(x\tan\theta_0 - y)}} \tag{3.3}$$

At the singular point, all of the velocity is contained in the perpendicular component. As a result, Equations 3.2 and 3.3 can be set equal to one other.

$$\sqrt{2gh} = \sqrt{\frac{x^2 g + g(x\tan\theta_0 - 1)^2}{2(x\tan\theta_0 - y)}} \tag{3.4}$$

Equation 3.4 is a relationship that the (*x*,*y*) coordinates of the singular point must satisfy for a given *h* and θ_0. Simplifying results in an expression involving *x* and *y* (both unknown), θ_0 (desired value for a unique jump takeoff angle, such as 25 degrees), and *h*. The result is Equation 3.5, which has an infinite number of solutions, since there is one relationship between two variables. The next sections will discuss a solution to finding the unique singular point for given *h* and θ_0.

$$x^2 = (4\cos^2\theta_0)(h + y)(x\tan\theta_0 - y) \tag{3.5}$$

B. METHOD TO DETERMINE SINGULAR POINT

In order to locate the singular point for a given *h* and θ_0, the (*x*,*y*) solution must satisfy Equation 3.5. One of the solutions is the coordinates of the singular point. However, the singular point cannot simply be any ordered pair that satisfies this equation. It must also possess the characteristic of a true singular point at this location: that the skier flight path angle is perpendicular to the landing surface only at this point. Plotting

Equation 3.5 on the (*x*,*y*) plane results in an ellipse. This section will make a conjecture about where the singular point lies on this ellipse, and then show that the singular point of the safe landing surfaces lies at the intersection of the rotated ellipse with its semi-minor axis.

1. Characteristics of a Rotated Ellipse

The general form for any quadratic curve (circle, ellipse, hyperbola, and parabola) is: [18].

$$c_1x^2 + 2c_2xy + c_3y^2 + 2c_4x + 2c_5y + c_6 = 0 \tag{3.6}$$

After defining the variables *P* and *Q*, [18]

$$P = \begin{vmatrix} c_1 & c_2 & c_4 \\ c_2 & c_3 & c_5 \\ c_4 & c_5 & c_6 \end{vmatrix} \neq 0 \tag{3.7}$$

$$Q = \begin{vmatrix} c_1 & c_2 \\ c_2 & c_3 \end{vmatrix} > 0 \tag{3.8}$$

$$if\ \frac{P}{R} < 0 \tag{3.9}$$

This quadratic curve is an ellipse, where $R = c_1 + c_2$.

Figure 23 shows a general ellipse with its major and minor axes, with the major axis defined as the longest. The semi-major and semi-minor axes are half of each full length axis, respectively. The axes are perpendicular where they intersect at the center of the ellipse. Equation 3.10 gives a formula for the length of the semi-major axis length a_e in terms of the coefficients in Equation 3.6 [18].

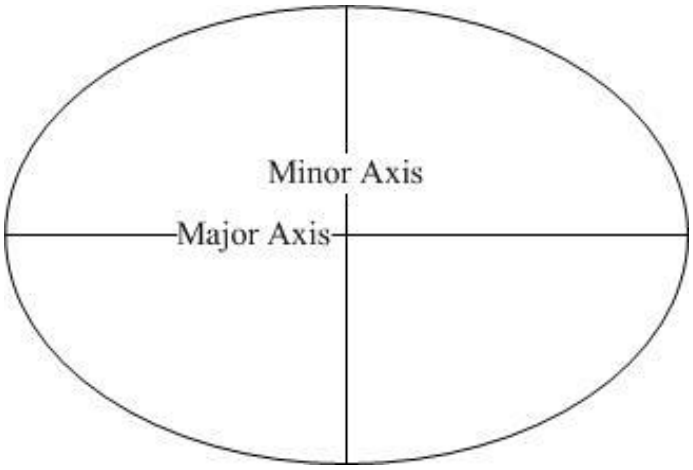

Figure 23. An ellipse showing major and minor axes

$$a_e = \sqrt{\frac{2(c_1{c_5}^2 + c_3{c_4}^2 + c_6{c_2}^2 - 2c_2c_4c_5 - c_1c_3c_6)}{({c_2}^2 - 4c_1c_3)(\sqrt{(c_1 - c_3)^2 + 4{c_2}^2} - (c_1 + c_3))}} \tag{3.10}$$

The semi-minor axis length b_e can also be found [18].

$$b_e = \sqrt{\frac{2(c_1{c_5}^2 + c_3{c_4}^2 + c_6{c_2}^2 - 2c_2c_4c_5 - c_1c_3c_6)}{({c_2}^2 - 4c_1c_3)(-\sqrt{(c_1 - c_3)^2 + 4{c_2}^2} - (c_1 + c_3))}} \tag{3.11}$$

The center of the ellipse (x_e, y_e) is given by the following expressions [18].

$$x_e = \left(\frac{c_3c_4 - c_2c_5}{{c_2}^2 - c_1c_3}\right) \tag{3.12}$$

$$y_e = \left(\frac{c_1c_5 - c_2c_4}{{c_2}^2 - c_1c_3}\right) \tag{3.13}$$

If an ellipse is rotated, the counterclockwise angle of rotation from horizontal α can be defined as either:

1. The angle through which the ellipse is rotated from the horizontal, which is the same as the angle between the x-axis and the semi-major axis, or

2. The angle between the y-axis and the semi-minor axis.

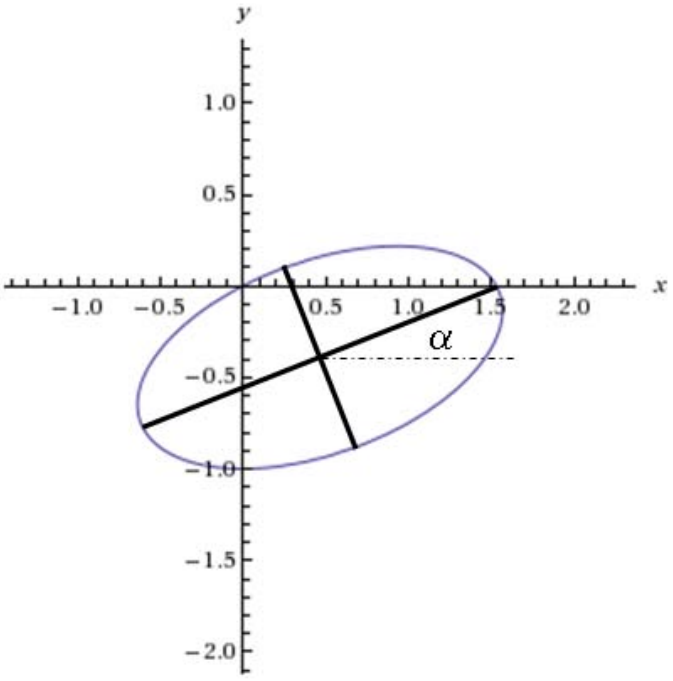

Figure 24. Ellipse rotated at angle α, showing the major axis and minor axes

This counterclockwise angle α is found through one of the following expressions [18].

$$\alpha = 0 \; for \; c_2 = 0 \; and \; c_1 < c_3 \tag{3.14}$$

$$\alpha = \frac{\pi}{2} \; for \; c_2 = 0 \; and \; c_1 > c_3 \tag{3.15}$$

$$\alpha = \frac{tan^{-1}(\frac{2c_2}{c_1 - c_3})}{2} \; for \; c_2 \neq 0 \; and \; c_1 < c_3 \tag{3.16}$$

$$\alpha = \frac{\pi}{2} + \frac{tan^{-1}(\frac{2c_2}{c_1 - c_3})}{2} \; for \; c_2 \neq 0 \; and \; c_1 > c_3 \tag{3.17}$$

2. Specific Rotated Ellipse Equation in Terms of h and θ_0

Combining like terms of Equation 3.5 reveals an equation for an ellipse rotated about the origin.

$$x^2 - 4\cos^2\theta_0 \tan\theta_0 xy + 4\cos^2\theta_0 y^2 - 4\cos^2 h\tan\theta_0 x + 4h\cos^2\theta_0 y = 0 \quad (3.18)$$

Comparing coefficients in Equation 3.18 with the general form in Equation 3.6, the values for c_1 to c_6 are easily identified.

$$c_1 = 1$$

$$c_2 = -2\cos^2\theta_0 \tan\theta_0 = -2\sin\theta_0 \cos\theta_0$$

$$c_3 = 4\cos^2\theta_0$$

$$c_4 = -2h\cos^2\theta_0 \tan\theta_0 = -2h\sin\theta_0 \cos\theta_0$$

$$c_5 = 2h\cos^2\theta_0$$

$$c_6 = 0$$

Notice that, for this rotated ellipse, c_2 is never zero for any value of $\theta_0 \neq 0$. Comparing coefficients c_1 and c_3 shows that for reasonable ski jump angles (less than 60 degrees), $c_1 < c_3$. At θ_0= 60 degrees, $c_1 = c_3$. The mostly like scenario is for any takeoff angle θ_0 less than 60 degrees, which is quite reasonable, considering that a skier must be comfortable with jumping at this steep angle. Therefore, we will not consider the cases where angles are greater than 60 degrees ($c_1 > c_3$), and thus we will only be using the third case for α (Equation 3.16).

Equation 3.18 presents a condition h and θ_0 that the singular point must satisfy. Using the known values for the coefficients c_1 to c_6, it is possible to rewrite Equations 3.10 and 3.11 in terms of h and θ_0 only as:

$$a_e = \frac{h\sqrt{2}\cos\theta_0(2\sin\theta_0 - 1)}{(\cos^2\theta_0 - 1)(\sqrt{(1 - 8\cos^2\theta_0 + 32\cos^4\theta_0)} - 4\cos^2\theta_0 - 1)} \quad (3.19)$$

$$b_e = \frac{h\sqrt{2}\cos\theta_0(2\sin\theta_0 - 1)}{(\cos^2\theta_0 - 1)(-\sqrt{(1 - 8\cos^2\theta_0 + 32\cos^4\theta_0)} - 4\cos^2\theta_0 - 1)} \quad (3.20)$$

Similarly, the center of the ellipse, found in Equations 3.12 and 3.13 can be rewritten in terms of h and θ_0, as:

$$x_e = h \tan\theta_0 \tag{3.21}$$

$$y_e = \tan^2\theta_0 - \frac{h}{2\cos^2\theta_0} \tag{3.22}$$

3. Rotated Ellipse Analysis

The singular point ellipse changes as h and θ_0 vary. In order to plot this ellipse Equation, it is necessary to choose an angle θ_0 and a value for h (EFH). Notice that the origin (0,0) is a solution to Equation 3.18. Plotting it produces an ellipse rotated clockwise at some angle. Consider the following plots (Figures 25, 26, 27) for various reasonable values of h and θ_0.

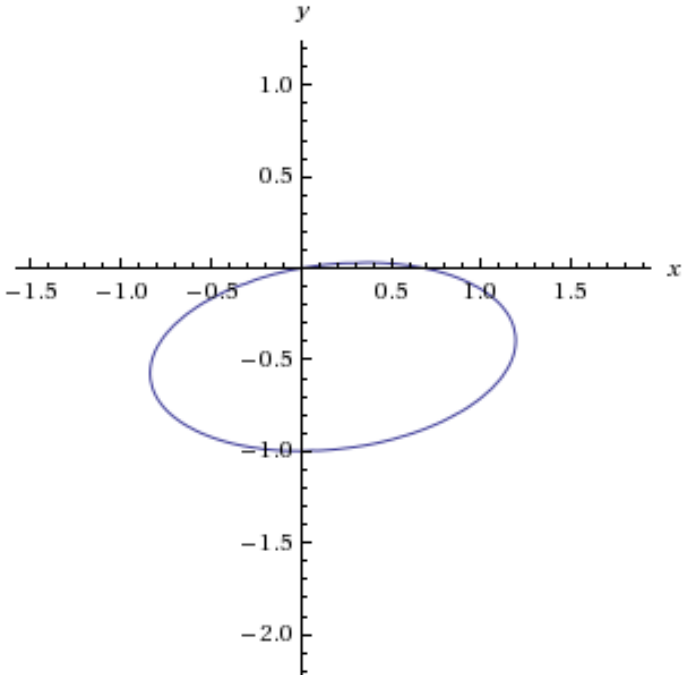

Figure 25. Ellipse of Equation 3.18 for θ_0=10° and h=1 m[1]

[1] Plots such as this one were made using a free online source, http://www.wolframalpha.com, a computational knowledge engine.

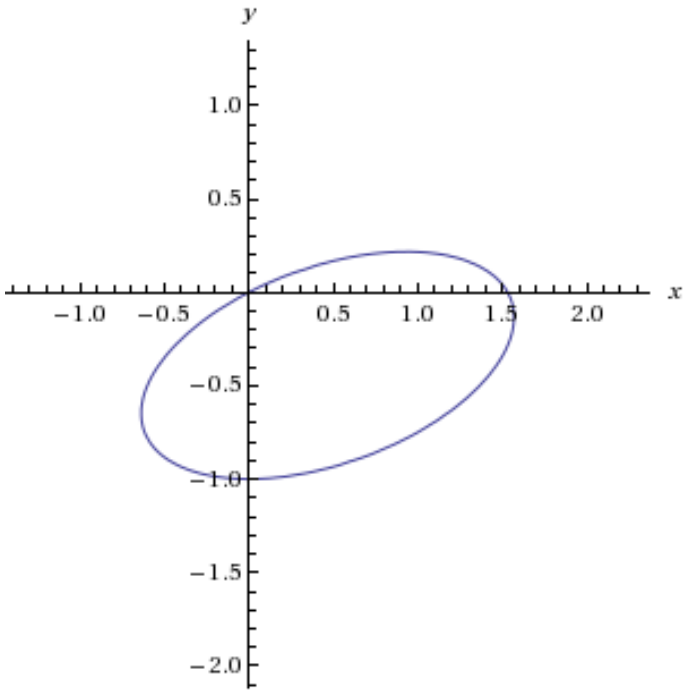

Figure 26. Ellipse of Equation 3.18 for θ_0=25° and h=1 m

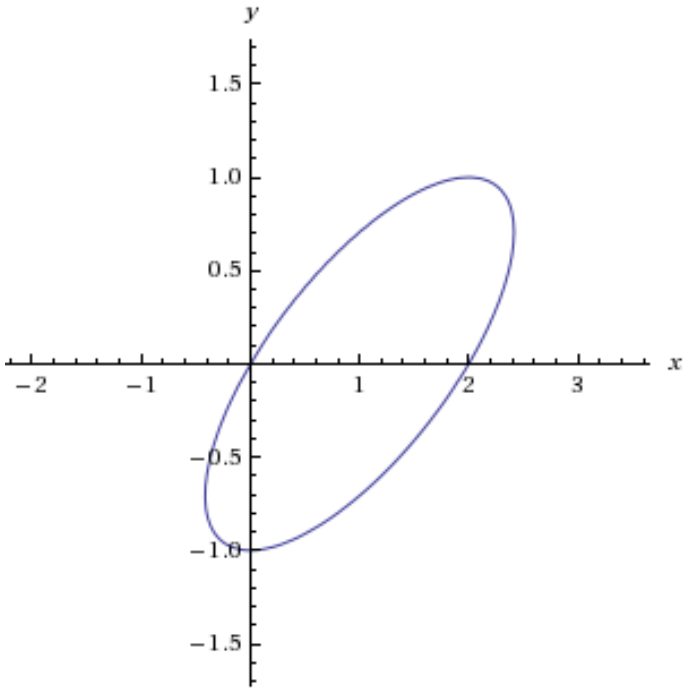

Figure 27. Ellipse of Equation 3.18 for θ_0=45° and h=1 m

Plotting five ellipses together in Figure 28 (for a constant h but different values of θ_0) verifies that the origin is common to all, while the ellipse rotation angle increases as θ_0 increases. All of these ellipses contain the origin. The unique singular point for each lies somewhere along the edge of the ellipse, and although the origin is always a solution to the ellipse equation, this is not the singular point. Rather, the origin of the ellipse plot is the origin of the jump takeoff.

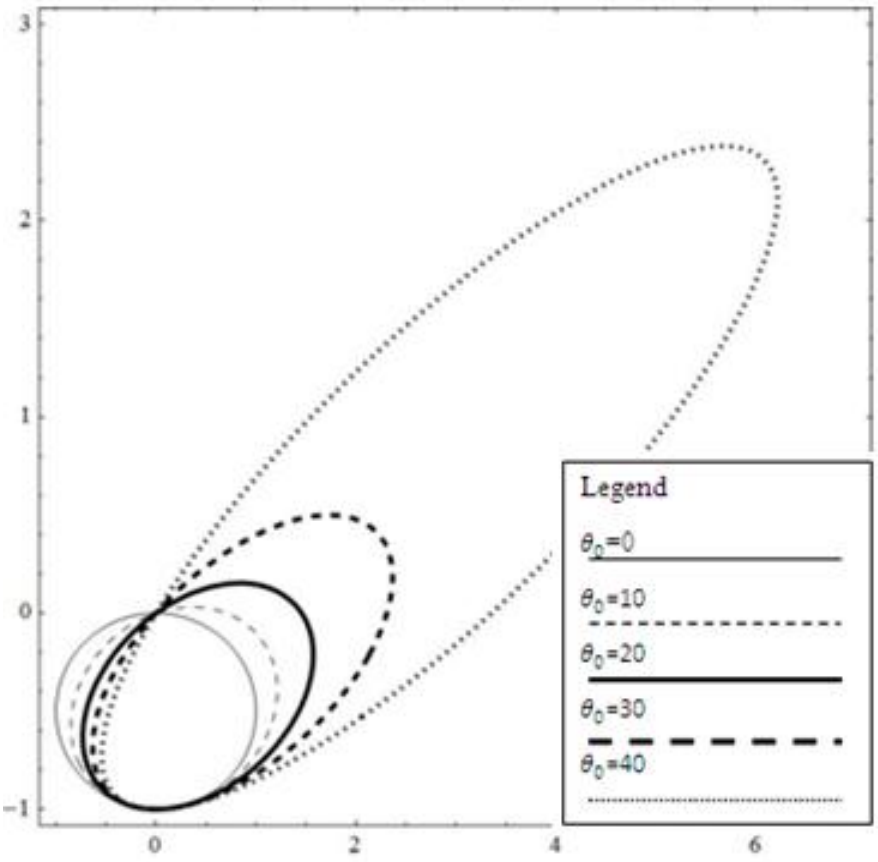

Figure 28. A family of rotated ellipses for h=1 meter, θ_0= 0°, 10°, 20°, 30°, 40°

The skier jump takeoff angle θ_0 relates to the angle of the rotated ellipse. As θ_0 increases, it is clear that α increases, but at what rate with respect to θ_0? Substituting the known values of c_1, c_2, and c_3 in for the definition of α in Equation 3.16 yields the following expression for α, in terms of the takeoff angle θ_0.

$$\alpha = \frac{tan^{-1}\left(\frac{-4\,cos\,\theta_0\,sin\,\theta_0}{1-4\,cos^2\,\theta_0}\right)}{2} \tag{3.23}$$

The value of θ_0 is the only variable that will change the value of α. Notice that gravity is not involved. Although h changes the size of the ellipse, it does not affect the angle α. Plotting Equation 3.23 for a general case α and θ_0 results in Figure 29.

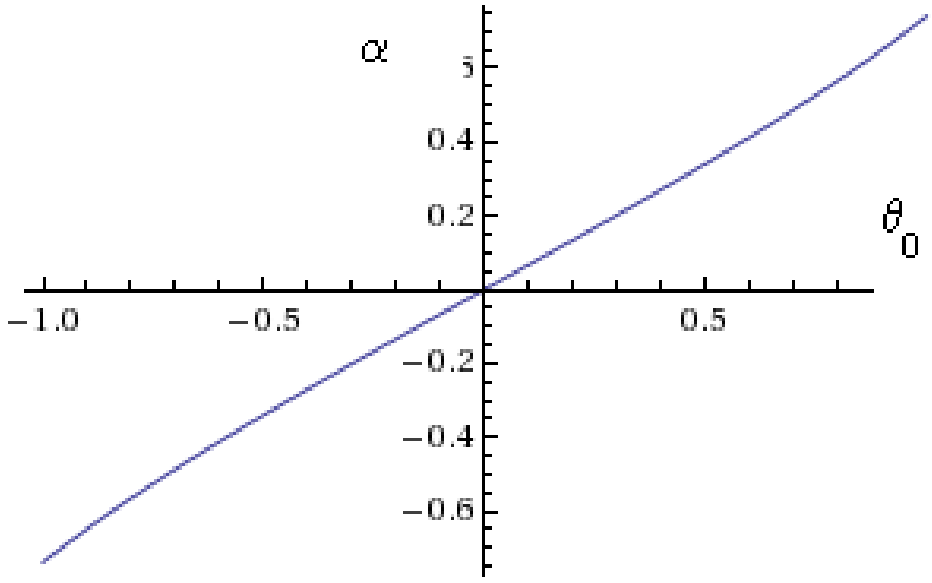

Figure 29. Singular point ellipse rotation α vs. skier takeoff angle θ_0

In this graph, θ_0 values are along the x-axis; α values are along the y-axis. Both are in radians. This arctangent curve appears to be nearly linear (although not exactly), with an approximate slope of 0.7. This plot verifies that, for a quick approximation of α, simply multiply θ_0 by 0.7. That is, $\alpha \cong 0.7\theta_0$.

4. Conjecture for Singular Point Location

Where exactly will the singular point be along the ellipse? As a skier jumps from the left to the right, the singular point must be at a location below and to the right of the origin. From inspection due to the physical location of the jumper path and safe slope intersection, it would appear near the lower right portion of the ellipse. This final section

on rotated ellipses will conjecture that the location of the singular point of a safe landing surface lies at the intersection of a rotated ellipse with its semi-minor axis, as seen in Figure 30.

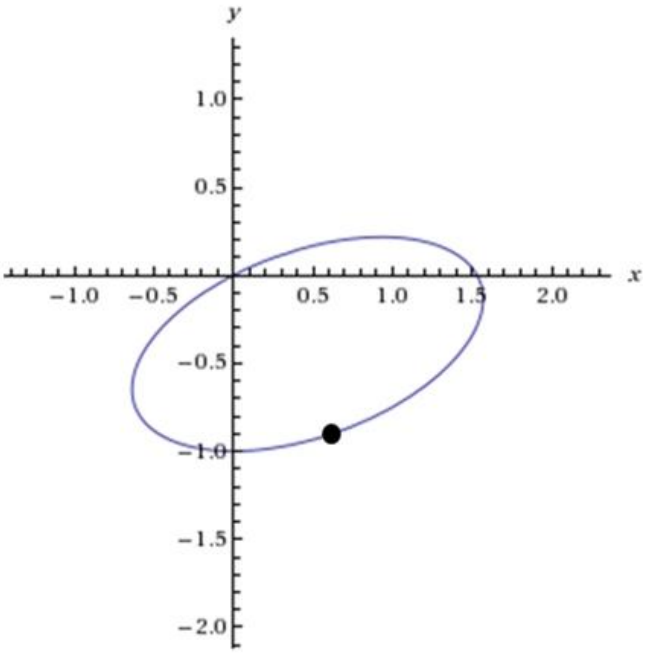

Figure 30. Singular point location on a rotated ellipse

Equation 2.15 gives the initial velocity required to reach a given (*x*,*y*) point. Using the conjecture for the location of the singular point, it is possible to solve for v_0 in terms of g, θ_0, and the singular point location (x_{sp}, y_{sp}). This new expression is Equation 3.24.

$$v_0 = \sqrt{\frac{{x_{sp}}^2 g}{2\,(x_{sp}\,tan\,\theta_0 - y_{sp})\,(cos\,\theta_0)^2}} \tag{3.24}$$

Equation 2.18 gives the velocity at any point along the skier flight path. Again, using the conjecture of the location of the singular point, it is possible to solve for v in terms of g, θ_0, and the singular point location (x_{sp}, y_{sp}). This new expression is Equation 3.25.

$$v = \sqrt{(v_0 \cos\theta_0)^2 + (v_0 \sin\theta_0 - \frac{g x_{sp}}{v_0 \cos\theta_0})^2} \qquad (3.25)$$

Table 1 compares impact velocities by varying θ_0, keeping h constant, and assuming the conjectured location of the singular point. The first velocity (line 4) is the velocity at impact using Equation 3.25. The second velocity (line 5) is the velocity at the actual singular point, which is defined to be $\sqrt{2gh}$.

	θ_0, in degrees	10	20	30	40
1	EFH (meters)	1	1	1	1
2	x_{sp} (conjectured)	0.235	0.485	0.768	1.114
3	y_{sp} (conjectured)	-0.986	-0.940	-0.847	-0.670
4	Velocity at impact (m/s) From Equation 3.25	4.428	4.428	4.428	4.428
5	Velocity at true singular point (m/s) From $v = \sqrt{2gh}$	4.428	4.428	4.428	4.428

Table 1. Test results to find velocity at singular point for constant *h* and increasing θ_0

Notice that the two velocity rows are identical for each value of θ_0. This is because if a skier lands at the conjectured singular point, it does not matter what angle he jumps from. His velocity at impact, found in Equation 3.25, is the same as the freefall velocity (line 5). These results seem to verify the conjecture that the singular point of a safe landing surface lies at the intersection of an associated rotated ellipse with its semi-minor axis. However, there is one more compelling reason why this location is correct.

One characteristic of a singular point is that the slope of the skier flight path is perpendicular to the slope of the landing surface. This relationship is seen in Equation 3.26.

$$\tan\theta = -\frac{1}{\tan\varphi} \qquad (3.26)$$

This expression can be written another way:

$$(tan\,\theta\,)(tan\,\varphi) + 1 = 0 \tag{3.27}$$

Using the known expressions for $tan\,\theta$ (Equation 2.20) and $tan\,\varphi$ (Equation 2.25), Equation 3.27 can be rewritten into Equation 3.28.

$$tan\left(tan^{-1}\left(tan\,\theta_0 - \frac{g x_{sp}}{(v_0 cos\,\theta_0)^2}\right) + sin^{-1}\left(\sqrt{\frac{2gh}{(v_0 cos\,\theta_0)^2 + (v_0 sin\,\theta_0 - \frac{g x_{sp}}{v_0 cos\,\theta_0})^2}}\right)\right)(\,tan\,\theta_0 - \frac{g x_{sp}}{(v_0 cos\,\theta_0)^2}) + 1 = 0 \tag{3.28}$$

If the conjectured singular point is correct, Equation 3.28 will be satisfied for any desired values of h, v_0, and θ_0. If Equation 3.28 can be solved with conjecture coordinates of the singular point, a check can be made using Equation 3.29, which is the same as Equation 3.18, but for a specific singular point conjecture (x_{sp}, y_{sp}). This equation should also be true for the same values of h and θ_0. Table 2 summarizes some results of this test.

$$x_{sp}{}^2 - 4\,cos^2\,\theta_0\,tan\,\theta_0 x_{sp} y_{sp} + 4\,cos^2\,\theta_0 y_{sp}{}^2 - 4\,cos^2\,h\,tan\,\theta_0\,x_{sp} + 4h\,cos^2\,\theta_0\,y_{sp} = 0 \tag{3.29}$$

	θ_0 (degrees)	10	20	30	40
1	EFH (meters)	1	1	1	1
2	x_{sp} (conjectured)	0.235	0.485	0.768	1.114
3	y_{sp} (conjectured)	-0.986	-0.940	-0.847	-0.670
4	Solution to Equation 3.28	5.5511e-016	2.2204e-016	4.6800e-008	1.1102e-016
5	Solution to Equation 3.29	9.7145e-017	8.3267e-017	5.5511e-016	-2.2204e-016

Table 2. Test results to verify singular point position for constant *h* and increasing θ_0

In Table 2, line 4 lists solutions to Equation 3.28, which verifies that the slope of the skier flight path is perpendicular to the slope of the landing surface. Line 5 takes the same coordinates of the conjectured singular point and substitutes them into Equation 3.29. The results, although not exactly zero, are so extremely small that they can be regarded as solutions to these equations. As a result, one can reason that the singular point conjectures are correct.

Figure 31 shows the locus of the singular point while increasing both θ_0 and *h*. As θ_0 increases for an individual *h*, the singular point moves up and to the right in a curved manner. For an individual θ_0 and increasing *h*, the singular point moves down and to the right linearly.

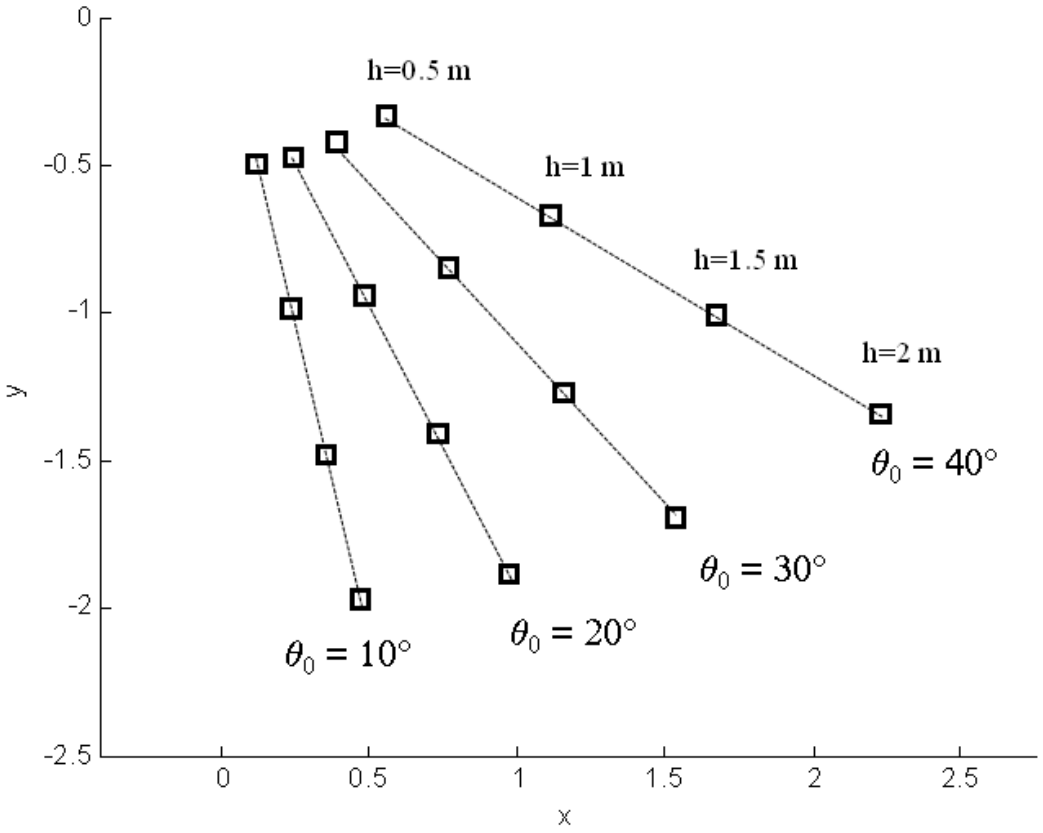

Figure 31. Singular point locations for h=0.5m, 1.0m, 1.5m, 2.0m and θ_0=10°, 20°, 30°, 40°

Figure 32 shows that keeping θ_0 constant and increasing h produces increasingly larger ellipses. These ellipses all share the origin as a common solution. The singular point gets pushes farther to the right and down as h increases. This makes physical sense, as an increased accepted fall height will produce a greater distance from the skier takeoff point (origin) to the singular point.

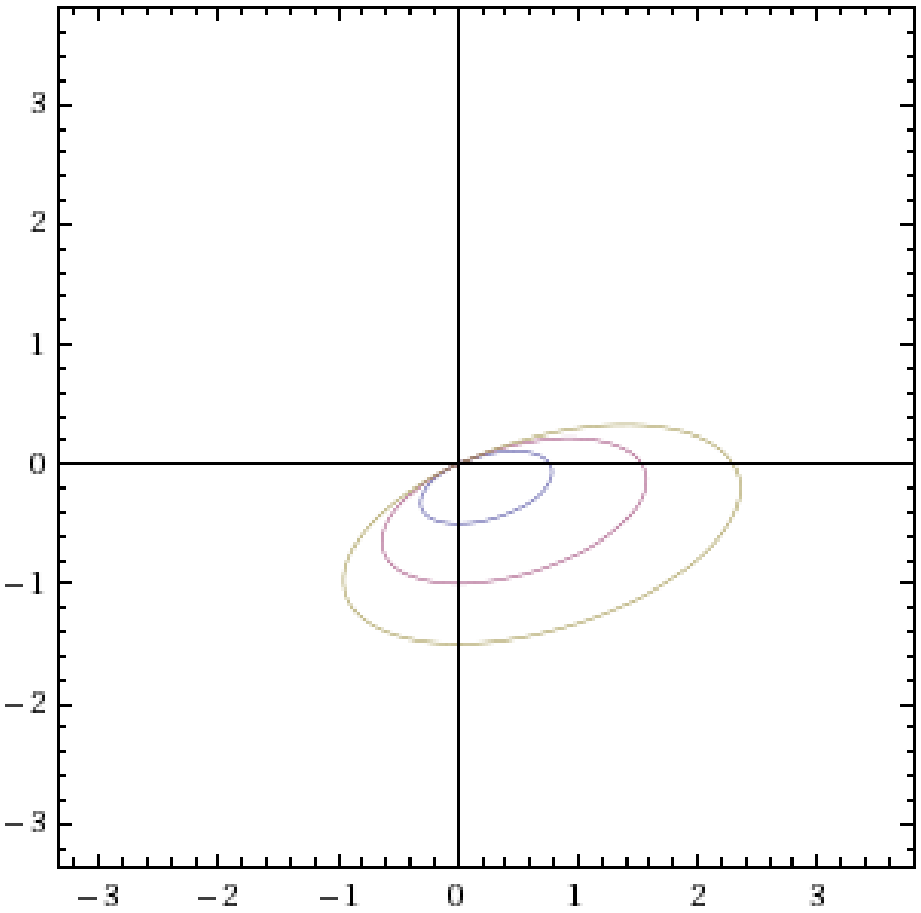

Figure 32. θ_0=25 degrees for h=0.5m (smallest ellipse), 1.0m (middle), 1.5m (largest ellipse)

C. NON LIPSCHITZ CONTINUITY OF SAFE SURFACE ODE

There are an infinite number of safe landing slope solutions, all of which begin at the singular point. Notice how, along with the uniqueness of the convergence point, (which is the singular point), the slope of the bundle of the safe landing surfaces asymptotically approach a distinct angle closer to the singular point. This angle is α, since at a specific singular point (given a value for h and θ_0), there exists an ellipse, of which the major axis is rotated at angle α.

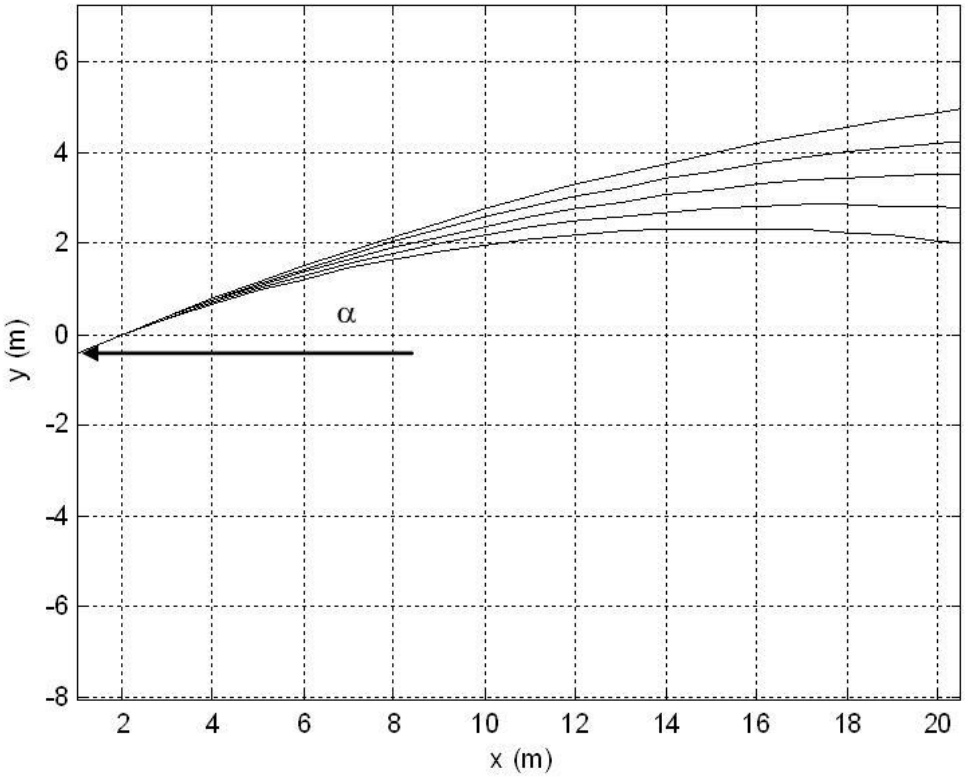

Figure 33. All safe landing slopes converge to the singular point

There are multiple solutions to the ODE (Equation 2.27) because the right hand side is not Lipschitz continuous at the singular point.

$$\frac{dy_s}{dx} = tan(tan^{-1}(\frac{2y}{x} - tan\,\theta_0) + sin^{-1}\sqrt{\frac{h}{\frac{x^2}{4\,(x\,tan\,\theta_0 - y)\,(cos\,\theta_0)^2} - y}})$$

A function *f(t,y)* satisfies a Lipschitz condition in the variable y on a set $D \subset \mathbb{R}^2$ if a constant L>0 exists with $|f(t,y_1) - f(t,y_2)| \leq L|y_1 - y_2|$, whenever (t,y_1), $(t,y_2) \in D$. The constant L is called a Lipschitz constant for f [19].

Close to the singular point, there is a lack of Lipschitz continuity. With no Lipschitz continuity, there may a lack of uniqueness in the solution. Furthermore, solving the ODE at the singular point can also lead to large errors in finding solutions. Typical error bounds for a numerical solution to an ODE have a factor $e^{L(t_2-t_1)}$ where *L*

is the Lipschitz constant and $y_1 - y_2$ is the change in the independent variable. At the singular point, L is infinite, so the error can be huge.

The inverse sine on the right hand side causes the ODE to not be Lipschitz continuous at the singular point. Figure 34 shows the function $y = \sin^{-1} x$ for $(-1 \leq x \leq 1)$. The function has a derivative at every point except at $x = 1$ and $x = -1$, as $\frac{d}{dx} sin^{-1} x = \frac{1}{\sqrt{1-x^2}} = \infty$ at these points. Since the slope is infinite at $x = 1$ and $x = -1$, the ODE becomes unsolvable when the inverse sine portion is 1.

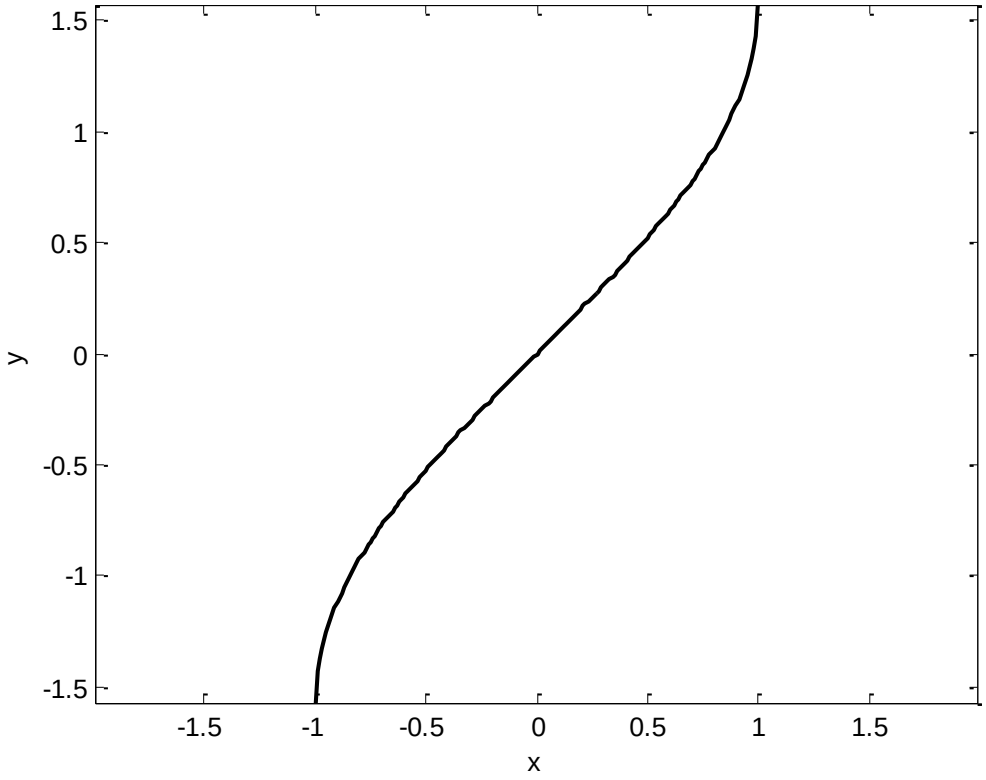

Figure 34. $y = \sin^{-1} x$ for $(-1 \leq x \leq 1)$

Moving to the left on the curve $y = \sin^{-1} x$ at $x = 1$ by an infinitesimal amount makes the ODE solvable.

IV. IN-RUN DESIGN

A. MOTIVATION FOR A TRANSITION DESIGN

The previous sections determined a procedure to develop a safe landing surface for a skier leaving a jump with a given takeoff angle. This section will outline a method to ensure a safe in-run and transition portion of the jump. The snow surface prior to the skier leaving the jump takeoff can be modeled with three distinct parts:

1. The in-run, a linear surface that a skier rides down from a given starting point.

2. The curved transition region that moves the skier from the linear surface to the linear takeoff ramp.

3. The straight takeoff ramp.

The goal for this section is to determine a good way to limit the rate of change of acceleration (jerk) upon the skier, which can be accomplished through design of the transition region, based on a unique curve known as a clothoid.

1. Problems With a Circular Transition

As a skier moves in the transition region, his velocity direction changes as he moves from downhill at angle $-\lambda$ to uphill at angle β. Figure 35 shows that a skier turns a total angle of $\lambda + \beta$ prior to jumping.

Figure 35. Total turn angle ($\lambda + \beta$) prior to jumping

In a circular transition, he will experience centripetal acceleration with magnitude $\frac{v^2}{r}$, r being the radius of the circular path. The linear in-run surface can be considered a circle with infinite radius, thereby producing no additional centripetal acceleration. The normal acceleration is not continuous at the point that a skier moves from this linear slope to a circular transition. As a result, he will feel infinite jerk, the time rate of change of acceleration. Making the radius of the transition circle larger allows for the magnitude of the normal acceleration to decrease, but even large radii (50 meters or more) still have the skier feeling infinite jerk at the two transition points. This jerk can cause balance problems for the skier in the transition and will not be advantageous to the skier's body and mind while preparing to jump and land safely.

2. Problems With a Circular Take-Off Ramp

The skier exits the transition to a takeoff ramp, which should be linear with angle β. If a ramp has any curvature to it, it may cause the skier to be propelled into an undesired back flip [11]. Figure 36 shows a terrain park jump with a curved takeoff ramp. Consider the mishaps a skier might have upon leaving the jump and flying through the air. The worst case is that he may accidentally rotate backwards, and find himself in a back flip. This can lead to him landing on his head, which is undoubtedly the worst way to land after leaving a jump. While some skiers desire to complete a back flip and land on their feet, most prefer to glide off of the jump and perform some other type of trick. Only a linear take off ramp should be considered for the jump.

Figure 36. Terrain park jump with a curved take off ramp [2]

Certain types of ski jumps purposely have a circular arc in the ski jump take off. As Figure 37 shows, aerial ski jumpers desire a back flip rotation, as this is often a standard beginning trick followed by numerous additional rotations and flips. The takeoff ramp in these jumps is specifically designed to have curvature. This requires the skier to sustain centripetal acceleration upon takeoff, and engenders backward angular velocity. However, for typical terrain park jumps found at ski areas, most skiers do not want backwards rotations after jumping.

[2] Side view photograph of a terrain park takeoff ramp. Jumps like this one exist in many terrain parks.

Figure 37. A course layout for an aerial ski jump, from [20]

B. DEVELOPMENT OF A MODEL FOR A CIRCULAR TRANSITION

1. Free Body Diagram

To find the velocity and normal acceleration at any point along the circular transition, we can find the forces acting on a particle (skier) at any point during the three distinct portions of a jump prior to takeoff: the in-run, the curved transition, and the linear takeoff ramp. During any part of the in-run, the velocity can be found through applications of Newton's second law ($F = ma$). Since acceleration is the time derivative of velocity, it is possible to solve for $\dot{v}$ numerically with MATLAB.

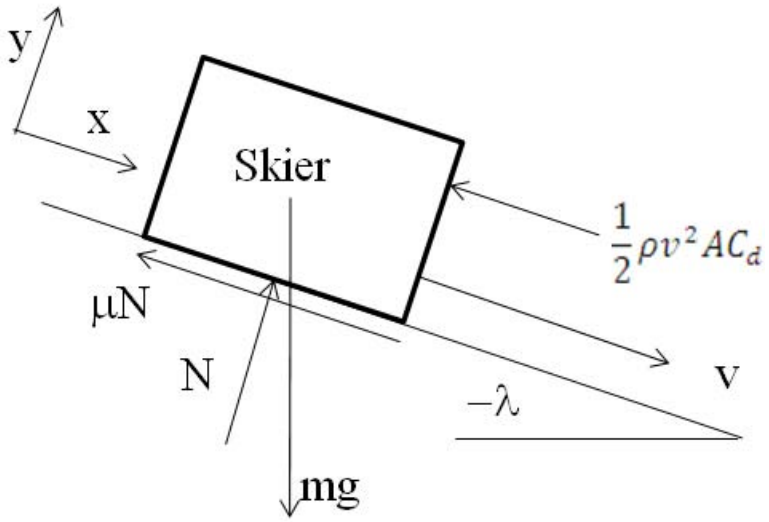

Figure 38. Free body diagram of a particle along the linear in-run

Figure 38 shows the forces acting on a skier along a linear in-run. Summing forces in the tangential direction results in an expression involving the coefficient of friction μ, normal force N, mass m, gravity g, angle λ, acceleration $\dot{v}$, and variables in the drag force: density of air ρ, cross sectional area A_{cs}, and drag coefficient C_d.

$$\sum F_T = m\dot{v} \tag{4.1}$$

$$-\mu N + mg\,sin\,\lambda - \frac{1}{2}\rho A_{cs} v^2 C_d = m\dot{v} \tag{4.2}$$

A similar expression results in summing the forces in the normal direction, which is algebraic since the normal velocity and acceleration are both zero.

$$\sum F_N = ma_N \tag{4.3}$$

$$N - mg\cos\lambda = 0 \tag{4.4}$$

Solving for N in Equation 4.4 and substituting into Equation 4.2 results in a differential equation that governs the velocity of a skier in the linear in-run.

$$\dot{v} = -\mu g\,cos\,\lambda + g\,sin\,\lambda - \frac{1}{2m}\rho A_{cs} v^2 C_d \tag{4.5}$$

Integrating Equation 4.5 with respect to time gives the velocity of the skier along the linear path (Equation 4.6), and integrating again (Equation 4.7)[3] gives the position x of the skier at time t [21].

$$v = \left(\sqrt{\frac{2m(g\sin\lambda - \mu g\cos\lambda)}{\rho A_{cs} C_d}}\right) tanh\left(t\sqrt{\frac{\rho A_{cs} C_d (g\sin\lambda - \mu g\cos\lambda)}{2m}}\right) \quad (4.6)$$

$$x = \frac{2m}{\rho A_{cs} C_d} ln\, cosh\left(t\sqrt{\frac{\rho A_{cs} C_d (g\sin\lambda - \mu g\cos\lambda)}{2m}}\right) \quad (4.7)$$

Solving for t in Equation 4.7 and substituting that in Equation 4.6 results in an expression for velocity at the end of linear path x (Equation 4.8). If $x = L_R$, this equation gives the velocity at the end of a linear in-run.

$$v = \left(\sqrt{\frac{2m(g\sin\lambda - \mu g\cos\lambda)}{\rho A_{cs} C_d}}\right) tanh\left(cosh^{-1}\left(e^{x\left(\frac{\rho A_{cs} C_d}{2m}\right)}\right)\right) \quad (4.8)$$

[3] Equation 4.7 was adapted from an equation in the article "Identification of Basketball Parameters for a Simulation Model" by H. Okubo and M. Hubbard. In the article, vertical displacement of a basketball from the floor is expressed as a similar expression to Equation 4.7. After applying the equation in the article to the linear in-run model, it was possible to find the time derivative solved for velocity (Equation 4.6).

A similar free body diagram approach is used for the circular transition (Figure 39).

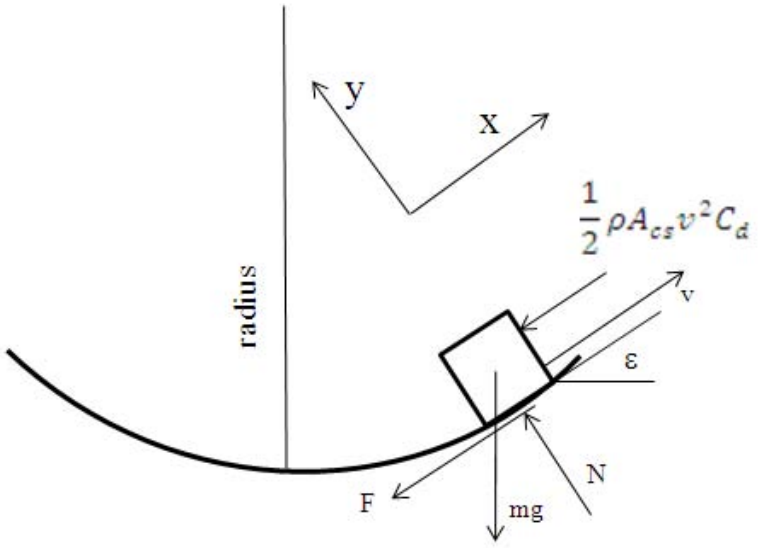

Figure 39. Free body diagram of a particle in the circular transition region

The sum of forces in the tangential direction is equal to the product of the mass and acceleration.

$$\sum F_T = m\dot{v} \tag{4.9}$$

$$-mg\ sin\,\varepsilon - \mu N - \frac{1}{2}\rho A_{cs} v^2 C_d = m\,\dot{v} \tag{4.10}$$

Equation 4.10 uses a new variable ε, which is the varying angle of the surface tangent relative to horizontal. The value of ε ranges from $-\lambda$ to β, as these are the angles of the in-run slope and take off ramp, respectively.

Similarly, the sum of forces in the normal direction is equal to the product of the mass and acceleration. In the circular transition, the centripetal acceleration is $\frac{v^2}{r}$, whereas in a linear portion, the centripetal acceleration is zero.

$$\sum F_N = m\dot{v} \tag{4.11}$$

$$-mg\cos\varepsilon + N = m\frac{v^2}{r} \tag{4.12}$$

Solving for N in Equation 4.12 and substituting it in Equation 4.10 results in Equation 4.13, the acceleration of a skier in a circular transition.

$$\dot{v} = -g\sin\varepsilon - \mu\left(\frac{v^2}{r} + g\cos\varepsilon\right) - \frac{1}{2m}\rho A_{cs} v^2 C_d \tag{4.13}$$

Because the skier path is a circle, velocity is the product of the radius and angular velocity ω.

$$v = r\omega = r\dot{\varepsilon}. \tag{4.14}$$

Solving for $\dot{\varepsilon}$ gives the rate of change of the interior and slope angle ε.

$$\dot{\varepsilon} = \frac{v}{r} \tag{4.15}$$

The final part of the transition is the take off portion. This free body diagram (Figure 40) is similar to the first linear section the in-run.

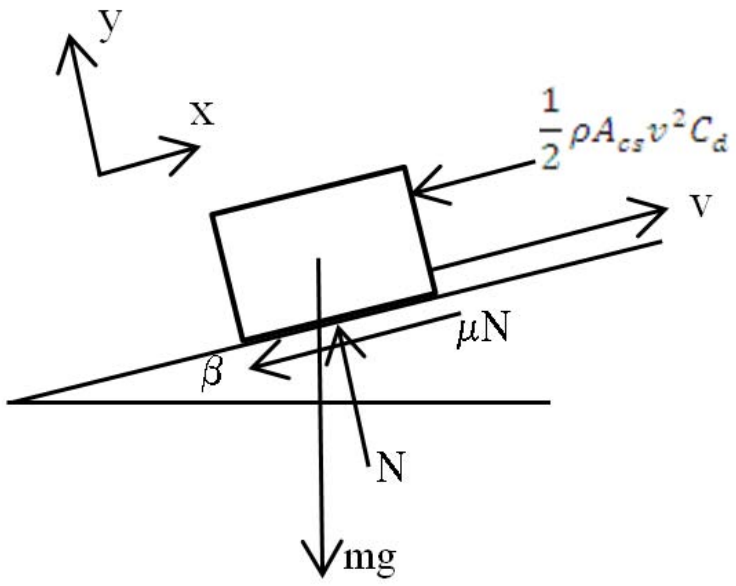

Figure 40. Free body diagram of a particle along the linear take off ramp

Summing forces in the tangential direction results in an expression involving the takeoff angle β.

$$-mg\,sin\,\beta - \mu N - \frac{1}{2}\rho A_{cs} v^2 C_d = m\,\dot{v}_t \tag{4.16}$$

Summing forces in the normal direction gives *N*.

$$N - mg\,cos\,\beta = 0 \tag{4.17}$$

Solving for N and substituting into Equation 4.16 results in Equation 4.18, an ODE which governs the velocity of a particle along the linear takeoff ramp.

$$\dot{v} = -\mu g\,cos\,\beta - g\,sin\,\beta - \frac{1}{2m}\rho A_{cs} v^2 C_d \tag{4.18}$$

Just as Equations 4.6, 4.7, and 4.8 show analytic solutions for velocity along the in-run slope, there are similar analytic solutions for velocity and position along the linear takeoff ramp. However, since the paths are not simply mirror images of one another, due to friction and drag, it is easier to integrate the ODE for the linear takeoff ramp in Table 3. Using MATLAB and one of its built-in integration functions will allow us to find the velocity at any desired point along the in-run. This velocity will then become v_0, the takeoff velocity. Table 3 presents a summary of equations that govern velocity for the linear in-run, circular transition, and linear takeoff ramp.

Jump portion	Governing Equations
Linear in-run	$\dot{v} = -\mu g \cos\lambda + g \sin\lambda - \frac{1}{2m}\rho A_{cs} v^2 C_d$ which has solution for in-run length L_R: $v = \left(\sqrt{\frac{2m(g \sin\lambda - \mu g \cos\lambda)}{\rho A_{cs} C_d}}\right) tanh\left(cosh^{-1}\left(e^{L_R\left(\frac{\rho A_{cs} C_d}{2m}\right)}\right)\right)$
Circular Transition	$\dot{v} = -g \sin\varepsilon - \mu(\frac{v^2}{r} + g \cos\varepsilon) - \frac{1}{2m}\rho A_{cs} v^2 C_d$ $\dot{\varepsilon} = \frac{v}{r}$
Linear takeoff ramp	$\dot{v} = -\mu g \cos\beta - g \sin\beta - \frac{1}{2m}\rho A_{cs} v^2 C_d$

Table 3. Differential equations used to find the velocity at any point in an in-run

2. Analysis of Circular In-Run Design

Figure 41 shows an example plot of velocity vs. time in a circular acceleration for $C_d = 0$, and for values of λ=35 degrees (incoming slope), β=10 degrees (takeoff ramp), $\mu = 0.05$ (coefficient of friction between skis and the snow), radius=7.1m, $L_R = 10$m, and a velocity upon entering the transition of 10.22 m/s (22.86 mph).

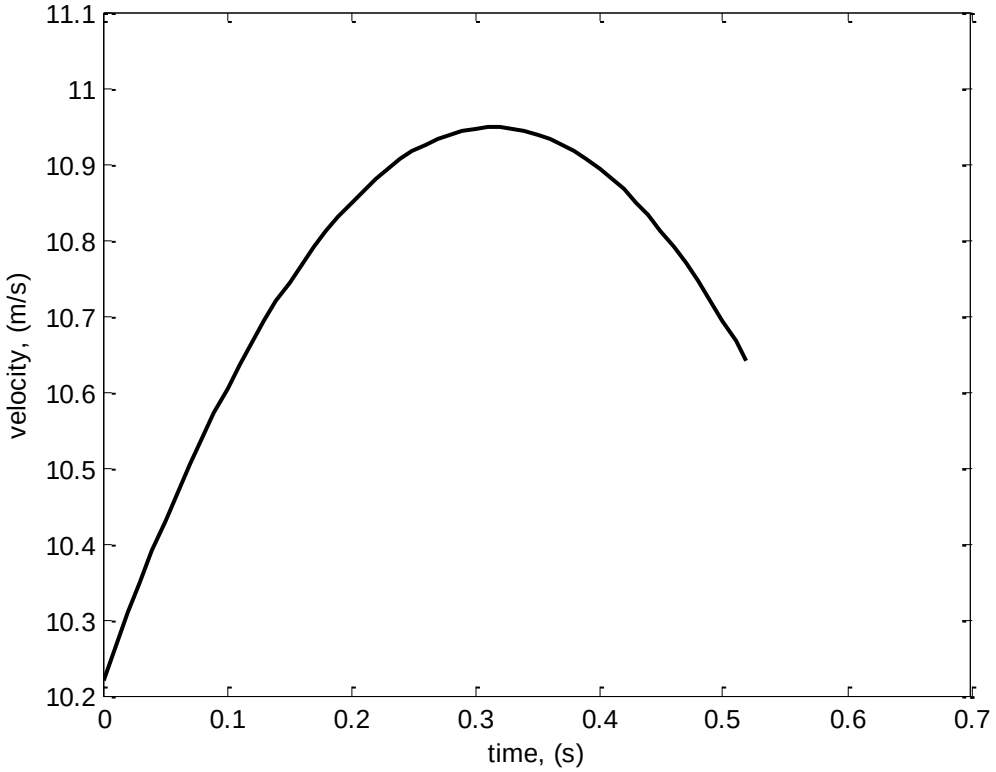

Figure 41. Velocity vs. time in a circular transition, with $\lambda = 35°$, $\beta = 10°$, μ=0.05, and $C_d = 0$

The skier increases in velocity to approximately 10.95 m/s before slowing down. In total, he will spend about 0.52 seconds in the transition. Figure 42 shows normal acceleration in g's vs. time in a circular transition.

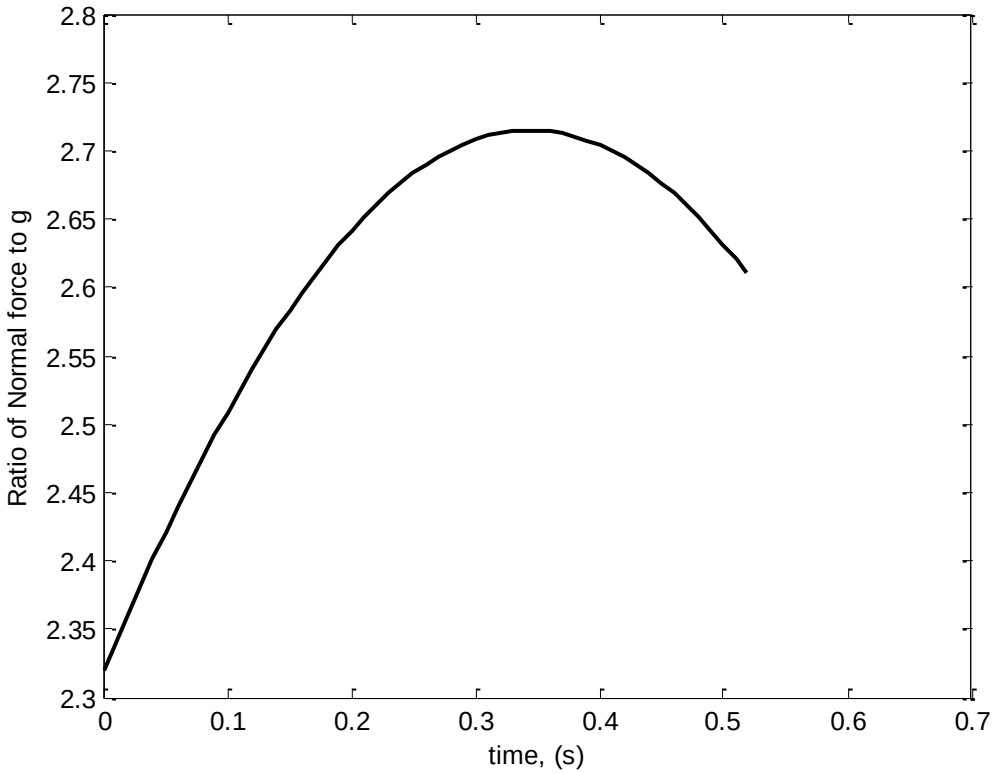

Figure 42. Ratio of normal acceleration vs. time in a circular transition, with $\lambda = 35°$, $\beta = 10°$, μ=0.05, and $C_d = 0$

In a circular transition, as a skier moves from the linear slope to the curve with constant radius, he will experience an instantaneous centripetal acceleration. This jerk occurs at the endpoints of the curve in Figure 42. At the left endpoint, where the skier enters the circular transition, he experiences an abrupt change in apparent gravitational acceleration, from $1g$ to about $2.32g$. This is similar to having someone of equal body weight suddenly jump on the skier's back and remain there to the end of the transition. At the right endpoint, the sudden shift from $2.6g$ back to $1g$ is even more profound. Keep in mind the skier must now negotiate the takeoff ramp that is just a few feet ahead of him. This is hardly an ideal situation. The next section presents a curved shape that will limit the jerk that a skier feels at the transition points, and will ultimately lead to a safer transition prior to jumping.

C. DEVELOPMENT OF A MODEL FOR A CLOTHOIDAL TRANSITION

1. The Clothoid

A clothoid is a unique design that will ease the transition from a linear slope to a curved section. It has a variable radius along its length, and it provides a smooth link between a straight line and a circular curve [22]. It has the unique property that the distance from the start of a transition s and the radius r at that point are inversely proportional to each other [23]. That is, $A^2 = rs$, where A^2 is a constant, to be discussed later. This shape at $s = 0$ initially has an infinite radius. Clothoids are frequently used in rollercoaster, highway and railway design, as they allow a car or train to travel around a loop or curve without experiencing infinite jerk [23].

Consider a straight highway that requires a necessary curve in a section. If the highway transitions suddenly from a straight section to a circular section, the vehicle will experience an infinite jerk the instant that it enters and exits the circular region [22]. A better way to allow the road to bend is through a clothoid, also known as a Cornu spiral or Euler's Spiral [24]. Similarly, if a rollercoaster car transitions from a straight to a circular section, there is a definable point where the track changes from being linear to circular with constant curvature [25]. This creates an undesirable effect on the riders, as the centripetal acceleration changes from zero to a nonzero magnitude instantly. A clothoid allows the acceleration to increase slowly while minimizing stress on the riders, yet still allows the roller coaster to complete a loop. The centripetal acceleration varies at a constant rate: from zero force at the linear ends, to the maximum force at the most curved part [25].

With two clothoids joined together at a certain point, so that they share a common radius, it is possible to design a proper transition for a ski jump. Instead of having the in run surface and takeoff ramp joined by a circular segment (which leads to infinite jerk), a clothoidal transition will have two clothoids joined together. One clothoid will start with zero curvature (infinite radius) and turn to having a minimum radius. The second clothoid begins where the first one ends, with minimum radius, and turns to having zero

curvature (infinite radius) at the straight slope of the takeoff ramp. The two clothoids will allow the skier to cope better with changing accelerations in the transition region.

A clothoid can be defined by the parametric equations [24].

$$f(t) = \int_0^t sin\frac{x^2}{2}\ dx \tag{4.19}$$

$$g(t) = \int_0^t cos\frac{x^2}{2} dx \tag{4.20}$$

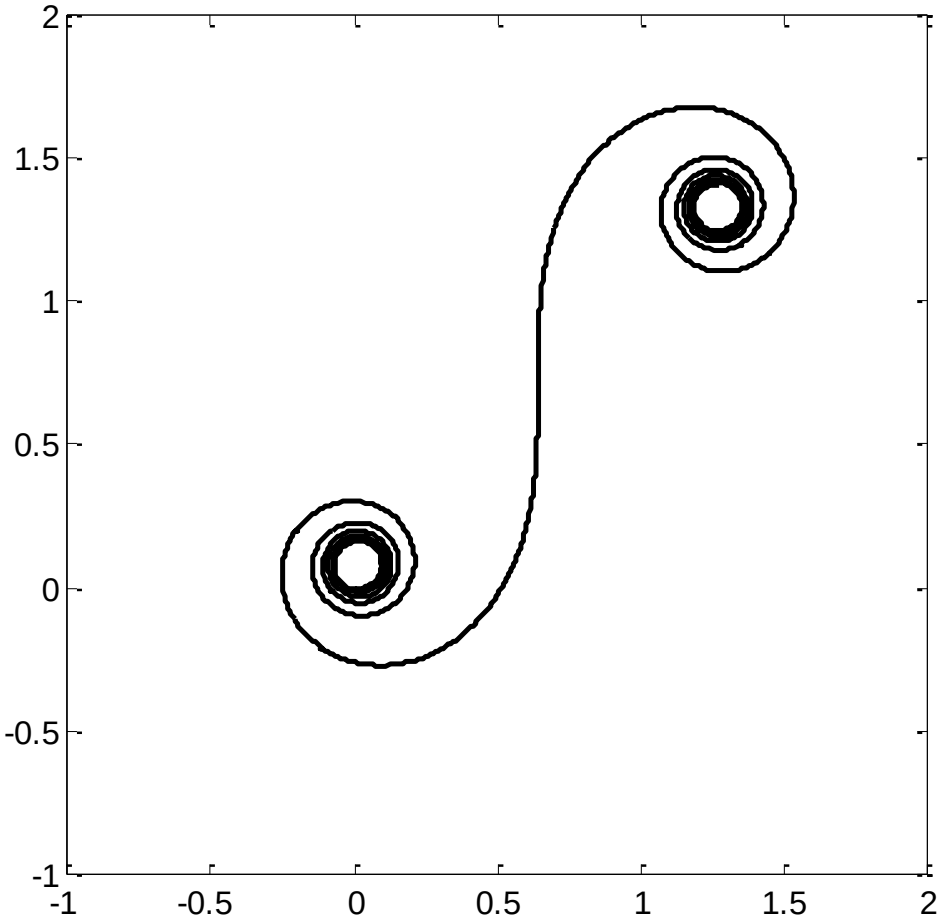

Figure 43. MATLAB plot of a clothoid (Euler's Spiral) [4]

[4] The MATLAB code used in this plot of a clothoid was taken from an open source online, found at www.mathworks.in/matlabcentral/newsreader/view_thread/170988

The clothoid possesses the characteristic that the curvature at any point is proportional to its arc length, measured from the origin. In Figure 43, notice that the spiral rapidly tightens as the arc length increases. The next sections will discuss the procedure to design a clothoid by using a tolerable gravitational acceleration and a minimum transition radius.

2. Minimum Transition Radius Limits Normal Acceleration

At sea level, objects at rest on the earth experience one unit of the acceleration of gravity g. However, humans daily experience acceleration that are both greater and less than the force of gravity. Let γ be the centripetal acceleration in g's.

The level of γ can be arbitrarily prescribed. It is the comfortable level tolerated by the human body. Although humans can endure forces of gravity beyond 6g, such as in a roller coaster [26], something closer to 1.5g is probably a much more reasonable estimate. Although some skiers can handle higher sustained gravitational acceleration, this discussion will focus on one that a child or beginner will be comfortable with.

The value of γ can be thought of as the allowable centripetal acceleration in units of g. It is possible to solve for the minimum radius r_{min} of a curve that corresponds to γ at a given velocity. Equations 4.21 to 4.23 present the steps to solve for the radius of such a curve.

$$\text{centripetal acceleration} = \frac{v^2}{r_{min}} = g\gamma \tag{4.21}$$

$$\gamma = \frac{v^2}{r_{min} g} \tag{4.22}$$

$$r_{min} = \frac{v^2}{\gamma g} \tag{4.23}$$

For any given desired γ and skier velocity at the beginning of the circular transition, it is possible to know the minimum radius required to ensure that the skier does not encounter a higher centripetal acceleration than desired.

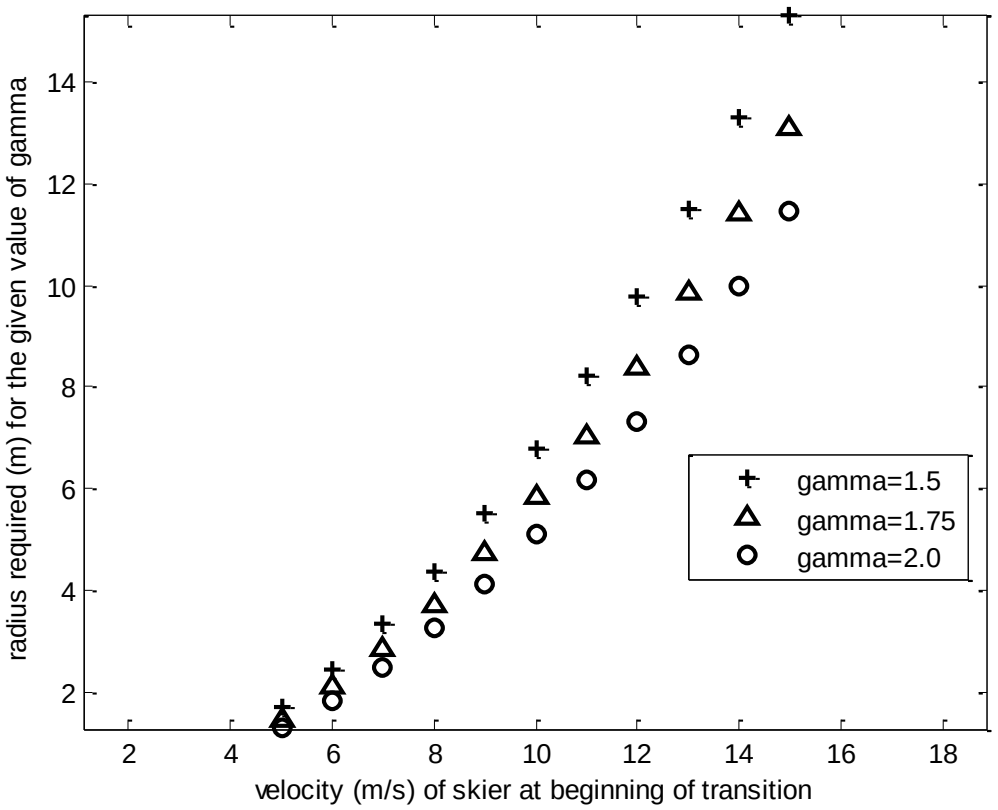

Figure 44. Circular transition radius vs. velocity for three values of centripetal acceleration γ

Figure 44 shows the minimum radius required to keep a skier feeling an additional acceleration of a desired γ level. Establishing a specific γ allows calculation of a minimum transition radius, which will then be used in designing an exact clothoid.

The arc length of this circular transition can be found by multiplying the minimum radius by the total angle $(\lambda + \beta)$ that the skier rotates in the transition.

$$s = r(\lambda + \beta) \tag{4.24}$$

Furthermore, the minimum radius required corresponds to a maximum approximation for the transition length since realistically, the sum of λ and β will unlikely be greater than 60 degrees. (60 degrees is just more than one radian = 57.29 degrees). As Equation 4.24 indicates, they are related linearly.

The circular length s_c is found by Equation 4.25.

$$s_c = \frac{v^2}{\gamma g}(\lambda + \beta) \tag{4.25}$$

The circular length gives a good approximation for a lower bound of how long the clothoid must be. Trials will show that a clothoid transition is approximately twice the length of a circular transition.

3. Development of Equations to Model a Clothoidal Transition

a. Relationship That Governs a Clothoid

The relationship that governs a clothoid can be expressed as the product of the arc distance along a clothoid and the radius of curvature at the point [23].

$$A^2 = sr \tag{4.26}$$

Where

A = Flatness of the curve; a constant

s = Distance from the start of the transition, where curvature is zero

r = Radius of curvature at distance s along the clothoidal transition

Figure 45. A family of clothoids is formed by fixing the length *s* while varying A and *r*, from [27]

Figure 45 shows a family of clothoids with varying curvature. In a clothoidal ski jump transition design, two clothoids will join in the middle of the transition at their shared point of maximum curvature and minimum radius. They are the same shape and the same length, but can be thought of as offset mirror images of one

another. One clothoid will be used to design the transition from the in run surface $-\lambda$ to the point of full maximum curvature at it's end. The second clothoid will start at the end of the first, where the radius is at a minimum, and take the skier to a desired linear jump takeoff slope β with zero curvature. As a skier enters the clothoid region from a constant slope $-\lambda$, there is a roughly linearly increasing feeling of centripetal acceleration until he reaches the end of the first clothoid.

b. Clothoid Parameters: Turning Angle, Spiral Flatness, Clothoid Length, and Angle From Horizontal

During a skier's time in a clothoidal transition, he will ultimately turn from $-\lambda$ to β, just as he would in a circular transition. Let ζ be the turning angle at any point along the clothoid. The differential change in arc length is the product of the radius and the differential change of its turning angle.

$$ds = r\, d\zeta \tag{4.27}$$

For a clothoid, the constant radius circular arc is replaced with a curve of varying radius.

$$d\zeta = \frac{ds}{r} \tag{4.28}$$

Since $A^2 = rs$, and

$$d\zeta = \frac{ds}{\frac{A^2}{s}} = \frac{s\, ds}{A^2} \tag{4.29}$$

Integrating both sides yields the turning angle in terms of the distance along the clothoid and the spiral flatness, or as the distance along the clothoid and the associated radius at that distance.

$$\zeta = \frac{s^2}{2A^2} = \frac{s}{2r} \tag{4.30}$$

With a given γ, λ, and β, it is possible to determine *A*, the spiral flatness. Since ζ must turn through a total angle $\lambda + \beta$, the turning angle of one of the (equal and symmetric) clothoids is $\frac{(\lambda+\beta)}{2}$.

$$\zeta = \frac{s^2}{2A^2} = \frac{s}{2r} = \frac{(\lambda + \beta)}{2} \tag{4.31}$$

$$\frac{s^2}{A^2} = \frac{s}{r} = (\lambda + \beta) \tag{4.32}$$

It is now possible to relate the spiral flatness *A* to the total turning angle and length of each clothoid segment L_C.

$$A^2 = \frac{{L_C}^2}{(\lambda + \beta)} \tag{4.33}$$

Since $L_C = r_{min}(\lambda + \beta)$, it is also possible to express A^2 in terms of the minimum radius.

$$A^2 = {r_{min}}^2(\lambda + \beta) \tag{4.34}$$

We now use Equation 4.33 to solve for L_c, the total length of each clothoid segment.

$${L_c}^2 = A^2(\lambda + \beta) \tag{4.35}$$

$$L_c = A\sqrt{(\lambda + \beta)} \tag{4.36}$$

The turning angle of a clothoid is the angle between the tangent to the curve at the beginning of the transition and the tangent to the curve at point along the clothoid. As shown above, this turning angle varies quadratically with the length of the clothoid. For a general case transition, where the incoming slope and jump take off ramp do not have the same angle, at the beginning of the first clothoid the turning angle will be zero. At the end of this clothoid, where *s* is at a maximum, the turning angle will be $\frac{\lambda+\beta}{2}$. The turning angle is the product of a constant *C* and the square of L_c, the maximum length of the clothoid.

$$\zeta = \frac{\lambda + \beta}{2} = C{L_c}^2 \tag{4.37}$$

After solving for *C* in Equation 4.37, the turning angle can now be found at any value of *s* along the clothoid.

$$\zeta = Cs^2 = \frac{(\lambda + \beta)}{2{L_c}^2} s^2 \tag{4.38}$$

In the first clothoid, a skier enters the transition at a point of infinite radius (zero curvature) and travels to a point of known minimum radius, at the end of the first clothoid. As he gets closer to the end of this clothoid, his rate of turning increases. At the end of the first clothoid, he enters the second clothoid. This clothoid begins at the point of minimum radius, and ends at a point of infinite radius, which is the beginning of the takeoff ramp with constant slope β. As a result, the skier feels a gradual centripetal acceleration, as opposed to in a circular transition, where there is an instant of infinite jerk.

Another meanginful characterization of a clothoid transition is based on Θ, the angle of the surface from horizontal. In the transition, at the point of intersection between the linear in-run surface and the clothoid, $\zeta = 0$ and $\Theta = -\lambda$. At the intersection of the two clothoids $\zeta = \frac{\lambda+\beta}{2}$ and $\Theta = \frac{\lambda-\beta}{2}$. At the end of the second clothoid, where the entire transition ends, the value of $\zeta = \lambda + \beta$, and the value of $\Theta = \beta$. A summary of these angles is seen in Figure 46 and Table 4.

The average rates of change of ζ and Θ are the same.

$$d\Theta = d\zeta \tag{4.39}$$

Integrating both sides yields an expression relating the turning angle and the angle from horizontal.

$$\Theta = \zeta + C \tag{4.40}$$

The value of *C* (constant of integration) is found from the initial condition of $\Theta = -\lambda$ when $\zeta = 0$. Therefore, everywhere along both clothoid segments, $\Theta = \zeta -$

λ. In general, the angle from horizontal at any point along a clothoid equals the total turning angle at any point plus the originating linear surface angle.

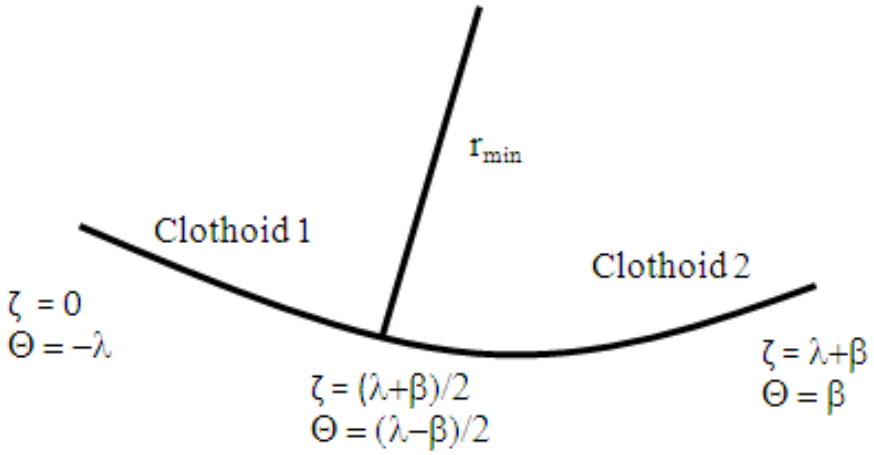

Figure 46. Relationship between turning angles and angles from horizontal

	Clothoid 1		Clothoid 2	
	Initial	Final	Initial	Final
Turning Angle ζ	0	$\frac{\lambda+\beta}{2}$	$\frac{\lambda+\beta}{2}$	$\lambda+\beta$
Angle from horizontal Θ	$-\lambda$	$\frac{\lambda-\beta}{2}$	$\frac{\lambda-\beta}{2}$	β

Table 4. Summary of turning angles and angles from horizontal in a clothoid transition

c. Free Body Diagram of a Skier in Clothoidal Transition

In a clothoidal transition region, the free body diagrams for the two linear portions (Figures 38 and 40) are the same as in a circular transition. The distinction is in the transition, which is now clothoidal. Figure 47 shows the free body diagram for a clothoidal transition.

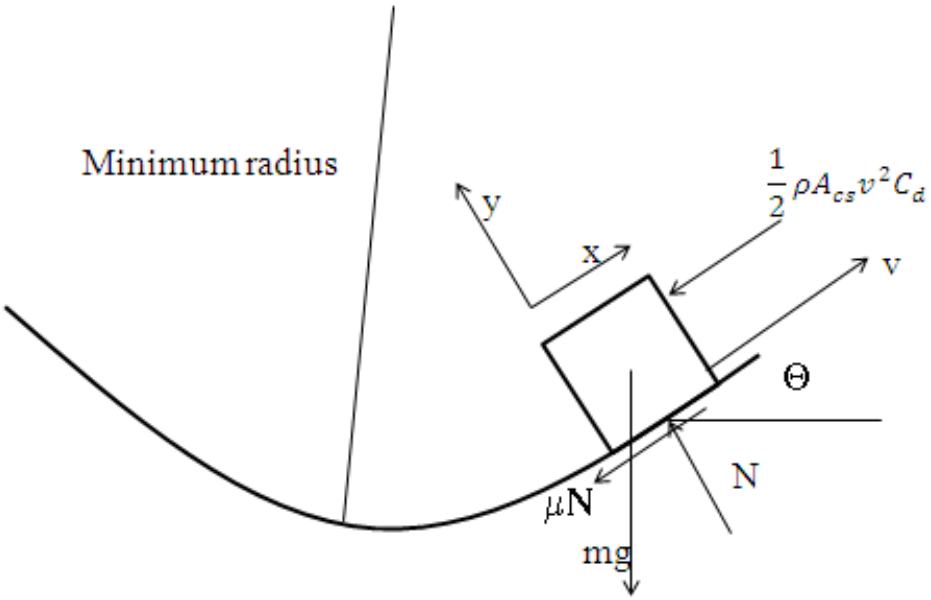

Figure 47. Free Body Diagram for a clothoidal transition

Summing the forces in the tangential direction produces an expression involving the angle from horizontal.

$$\sum F_T = m\dot{v} \tag{4.41}$$

$$-mg\,sin\,\Theta - \mu N - \frac{1}{2}\rho A_{cs} v^2 C_d = m\,\dot{v} \tag{4.42}$$

Summing forces in the normal direction produces a similar expression.

$$\sum F_N = m\dot{v} \tag{4.43}$$

$$-mg\,cos\,\Theta + N = m\frac{v^2}{r} \tag{4.44}$$

Solving for N in the Equation 4.44 and substituting it in Equation 4.42 yields the following expression:

$$\dot{v} = -g\,sin\,\Theta - \mu\left(\frac{v^2}{r} + g\,cos\,\Theta\right) - \frac{1}{2m}\rho A_{cs} v^2 C_d \tag{4.45}$$

Along the path of a clothoid, the velocity of a particle is the rate of change of its position at that point.

$$v = \frac{ds}{dt} = \dot{s} \tag{4.46}$$

d. Clothoidal Transition Velocity Equations

For the first clothoid, the formula for the velocity at any point in the clothoid can be written as seen in Equation 4.45. This can be rewritten using the turning angle ζ, angle λ, position along the clothoid *s*, spiral flatness *A*, density of air ρ, cross sectional area A_{cs}, and drag coefficient C_d.

$$\dot{v} = -g\,sin(\zeta - \lambda) - \mu(\frac{s}{A^2}v^2 + g\,cos(\zeta - \lambda)) - \frac{1}{2m}\rho A_{cs} v^2 C_d \tag{4.47}$$

And finally, using only *v*, *s*, λ, *A*, ρ, A_{cs}, and C_d.

$$\dot{v} = -g\,sin(\frac{s^2}{2A^2} - \lambda) - \mu(\frac{s}{A^2}v^2 + g\,cos(\frac{s^2}{2A^2} - \lambda)) - \frac{1}{2m}\rho A_{cs} v^2 C_d \tag{4.48}$$

For the second clothoid, if the turning angle ζ is measured from the beginning of the second clothoid, Equation 4.45 can also be rewritten using turning angle ζ, takeoff ramp angle β, position along the clothoid *s*, spiral flatness *A*, density of air ρ, cross sectional area A_{cs}, and drag coefficient C_d.

$$\dot{v} = -g\,sin(\zeta + \beta) - \mu(\frac{s}{A^2}v^2 + g\,cos(\zeta + \beta)) - \frac{1}{2m}\rho A_{cs} v^2 C_d \tag{4.49}$$

And finally, using only *v*, *s*, β, *A*, ρ, A_{cs}, and C_d.

$$\dot{v} = -g\,sin(\frac{s^2}{2A^2} + \beta) - \mu(\frac{s}{A^2}v^2 + g\,cos(\frac{s^2}{2A^2} + \beta)) - \frac{1}{2m}\rho A_{cs} v^2 C_d \tag{4.50}$$

The differential equations for the velocity (Equations 4.47 and 4.49) and the rate of change of the turning angle (Equation 4.51) make it possible to find the velocity of a skier at any point in the clothoidal transition region using an automated integration function in MATLAB.

$$d\zeta = \dot{\zeta} = \frac{s\, ds}{A^2} \tag{4.51}$$

A summary of equations that govern velocity in a clothoidal transition is seen in Table 5.

Jump portion	Governing Equations
Linear in-run	$\dot{v} = -\mu g \cos\lambda + g \sin\lambda - \frac{1}{2m}\rho A_{cs} v^2 C_d$ which has solution for in-run length L_R: $v = \left(\sqrt{\frac{2m(g \sin\lambda - \mu g \cos\lambda)}{\rho A_{cs} C_d}}\right) tanh\left(cosh^{-1}\left(e^{L_R\left(\frac{\rho A_{cs} C_d}{2m}\right)}\right)\right)$
Clothoidal Transition	$\dot{v} = -g \sin\Theta - \mu\left(\frac{v^2}{r} + g \cos\Theta\right) - \frac{1}{2m}\rho A_{cs} v^2 C_d$ $v = \frac{ds}{dt} = \dot{s}$ $\dot{\zeta} = \frac{s\,\dot{s}}{A^2}$
Linear takeoff ramp	$\dot{v} = -\mu g \cos\beta - g \sin\beta - \frac{1}{2m}\rho A_{cs} v^2 C_d$

Table 5. Summary of velocity ODEs for a clothoidal transition

e. Physical Coordinates of a Clothoid

The (*x*,*y*) coordinates of any point on the clothoid can be expressed as functions of *s*, the distance at any point along a clothoid [28]. The (*x*,*y*) coordinates when plotted, result in a clothoid that starts at the origin, beginning with zero curvature.

$$x = s - \frac{s^5}{40A^4} + \frac{s^9}{3456A^8} + \cdots \tag{4.52}$$

$$y = \frac{s^3}{6A^2} - \frac{s^7}{336A^6} + \frac{s^{11}}{42240A^{10}} + \cdots \tag{4.53}$$

Neither of the two conjoined clothoids satisfy the conditions met in Equations 4.52 and 4.53. The (*x*,*y*) coordinates must be translated, rotated, and reflected to give the true coordinates that are needed in building the correct clothoid transition. Consider the following example clothoid plots, all which use γ=1.5 and L_R=10 meters.

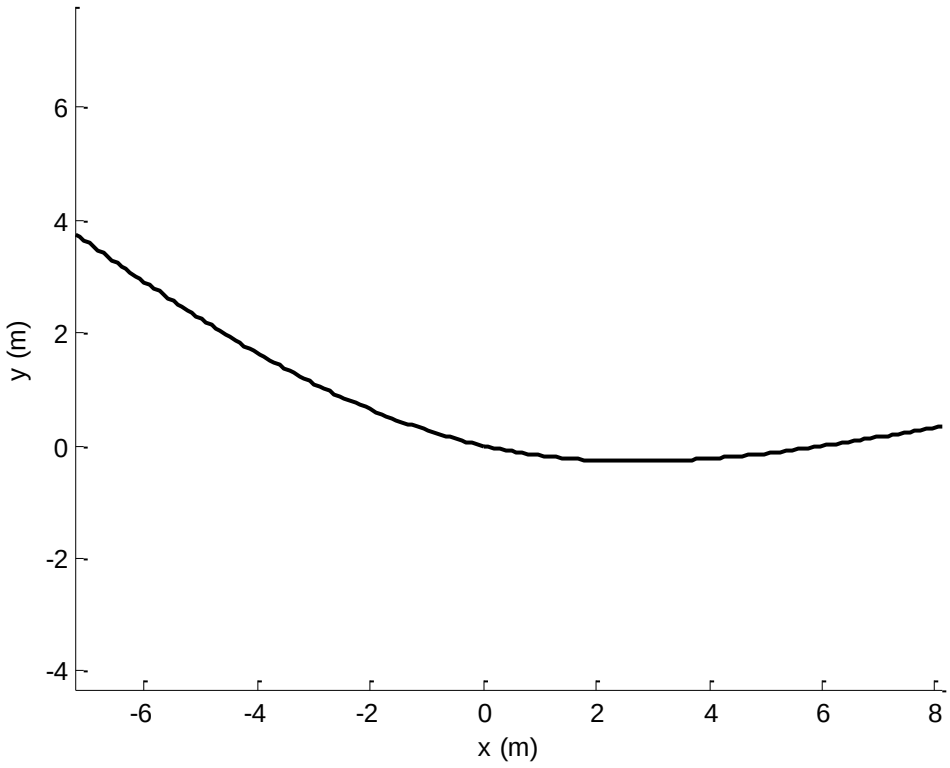

Figure 48. Complete transition composed of two clothoids, with λ = 35°, β = 10°, γ=1.5, L_R=10m, C_d=0, μ=0.05

In Figure 48, the clothoid transition begins at λ = 35° and ends at β = 10°. This plot is actually two clothoids, joined together at the point with minimum radius, which is determined by skier velocity and desired γ level. Figures 49 and 50 show other examples of clothoid transitions for different values of λ and β.

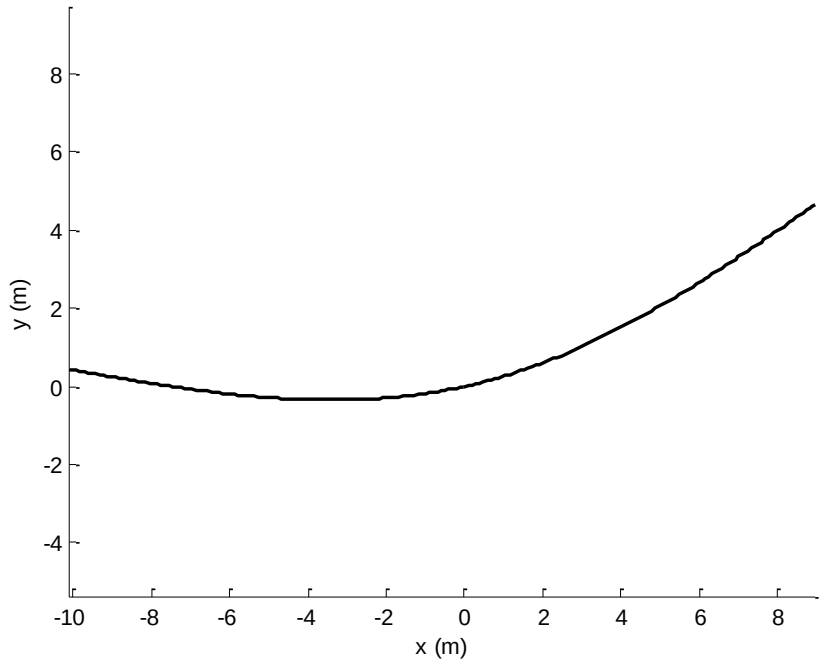

Figure 49. Complete transition composed of two clothoids, with λ = 10°, β = 35°, γ=1.5, L_R=10m, C_d=0, μ=0.05

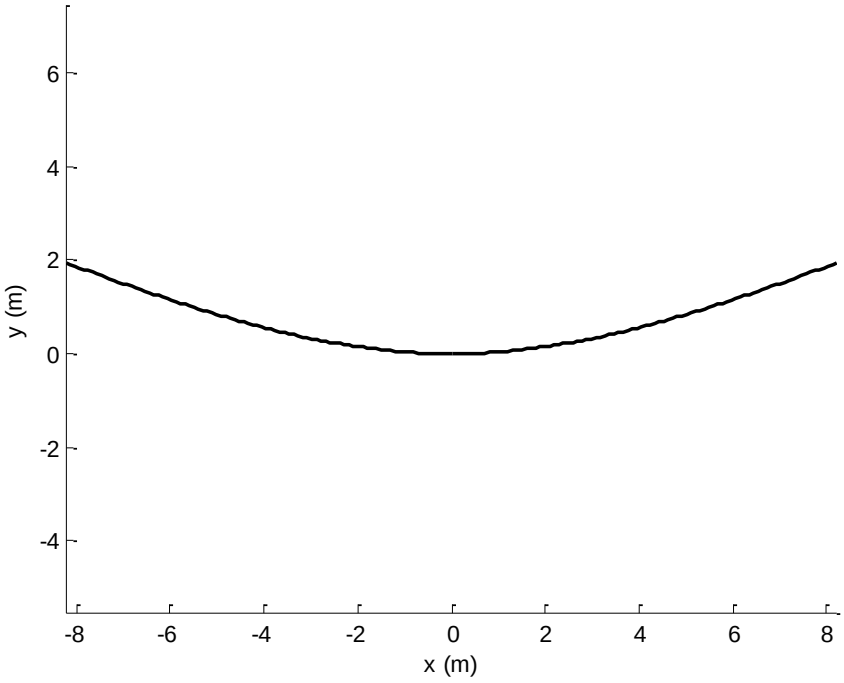

Figure 50. Complete transition composed of two clothoids, with λ = 20°, β = 20°, γ=1.5, L_R=10m, C_d=0, μ=0.05

4. Design Algorithm for Finding a Clothoidal Shape

A design algorithm for finding the needed clothoid shapes can be summarized with this algorithm:

1. Specify the degree of the incoming slope λ (in degrees) and the desired takeoff ramp slope angle β (in degrees).

2. Specify the length (in meters) of the incoming slope L_R.

3. Determine the velocity of the skier upon entering the transition,

$$v_{tr} = \left(\sqrt{\frac{2m(g\sin\lambda - \mu g\cos\lambda)}{\rho A_{cs} C_d}}\right) tanh\left(cosh^{-1}\left(e^{L_R\left(\frac{\rho A_{cs} C_d}{2m}\right)}\right)\right).$$

4. Establish γ, the lateral acceleration in g's that is can be tolerated by a skier. Realistically, the value should not be greater than 2.0.

5. Determine the minimum radius required, with $r_{min} = \frac{{v_{tr}}^2}{\gamma g}$.

6. Find *A*, the spiral flatness, (constant clothoid design parameter), from $A = r_{min}\sqrt{(\lambda + \beta)}$.

7. Find L_c, the total length of each clothoid, by $L_c = A\sqrt{(\lambda + \beta)}$.

8. Draw the generic (*x*,*y*) coordinates of a clothoid found by using a uniformly increasing *s* value and *A*.

$$x = s - \frac{s^5}{40A^4} + \frac{s^9}{3456A^8} + \cdots$$

$$y = \frac{s^3}{6A^2} - \frac{s^7}{336A^6} + \frac{s^{11}}{42240A^{10}} + \cdots$$

9. Translate and rotate both clothoid segments, and reflect only the second clothoid to calculate the (*x*,*y*) coordinates of the entire clothoidal transition region.

5. Analysis of a Clothoidal In-Run Design

Figure 51 shows that the pattern of velocity vs. time in a clothoid transition is very similar to that of a circular transition. The velocity increases to about 1.05 m/s more than in a circular transition, and the time spent in the clothoid is nearly double that of a circle.

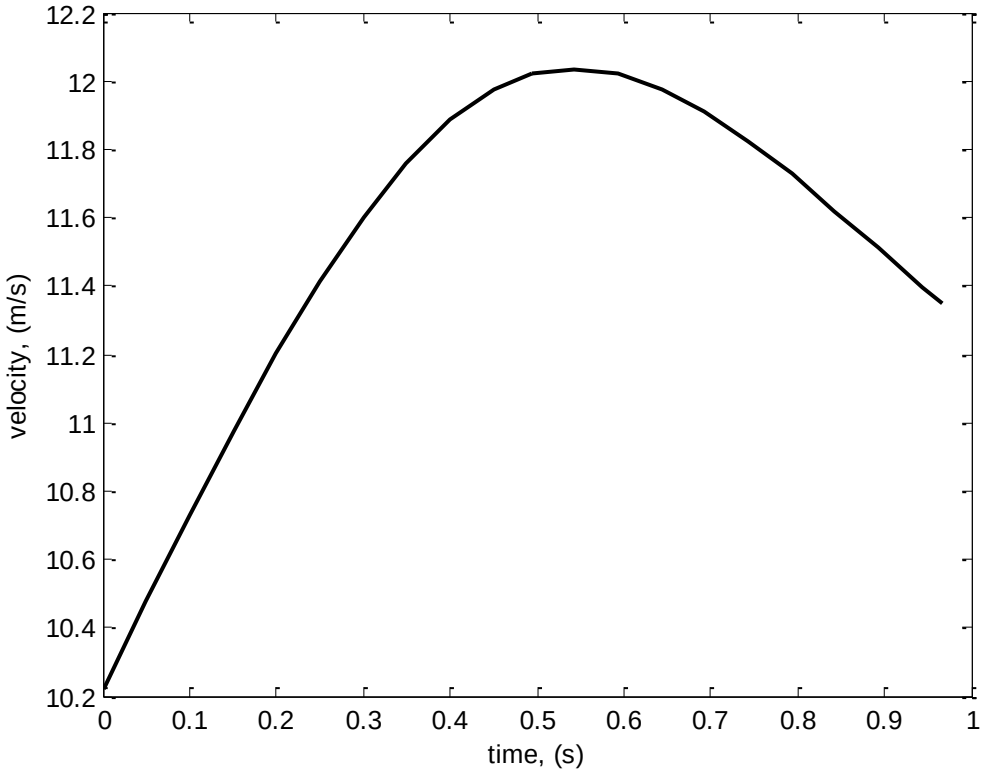

Figure 51. Velocity vs. time for a clothoidal transition for λ=35°, β=10°, μ=0.05, $\gamma = 1.5$, and $C_d = 0$

Figure 52 shows that in a clothoidal transition, the normal acceleration increases gradually and then decreases gradually after about halfway through the transition. This is because the unique shape of the clothoid takes a skier from the linear in-run (with around 1g) to a point of minimum radius, where the gravitational acceleration matches that felt in a circular transition, and then back to a linear surface (the takeoff ramp).

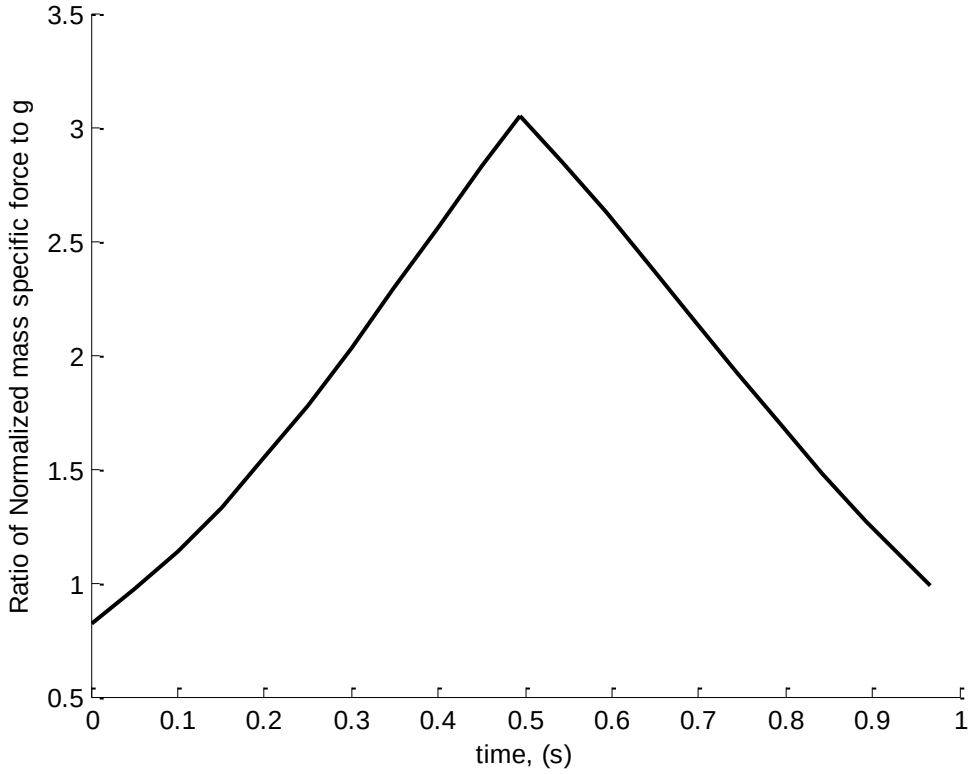

Figure 52. Ratio of normalized mass specific force to g vs. time in a clothoid transition, for $\lambda = 35°$, $\beta = 10°$, μ=0.05, $\gamma = 1.5$, and $C_d = 0$

D. ADVANTAGES OF A CLOTHOIDAL TRANSITION OVER A CIRCULAR TRANSITION

The clothoid shaped transition is an improvement over a circular transition, as the skier experiences a gradual change in apparent normal acceleration rather than one with sudden changes in acceleration and infinite jerk. Considering a specific case of defined parameters, an analysis of velocities and forces in the transitions can be conducted.

Notice how, in a clothoidal transition, the time spent in the transition is nearly double that for the circular transition. This is because the clothoid shaped transition is about twice the length of a circular shaped transition. In both plots, the skier enters the transition from the linear existing slope at the same speed, and the skier experiences an increase in velocity, then an instant where the velocity begins to decrease. The velocity will decrease throughout the remainder of the transition. Although these velocity plots

(Figures 41 and 51) are useful, a comparison of the normal forces (Figure 42 and 52) in the transitions will uncover the advantage that a clothoid transition has over a circular transition.

In a circular transition, as a skier moves from the in-run to the beginning of the circular arc, he will encounter infinite jerk (Figure 53). From -2 to 0 seconds, the skier is on the in-run. From 0 to 0.5 seconds, the skier is in the circular transition, and at 0.5 seconds, the skier begins moving along the linear takeoff ramp. Notice the infinite jerk that the skier experiences at the ends of the circular transition, represented by the vertical lines.

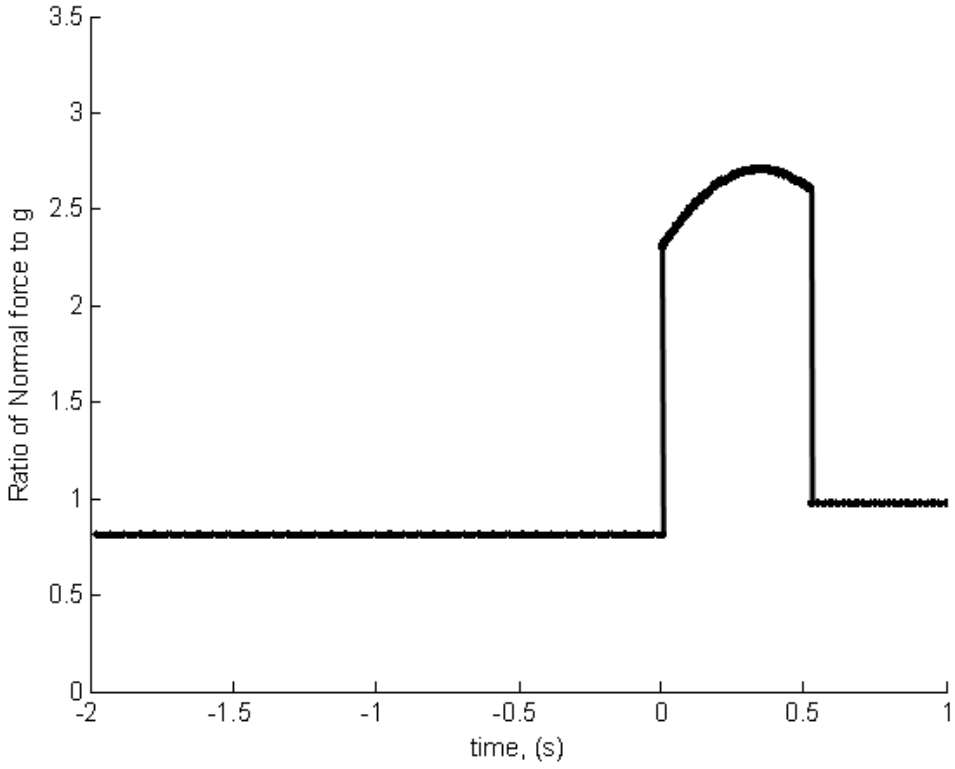

Figure 53. Ratio of normal acceleration vs. time in the in-run, circular transition, and takeoff ramp for λ=35°, β=10°, μ=0.05, $\gamma = 1.5$, and $C_d = 0$

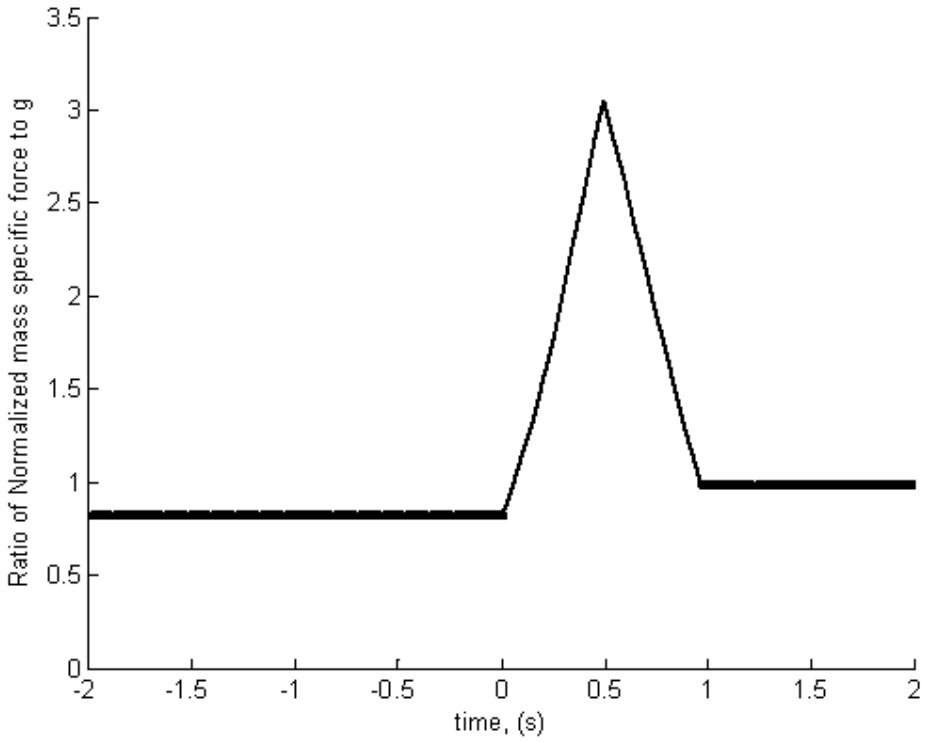

Figure 54. Ratio of normal acceleration vs. time in the in-run, clothoidal transition, and takeoff ramp for λ=35°, β=10°, μ=0.05, $\gamma = 1.5$, and $C_d = 0$

In a clothoidal transition, as a skier moves from the in-run to the beginning of the clothoidal arc, he will encounter a measureable amount of jerk. The lateral acceleration begins just under 1g, and increases to just over 3g, where it decreases again to the previous value. In Figure 54, from -2 to 0 seconds, the skier is on the in-run. From 0 to 1 second, the skier is in the transition, and at 1 second, the skier begins moving along the linear takeoff ramp.

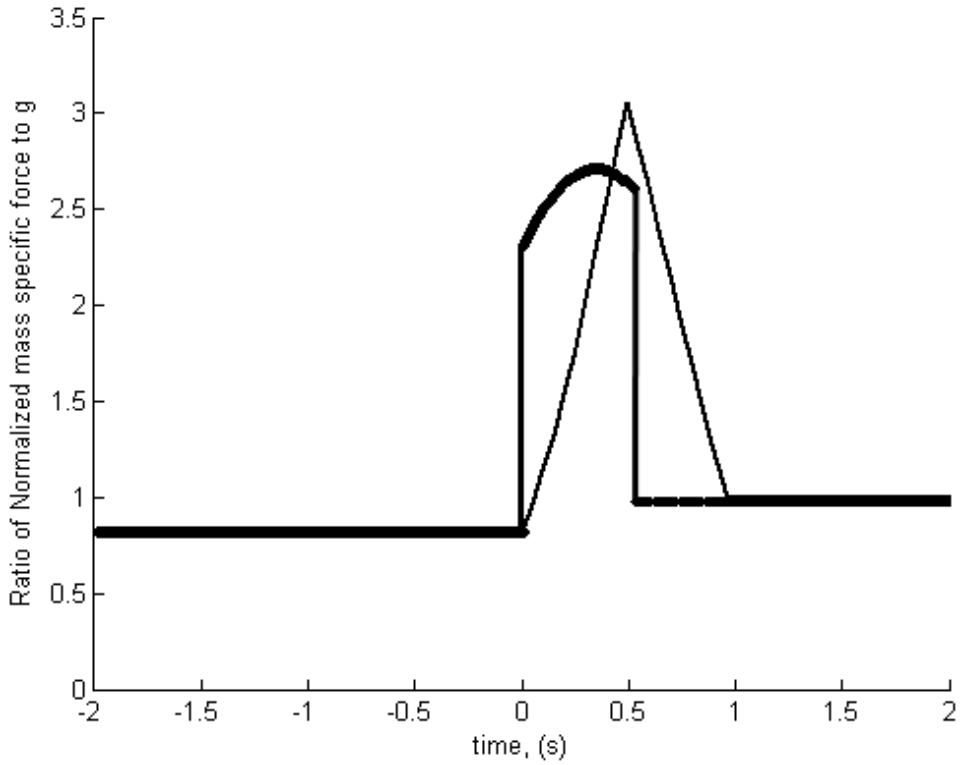

Figure 55. Comparison of the ratio of normal acceleration vs. time for circular and clothoidal transitions in the in-run, transition, and takeoff ramp for $\lambda = 35°$, $\beta = 10°$, μ=0.05, $\gamma = 1.5$, and $C_d = 0$

Figure 55 shows an overlay of Figure 53 and 54. In the circular transition, a skier encounters an instantaneous jump of approximately $2.5g$ at the beginning and the end of the transition. Conversely, in a clothoidal transition, a skier does not have any instantaneous jump at all. Rather, the normal acceleration builds to a reasonable level, and then decreases in roughly the same manner. Following each transition, (0.5 seconds for the circular and 1 second for the clothoidal) the skier begins moving along the linear takeoff ramp. Realistically, a skier will not be on a takeoff ramp for as long as 1 or 1.5 seconds, but this figure's purpose is to show how the two transition shapes allow for different methods to handling jerk along a vertical curve.

A clothoidal transition will better enable skiers to cope with the centripetal acceleration that must be endured while transitioning from a linear in-run to a takeoff ramp.

V. TERRAIN PARK JUMP MAINTENANCE

A. NEED FOR JUMP MAINTENANCE PROGRAM

In order to ensure that these jumps consistently allow the skier to jump safely, a maintenance program must be in place. If, through repeated landings in the same spot, the safe landing slope develops a sort of pothole appearance, the jump should be closed while repairs are made. The landing area should be level across the width of its surface, as all landings should have an even surface. Currently, little is known about how snowfall affects the surface of a ski jump transition, ramp, and landing surface. However, this section gives a short analysis of snowmelt and fall.

B. SNOWMELT

The amount of snow that melts can be determined by a simple expression [29].

$$M = C(T_a - T_b) \tag{5.1}$$

with

$$M = \text{Snowmelt, inches per day}$$

$$C = \text{Melt rate coefficient } (\frac{\text{in}}{°\text{F day}})$$

$$T_a = \text{Air temperature, °F}$$

$$T_b = \text{Base temperature at which snow melts, °F}$$

The melt rate factor typically varies between 0.04 and 0.08 in/°F day, and the base temperature is generally set to 32 °F. Figure 56 shows a plot of snowmelt per day vs. temperature.

This simple model is probably adequate for terrain park snowmelt analysis. It does not take any additional snowmelt induced by wind or rain, but it provides a conservative estimate of the amount of snow that melts by air temperature alone. The plot below gives snowmelt estimates for various typical values of snowmelt rate coefficients, as the ambient air temperature increases. Naturally, for snow to melt, the

temperature must be above freezing. The higher the outside temperature is, the greater that the snowmelt will be. It must be noted that at a reasonable outside temperature, such as 50 degrees, the ski area's overall snowpack will not be sustainable, and conditions will rapidly deteriorate. For a nice spring temperature of 50 degrees °F, with a high melt rate coefficient, snow will melt at about 1.5 inches per day. As the daily temperatures generally get warmer, with this fast rate, the ski area might begin to close runs and shut down winter operations.

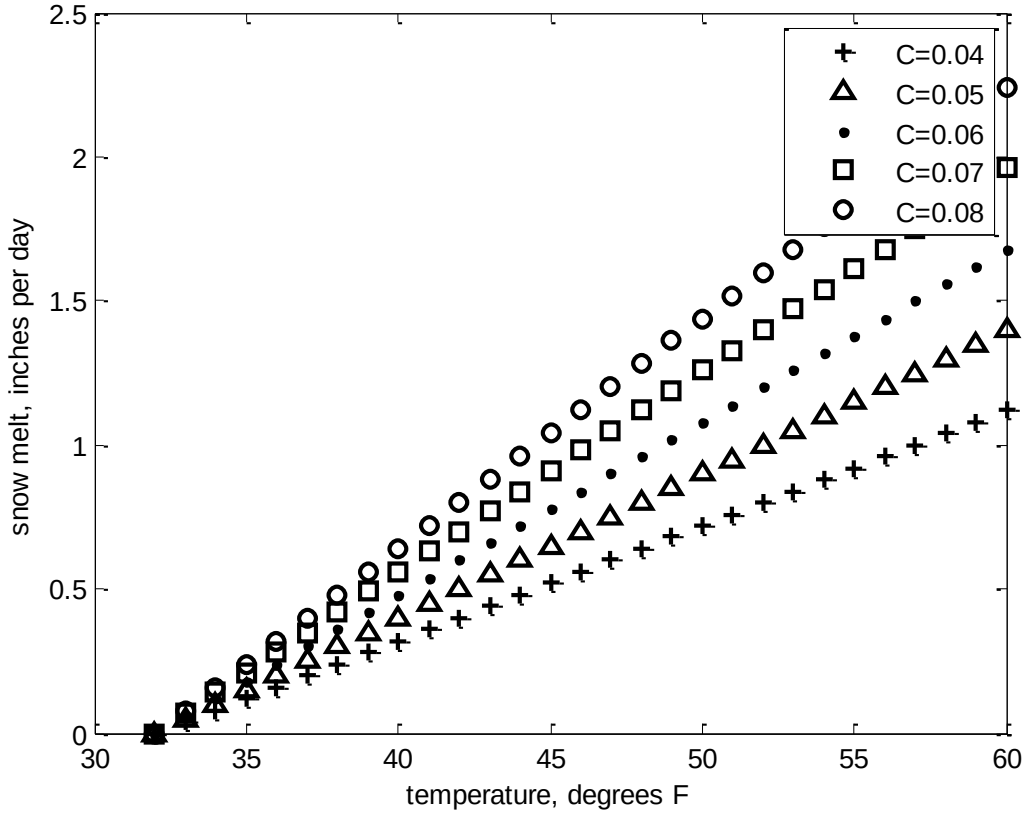

Figure 56. Snowmelt per day vs. temperature

In freezing temperatures, the coefficient of friction of skis against the snow will be around 0.05. For temperatures above freezing, the apparent coefficient of friction will increase, as the snow becomes slushy.

C. SNOWFALL

As new snow falls and builds depth on a terrain park jump, special care must be taken to ensure the jumps are maintained. A terrain park manager should ensure that the additional snow is packed down equally throughout the surface of the transition, takeoff ramp, and landing surface, so that the takeoff angle and safe slope surface remain relatively constant. Little is known about how heavy snowfall affects the surface dimensions and characteristics of a ski jump.

THIS PAGE INTENTIONALLY LEFT BLANK

VI. FINAL ALGORITHM

In determining a jump design, there is freedom in defining many parameters. First, as there is an infinite family of safe landing surfaces, there is freedom in determining how long and high the landing surface should be. Although there is a restriction on the degree of the existing linear in-run surface, there is then freedom in choosing the takeoff angle.

1. Find a region on a ski hill where one wishes to build the jump.

2. Determine the mean slope of the hill λ and establish an in-run length L_R.

3. Determine the desired maximum height and length of the entire jump at the highest velocity. These will be the (x_L, y_L) constraints.

4. Determine the desired EFH (ideally should be 0.5 to 1.5 meters)

5. Choose a reasonable takeoff angle β.

6. Run the clothoid algorithm for the chosen angle. Determine the velocity on takeoff.

7. Calculate a set of safe jump landing surfaces for the chosen takeoff angles that fit within the (x_L, y_L) limitations. These safe landing surfaces all have the same horizontal extent x_L but vary in height y_L at their end.

8. With this set of landing surfaces, determine where to best place one on the chosen region on the hill. This can be accomplished by shifting the set of safe landing surfaces so that the area between the existing slope and safe landing surface is minimized. Choose the one safe surface that minimizes this area. This will result in the least movement of snow to build the landing surface.

THIS PAGE INTENTIONALLY LEFT BLANK

LIST OF REFERENCES

[1] G.C. Louie, "History." 2010 [Online] Available: http://www.randosaigai.com/history.html [Accessed: February 24, 2010].

[2] Janne Tervonen, Helsinki University of Technology, Department of Computer Science, "The History of Cross Country Skiing in Finland" [Online] http://www.niksula.hut.fi/~jptervon/cross.html [Accessed: February 24, 2010].

[3] "The Progression of an Obsession: Ski History 4,000 B.C. – 1930," February 20, 2009. [Online]. Available: http://www.skiingthebackcountry.com/Early_Skiing_History.php [Accessed: February 25, 2010].

[4] M. Lund, "A Short History of Alpine Skiing," *Skiing Heritage*, Winter 1996, vol. 8, no. 1, [Online]. http://www.skiinghistory.org/History.html [Accessed: February 25, 2010].

[5] "Ski Jumping," April 12, 2010. [Online]. Available: http://en.wikipedia.org/wiki/Ski_jumping [Accessed: February 15, 2010].

[6] "Freestyle Skiing," April 12, 2010. [Online]. Available: http://en.wikipedia.org/wiki/Freestyle_skiing [Accessed: February 15, 2010].

[7] "Goode," *Goode Ski Technologies*, April 12, 2010. [Online]. Available: http://www.goode.com/images/ericsite.gif [Accessed: March 9, 2010].

[8] "Teton Gravity Research," April 12, 2010. [Online]. Available: http://www.tetongravity.com/photos/Seth-Morrisonin-Big-Alaska-5082651.htm [Accessed: March 23, 2010]. *Photo taken by Adam Clarke while filming Teton Gravity Research's movie Re: Session.*

[9] "Terrain Park," April 12, 2010. [Online]. Available: http://en.wikipedia.org/wiki/Terrain_park [Accessed: March 11, 2010].

[10] M. Hubbard "Safer Ski Jump Landing Surface Design Limits Normal Impact Velocity" *Journal of ASTM International*, vol. 6, no 1. Paper ID JAI101630

[11] J.A. McNeil, and J.B. McNeil, "Dynamical Analysis of Winter Terrain Park Jumps" *International Sports Engineering Association*, vol. 11, no. 3, 2009.

[12] "How to throw a rode 540," *www.skinet.com* [Online]. Available: http://www.skinet.com/skiing/how-to/how-to-ski/2008/08/how-to-throw-a-rodeo-540 [Accessed: March 11, 2010].

[13] P.C. Fosse, "Blogspot – P.C. Fosse" [Online]. Available: http://pcfosse.blogspot.com/2009/06/fonna-shoot-09.html [Accessed: April 12, 2010].

[14] H. Seino, S. Kawaguchi, M. Sekine, T. Murakami, and T. Yamashita, "Traumatic Paraplegia in Snowboarders," *Spine*, vol. 26, no. 11, 2001, pp. 1294—1297 [Online]. Available: http://www.biomedsearch.com/nih/Traumatic-paraplegia-in-snowboarders/11389402.html [Accessed: April 7, 2010].

[15] "Newton's Second Law," April 16, 2010 [Online]. Available: http://en.wikipedia.org/wiki/Newton%27s_second_law#Newton.27s_second_law [Accessed: March 2, 2010].

[16] "Impulse" March 25, 2010 [Online]. Available: http://en.wikipedia.org/wiki/Impulse_(physics) [Accessed: March 2, 2010].

[17] E. Harley, I. Scher, J. Shealy, and L. Stepan, "Jumper Kinematics on Terrain Park Jumps: Relationship Between Speed and Distance Traveled," Journal of *ASTM International*, vol. not available, p. 2, 2002.

[18] Wolfram Mathworld, April 2010, "Ellipse" [Online]. Available: http://mathworld.wolfram.com/Ellipse.html [Accessed: November 19, 2010].

[19] R. Burden and J. Faires, *Numerical Analysis*, 7th ed, Pacific Grove, CA: Brooks/Cole, 2001, Section 5.1, "The Elementary Theory of Initial-Value Problems," p. 251.

[20] "Aerial Freestyle Skiing-It's a Sport too, you know." [Online]. Available: http://www.everyjoe.com/articles/aerial-freestyle-skiing-its-a-sport-too-you-know-92/ [Accessed: March 11, 2010].

[21] M. Hubbard and H. Okubo, "Identification of Basketball Parameters for a Simulation Model" *8th Conference of the International Sports Engineering Association (ISEA)*, 2009.

[22] "Clothoid," [Online]. Available: http://en.wikipedia.org/wiki/Clothoid [Accessed: April 14, 2010].

[23] DHV Environment and Transportation, *Sustainable Safe Road Design*, World Bank and the Dutch Ministry of Transport, Public Works and Water Management, September 2005, version 5, p. 72 [Online] http://www.irfnet.ch/files-upload/knowledges/designsaferoads6.pdf [Accessed: December 22, 2010]

[24] R. Seng and M. Severida, "The Clothoid," *College of the Redwoods: Mathematics, Science, and Engineering Division*. December 9, 2007. [Online]. Available: http://online.redwoods.cc.ca.us/instruct/darnold/CalcProj/Fall07/MollyRyan/Paper.pdf [Accessed December 22, 2010].

[25] A.M. Pendrill, "Rollercoaster Loop Shapes," *Physics Education*, vol.40, no. 6, November 2005, [Online]. Available: http://physics.gu.se/LISEBERG/eng/loop_pe.html [Accessed: April 14, 2010].

[26] "G-Force," [Online]. 13 April 2010, Available: http://en.wikipedia.org/wiki/G-force [Accessed: February 1, 2010].

[27] J. McCrae and K. Singh, "Sketching Piecewise Clothoid Curves," Dynamics Group Project, University of Toronto, Canada. The Eurographics Association, (2008). [Online] http://www.dgp.toronto.edu/~karan/papers/sbim2008mccrae.pdf [Accessed: December 22, 2010].

[28] J.H. Banks, "Chapter 4: Geometric Design," in *Introduction to Transportation Engineering*, Second Edition. McGraw Hill, 2002, [Online] http://www.mhhe.com/engcs/civil/banks/graphics/chap4.pdf [Accessed: December 22, 2010].

[29] US Army Corps of Engineers, *Engineering and Design - Runoff from Snowmelt.* Publication Number: EM 1110-2-1406, Washington, D.C., March 31, 1998. Chapter 6 – Snowmelt, [Online] http://140.194.76.129/publications/eng-manuals/em1110-2-1406/c-6.pdf [Accessed: February 10, 2010].

THIS PAGE INTENTIONALLY LEFT BLANK

APPENDIX. RELEVANT MATLAB CODES

The MATLAB Codes presented in this section are actual codes used to produce the results in this thesis.

A. SAFE LANDING SURFACE CODES

1. Impact Events

```
%----------------   Function events -----------------------
function [value, isterminal, direction] = impactevents(t,y)
global xs ys dysdxs
% There are two events: to stop integrating
% 1.  When the skier hits the slope, stop integrating
% 2.  When the slope of the jumper path = slope of landing slope
%     When the jumper is at the max air height
% slope of jumper path=slope of landing surface = max height
format long
%states z =[ x vx y vy] These are the states required for ODE45
%if t> 0.05
xtraj=y(1); % distance in the x direction
vxtraj=y(2);    % velocity in the x direction
ytraj=y(3);   % distance in the y direction
vytraj=y(4);    % velocity in the y direction
ty=[t y'];      % establish a vector
    yslope=spline(xs,ys,xtraj);
    value(1) = ytraj-yslope;   % path height above surface
                             % jumper height - yslope
% when this goes to zero, the event happens.
% Looks for a time when quantity goes to zero
    isterminal(1) = 1;
            % when this happens, it tells ODE45 to stop integrating
    direction(1) = -1;
        % when this happens, program looks for value of when solution
        % crosses 0 to 1
       dydxtraj=vytraj/vxtraj;
    %dydxslope=interp1(xs,dysdxs,xtraj,'spline')
    if xtraj>xs(1)
        dydxslope=interp1(xs,dysdxs,xtraj);
    else
        dydxslope=dysdxs(1);
    end
    value(2)=dydxtraj-dydxslope; % slope of path wrt snow slope
    % = difference between trajectory derivative and slope derivative
    % helps determine vertical distance where the skier will be
    isterminal(2)=0;
    direction(2)=-1;
    results_impactevents=[xs(1) xtraj dydxtraj dydxslope value(2)];
format short
return
```

2. Jump Events

```
    %----------------   Function events -----------------------
function [value, isterminal, direction] = jumpevents(t,z)
global Xend
%states z =[ x vx y vy] These are the states required for ODE45
x = z(1);   % distance in the x direction
% FINISH EVENT
    value(1) = Xend-x;   % distance to go to path end
    isterminal(1) = 1;
    direction(1) = -1;
return

      % integrates until x equals end value that we want
      % Xend is in global
```

3. Initial Velocity

```
function  [vo v theta]=initvel(x,y)
%Initial velocity of the skier before the skier jumps to reach point
(x,y)
%Includes calculation for drag and skier pop
% once the skier gets there, what is x and y?
% iterate through while loop
format compact
global rho area mass g del_v betao sbo cbo tbo;
global Xend
    xandy_initvel=[x y];
    sbo=sin(betao);
    cbo=cos(betao);
    tbo=tan(betao); % line 11 is drag free velocity
    vo=sqrt(x^2*g/(2*cbo^2*(x*tbo-y)))  ; %velocity of jumper just
before jumping
dely=1;              %preallocates value of jumper height to slope
                    %height
                    % at value of x
                    % integrate jump flight; calculate y
                    % if not the right y, go back
                    % dely from last time and the one I want.
i=0;%allows for increment change in line 49
while abs(dely)> 1.0e-5 %runs loop until moment of impact
    i=i+1; % counter
    tspan=[0:0.1:5]; %betao is increased by delta_theta
    delta_theta=atan(del_v/vo); % takeoff angle increment after pop
    thetao=betao + delta_theta;   %total initial jumper angle with
horizontal
% jumper velocity is vj
    vj=(vo^2+del_v^2)^.5   ;        %calculates the jumper velocity
                                    %adding skier pop
                                    %component
    z0=[0  vj*cos(thetao)     0  vj*sin(thetao) ]; % state variable x,
vx, y, vy
    options = odeset('Events',@jumpevents); %look for event
```

```
    %
    Xend=x; %jumpflight has drag already in it %x is value we want,
with drag
    [t,z]=ode45(@jumpflight,tspan,z0,options); %already includes pop
    tz=[t z];%solves for vx, the x component
             %of skier velocity including drag
    xi=z(:,1); %x y vxi vyi are columns of z
    yi=z(:,3);
    vxi=z(:,2);
    vyi=z(:,4);
    xiyi=[xi yi];
    yact = z(end,3); % actual value of y is third column of z.
    vxa = z(end,2);
    vya = z(end,4);
    theta=atan(vya/vxa); % at end value
    v=sqrt(vxa^2+vya^2); %value of y at v
    dely=yact-y; % if vo is not correct, then y is not correct.
                %yact is less than y.
    if i==1 % first time through
        d_dely_dvo=x*x*g/(vo^3*cos(thetao)^2) ; % derivative
    else
        del_dely=dely-delyold;
        d_dely_dvo=-del_dely/delvo;
    end % change vo.  Divide dely we need by d_dely_dvo
    delvo=(dely/d_dely_dvo);
    vo=vo-delvo;
    delyold=dely;
end
```

4. Safe Surface

```
function yprime=safesurface(x,y) % output is yprime; input is (x,y)
% this routine implements the differential
% equation satisfied by a ski jump surface of
% constant equivalent fall height h for all speeds vo
% with a takeoff ramp of tho degrees assuming no drag
global h g betao % tho cto sto tto
% betao is ramp angle; not jump angle
xandy_safesurface=[x y];
cons=[h g betao]; % cto sto tto tho
    sbo=sin(betao);
    cbo=cos(betao);
    tbo=tan(betao);
vo=sqrt(x^2*g/(2*cbo^2*(x*tbo-y))); %initial velocity needed to impact
at x,y
                                    % with no drag or lift
                                    % same as eqn (2) on page 4
% v=total velocity.  The perpendicular component is sqrt(2gh) for a
given h
[vor v theta]=initvel(x,y); % routine to iterate
                        % init v reqd to get to x and y
% v=total velocity.  The perpendicular component is sqrt(2gh) for a
given h
xy=[x y];   % establishes a vector of x and y
% theta is the impact angle between the velocity vector and horizontal
```

```
            % same as eqn (4) on page 4
    if v < sqrt(2*g*h)
        v=sqrt(2*g*h);
    end;
    zeta=-asin(sqrt(2*g*h)/v);

% zeta is the allowed angle between slope and path at speed v
% zeta is the angle whose sine is sqrt(2gh)/v = v(perp)/v
% therefore, sin (zeta)=v(perp)/v
% if v is too small, then sqrt (2gh) is greater than v, and imaginary
phi=(theta-zeta); % gamma = theta-beta
% phi is the angle between the slope and horizontal at an impact point
yprime=tan(phi);  % surface slope relative to horizontal
% If the direction of the velocity vector is known, and
% the magnitude at impact is known, and
% the angle between v and the slope is known, then we can find out how
the
% slope should be oriented.
yprime(1);

format long;
rssur=[x y vor v theta zeta yprime] ;
format short;
```

5. Safe Jump

```
% Original code by Mont Hubbard, 1 March 2007
% Additional/changed code by Andrew Swedberg, 24 July 2009
% This program calculates the shape of a ski jump landing surface
% that results in a constant equivalent fall height at the impact point
% of skier trajectory on the jump surface as a function of takeoff
angle.
%
% The design uses a drag free approximation and the
% concept of the zenith in the design of the safe landing slope
% The slope is tested using a simulation including drag however.
%
clear
clf
hold off
global h g betao rho mass area del_v % tho cto sto tto
global ft2m m2ft deg2rad mps2mph mph2mps
global hnom
global xs ys dysdxs
%
format compact; hold off;
rad2deg=180/pi; % converts radians to degrees
ft2m=0.3048;    % converts feet to meters
m2ft=1/ft2m;    % converts meters to feet
deg2rad=pi/180;% converts degrees to radians
mps2mph=2.23693629; % converts meters/second to miles/hour (changed
from 2.237)
mph2mps=1/mps2mph;% miles per hour to meters per second conversion
g=9.80665;   % meters per second (changed from 9.81)
```

```
%
% to convert lb/ft3 to kg/m3, multiply by 16.0185
% to convert kg/m3 to lb/ft3, multiply by 0.0624
% Squaw Valley Base elevation: 6,200 ft (1,890 m)
% Squaw Valley Top elevation: 9,050 ft (2,760 m)
% Aspen Highlands Base elevation: 8,040 feet (2,450 m)
% Aspen Highlands Top elevation: 11,678 feet (3,559 m)
% Jackson Hole Base elevation: 6,311 feet (1,924 m)
% Jackson Hole Top elevation: 10,450 feet (3,190 m)
%
% From: http://www.denysschen.com/catalogue/density.asp
%
% Uncomment any rho_US desired, depending on elevation of jump
% rho_US is measured in lb/ft^3 ; see conversion

% rho_US=0.0645;  % For 5000 feet at (10C, 50F)
% rho_US=0.0658;  % For 5000 feet at (4.44C, 40F)
% rho_US=0.0668;  % For 5000 feet at (0C, 32F) freezing
% rho_US=0.0685;  % For 5000 feet at (-6.67C, 20F)
% rho_US=0.07;    % For 5000 feet at (-12.22C, 10F)
% rho_US=0.0715;  % For 5000 feet at (-17.77C, 0F)
% rho_US=0.0731;  % For 5000 feet at (-23.33C, -10F)

% rho_US=0.0621;  % For 6000 feet at (10C, 50F)
% rho_US=0.0633;  % For 6000 feet at (4.44C, 40F)
% rho_US=0.0644;  % For 6000 feet at (0C, 32F) freezing
% rho_US=0.066;   % For 6000 feet at (-6.67C, 20F)
% rho_US=0.0674;  % For 6000 feet at (-12.22C, 10F)
% rho_US=0.0688;  % For 6000 feet at (-17.77C, 0F)
% rho_US=0.0704;  % For 6000 feet at (-23.33C, -10F)
%
% rho_US=0.0598;  % For 7000 feet at (10C, 50F)
% rho_US=0.061;   % For 7000 feet at (4.44C, 40F)
% rho_US=0.062;   % For 7000 feet at (0C, 32F) freezing
% rho_US=0.0635;  % For 7000 feet at (-6.67C, 20F)
% rho_US=0.0649;  % For 7000 feet at (-12.22C, 10F)
% rho_US=0.0663;  % For 7000 feet at (-17.77C, 0F)
% rho_US=0.0678;  % For 7000 feet at (-23.33C, -10F)
%
% rho_US=0.0575;  % For 8000 feet at (10C, 50F)
% rho_US=0.0587;  % For 8000 feet at (4.44C, 40F)
rho_US=0.0597;    % For 8000 feet at (0C, 32F) freezing
% rho_US=0.0611;  % For 8000 feet at (-6.67C, 20F)
% rho_US=0.0624;  % For 8000 feet at (-12.22C, 10F)
% rho_US=0.0638;  % For 8000 feet at (-17.77C, 0F)
% rho_US=0.0652;  % For 8000 feet at (-23.33C, -10F)

% rho_US=0.0554;  % For 9000 feet at (10C, 50F)
% rho_US=0.0565;  % For 9000 feet at (4.44C, 40F)
% rho_US=0.0574;  % For 9000 feet at (0C, 32F) freezing
% rho_US=0.0588;  % For 9000 feet at (-6.67C, 20F)
% rho_US=0.0601;  % For 9000 feet at (-12.22C, 10F)
% rho_US=0.0614;  % For 9000 feet at (-17.77C, 0F)
% rho_US=0.0628;  % For 9000 feet at (-23.33C, -10F)
%
```

```
% range for rho_US:
% from 0.0554 (warm, high altitude) to 0.0731 (cold, low altitude)
%
% rho=1*1.15;  % atmospheric density Kg/m^3 from Muller (1997)
(original)
% rho=1.2 at sea level and 20 °C
%
% Density of Air = P/(R*T)
%   D = density, kg/m3
%   P = pressure, Pascals ( multiply mb by 100 to get Pascals)
%   R = gas constant , J/(kg*degK) = 287.05 for dry air
%   T = temperature, deg K = deg C + 273.15

%
rho=rho_US*16.0185; % kg/m3 % conversion
%
mass=70;     % kg from Muller(1997)...I want to have other weights
area=0.4;    % half avg drag and lift area (m^2) from Muller(1997)
             % I determined this to be 1.0 m^2 for a 6' tall skier
             % I want to vary this with time, as a skier changes
             % position during flight
%Choose a fall height and takeoff angle
del_v=1*2.25; % additional pop off of the jump
betaod=25; % Jump angle in degrees    % new name for thod
       % this will vary
betao=betaod*pi/180;% takeoff ramp angle in radians
sbo=sin(betao); % sine of beta
cbo=cos(betao); % cosine of beta
tbo=tan(betao);  % tangent of beta
h=1;  %meters
%hnom=h;      % nominal fall height to taper to
% reference frame origin is at takeoff point
% choose initial surface point at zenith of surface
%
% The next sequence finds the critical point for given parameters
a=1;
b=-2*cbo*sbo;
c=4*cbo^2;
d=-2*h*cbo*sbo;
f=2*h*cbo^2;
%
xc=(c*d-b*f)/(b^2-a*c) % center (x) of ellipse for critical point
search
yc=(a*f-b*d)/(b^2-a*c) % center (y) of ellipse for critical point
search
% rotation angle (alpha):  from x-axis to major axis
% same as from y-axis to minor axis
alpha=.5*atan((2*b)/(a-c)); % in radians
alpha_degrees=alpha*180/pi;
j= 2*((a*f^2)+(c*d^2)-(2*b*d*f));%numerator
k=(b^2-a*c)*(-sqrt(((a-c)^2)+(4*b^2))-(a+c)); % denominator
%
% L = half of semi minor axis length
L=(sqrt(j/k)); %L=(sqrt(j/k)/2)
%
```

```
critical_pt_x=xc+(L*sin(alpha))
critical_pt_y=yc-(L*cos(alpha))
%
% Choose a set of velocities
for yL=[5, 2.5, 0, -2.5, -5];
%for yL=[5, 0,-5,-10,-15];
%yL=-8.5
%for yL=[1, -1,-3.5,-7,-8.5];  % won't work for xL=40
    % 5 yL's at x=40, bring to x=10.  Overshoot with some velocity
    % higher and closer together that xL should be
    % xL=40; look at x=10; all between 2 and 3.
% purpose is to generate four safe slopes, at vo= 20,16,12,8
%
%xL=15;
xL=40; %xL=50;    % horizontal length of jump (m)
%
dx=1;% dx=.01; % spacing of slope calculation interval
x=xL:-dx:critical_pt_x+eps; % backwards integration from xL to crit.
pt.
options = odeset('MaxStep',1);
%[xsf,ysf]=ode15s(@safesurface,x,yL,options);
[xsf,ysf]=ode45(@safesurface,x,yL,options);
xysf=[xsf ysf];
xsf=flipud(xsf);  % integrate from right to left
ysf=flipud(ysf);  % backwards because integrating
% makes a difference in uses of safe surfaces later on, in impact
events
%
xs=xsf; % flipped up above
ys=ysf;
%
slopeshape=[xsf ysf] ; % calculate const fall ht surface % is this
needed?
dy=diff(ysf);
%
dysdxs=[dy(1); dy];  % note assumes dx=1 % is this even needed?
figure(1);
plot(xsf,ysf,'k','linewidth',2.0); % plot in meters
axis equal;
grid on;
xlabel( ' x (m)');
ylabel( ' y (m)');
hold on;
end
%
    % plot trajectories and verify efh
    % integrate flight equations including drag to
    % check whether safe slope
    % designed neglecting drag is still safe
heq=1;
dx=0.01;
tmax=9;
dt=tmax/50;
options = odeset('Events',@impactevents);
    for i=1:1:8;    % add pop by adding delta theta to betao
```

```
        vimph=i*5;% max speed 40 mph
        vi=vimph*mph2mps;
        delta_theta=atan(del_v/vi); % takeoff angle increment after pop
        thetao=betao + delta_theta ;  %total initial jumper angle with
horizontal
        cto=cos(thetao);
        sto=sin(thetao);
        tto=tan(thetao);
        vo=(vi^2+del_v^2)^.5;       %calculates the jumper velocity
                                    %adding skier pop
        vTO(i)=vo*mps2mph;          %vo=voV(i);
        tspan=[0:dt:tmax];
        vox=vo*cto;
        voy=vo*sto;
        ics=[0 vox 0 voy   ];

    [t,y,tE,yE,iE]=ode45(@jumpflight,tspan,ics,options);
    eventE=[tE yE iE];
    xtraj=y(:,1);
    ytraj=y(:,3);
    tflight(i)=t(end);
    %tflight(i)=tE(2);
    vximp=yE(2,2);  % impact is always the second event to occur
    vyimp=yE(2,4);
    lenimp(i)=sqrt(yE(2,1)^2+yE(2,3)^2);
    %lenimpft(i)=lenimp/ft2m;
    vimp=sqrt(vximp^2+vyimp^2); % impact velocity
    thimp=atan( yE(2,4)/yE(2,2) ); % impact angle
    tpk=tE(1);   % peak ht is always first event
    ypk=interp1(t,ytraj,tpk,'spline');
    xpk=interp1(t,xtraj,tpk,'spline');
    ysurfpk=interp1(xs,ys,xpk,'spline');
    airht(i)=ypk-ysurfpk;
    % independently calculate slope angle at impact point from xs, ys
    %dx=0.001; %meters
    yplusdy=spline(xs,ys,yE(2,1)+dx);
    dydx=(yplusdy-yE(2,3))/dx;
    slopeangledeg=atan(dydx)/deg2rad; % point of this is to calculate
    % vperp and equivalent fall ht.
    slopeR(i)=slopeangledeg;
    vperp=-vimp*sin(thimp-slopeangledeg*deg2rad);
    heq(i)=(vperp.^2)/(2*g) ; %heq is equivalent fall ht.
    %
    figure(2);
    hold on
    subplot(2,1,1);
    plot(lenimp(i),heq(i),'ko',0,0);
    xlabel('jump length (m)');
    ylabel(' equivalent fall height (m)');
    title(['For takeoff angle = ',num2str(betao*180/pi),'deg and
nominal fall height =', num2str(hnom),'m']);
    hold off
    %
    hold on
    subplot(2,1,2);
```

```
    plot(lenimp(i),-slopeangledeg,'ko');
    xlabel('jump length (m)');
    ylabel(' landing slope angle (deg)');
    hold off

    figure(3);
    hold on
    subplot(2,1,1);
    plot(lenimp(i),tflight(i),'ko',0,0);
    xlabel('jump length (m)');
    ylabel(' flight time (s)');
    title(['For takeoff angle = ',num2str(betao*180/pi),'deg and
nominal fall height =', num2str(hnom),'m']);
    hold off
    hold on
    subplot(2,1,2);

    plot(lenimp(i),airht(i),'ko');
    xlabel('jump length (m)');
    ylabel(' jump air height (m)');
    hold off

   figure (1);
   subplot(1,1,1);
    hold on
    axis equal
    plot(xtraj,ytraj,'k');
    xlabel(' x (m)')
    ylabel(' y (m)')
    title(['For takeoff angle = ',num2str(betao*180/pi),'deg and
nominal fall height =', num2str(hnom),'1m'])
    hold off

    end

    takeoff_angle_______nominal_fallht=[betao*rad2deg h];
    results=[vTO' airht' heq' lenimp' slopeR' tflight'];

    [mm,nnn]=size(results);
   disp(sprintf('For takeoff angle = %-5.1f(deg) and nominal fall
height = %-4.1f(m)', betao*180/pi,hnom))
   disp(sprintf('vTO(mph)  airht(m)  heq(m) lenimp(m) slope(deg)
tflight(s)  ' ))
   for i=1:mm
       disp(sprintf('%-10.4f',results(i,:)))
   end
   delxL=xL-lenimp;
   delhimp=h-heq;
```

B. SINGULAR POINT LOCATION CODE

```
format compact;
rad2deg=180/pi; % converts radians to degrees
```

```
ft2m=0.3048;    % converts feet to meters
m2ft=1/ft2m;    % converts meters to feet
deg2rad=pi/180;% converts degrees to radians
mps2mph=2.23693629; % converts meters/second to miles/hour (changed
from 2.237)
mph2mps=1/mps2mph;% miles per hour to meters per second conversion
g=9.80665;   % meters per second (changed from 9.81)
%
% to convert lb/ft3 to kg/m3, multiply by 16.0185
% to convert kg/m3 to lb/ft3, multiply by 0.0624

% From: http://www.denysschen.com/catalogue/density.asp
%
% Uncomment any rho_US desired, depending on elevation of jump
% rho_US is measured in lb/ft^3 ; see conversion

rho_US=0.0597;    % For 8000 feet at (0C, 32F) freezing
%
rho=rho_US*16.0185; % kg/m3 % conversion
%
mass=70;     % kg from Muller(1997)...I want to have other weights
area=0.4;    % half avg drag and lift area (m^2) from Muller(1997)
%Choose a fall height and takeoff angle
del_v=1*2.25; % additional pop off of the jump
betaod=25; % Jump angle in degrees    % new name for thod
       % this will vary
betao=betaod*pi/180;% takeoff ramp angle in radians
sbo=sin(betao); % sine of beta
cbo=cos(betao); % cosine of beta
tbo=tan(betao);  % tangent of beta
h=1;  %meters
%hnom=h;      % nominal fall height to taper to
% reference frame origin is at takeoff point
% choose initial surface point at zenith of surface
%
% The next sequence finds the critical point for given parameters
a=1;
b=-2*cbo*sbo;
c=4*cbo^2;
d=-2*h*cbo*sbo;
f=2*h*cbo^2;
%
xc=(c*d-b*f)/(b^2-a*c); % center (x) of ellipse for critical point
search
yc=(a*f-b*d)/(b^2-a*c); % center (y) of ellipse for critical point
search
% rotation angle (alpha):  from x-axis to major axis
% same as from y-axis to minor axis
alpha=.5*atan((2*b)/(a-c)); % in radians
alpha_degrees=alpha*180/pi;
j= 2*((a*f^2)+(c*d^2)-(2*b*d*f));%numerator
k=(b^2-a*c)*(-sqrt(((a-c)^2)+(4*b^2))-(a+c)); % denominator
%
% L = half of semi minor axis length
L=(sqrt(j/k)); %L=(sqrt(j/k)/2)
```

```
%
singular_pt_x=xc+(L*sin(alpha))
singular_pt_y=yc-(L*cos(alpha))
```

C. VELOCITY WITH DRAG ALONG IN-RUN CODE

```
% rho_US is measured in lb/ft^3 ; see conversion
rho_US=0.0597;    % For 8000 feet at (0C, 32F) freezing
rho=rho_US*16.0185; % kg/m3 % conversion
A=0.5; % cross sectional area, m^2
Cd=0.42;% Drag coefficient, for a half sphere
g=9.80665;
lambda_degrees=25;
lambda=lambda_degrees*pi/180;
muu=0.05;
m=40; %kg
gg=g*sin(lambda)-muu*g*cos(lambda);
t=[0:0.1:2];
K=rho*A*Cd;
L=10; % in-run (meter)
%
a=sqrt(2*m*gg/(rho*A*Cd));
%
distance=((a^2)/gg)*log(cosh(gg/a*t)); % distance for a time t
velocity=sqrt(2*m*gg/K)*tanh(t*sqrt(K*gg/2*m)); % velocity for a time t

velocity2=sqrt(2*m*gg/K)*tanh(acosh(exp(L*K/(2*m))))
% velocity for a linear in-run length L
```

D. EQUIVALENT FALL HEIGHT CODES

1. Tabletop EFH Code

```
% EFH for tabletop jump
% Andrew Swedberg
% NPS, April 2010
% yt=height above tabletop (m), written as negative value
% xt is length of tabletop (m)
% phi is angle of landing slope (radians), written as negative value
% theta_zero is angle of takeoff ramp (degrees)
% EFH is equivalent fall height
% x is range for length of jump, (m)
%
clear
format compact
g=9.80665;
x=[0:1:40];
grid on
%

yt=0; % 0, -1, -2, -3; % meters (negative)
phi_degrees=-30; % degrees (negative)
```

```
theta_zero_degrees=25; % degrees
%
%
phi=phi_degrees*(pi/180); % converts to radians
theta_zero=theta_zero_degrees*(pi/180); % converts to radians
cto=cos(theta_zero);
tto=tan(theta_zero);
sto=sin(theta_zero);
%
h2=-yt;
h1=((x.^2)*tto^2)./(4*(x.*tto+h2));
EFH=h1+h2;
%
hold on
figure (1)
plot (x,EFH,'k.','linewidth' ,2.0) ;% axis equal
axis([0 40 0 15]) ;
xlabel ('horizontal length of jump x (m)')
ylabel ('EFH (m)');
%
%
g=9.80665;
x=[0:1:40];
%
xt=10;
yt=-1; % 0, -1, -2, -3; % meters (negative)
phi_degrees=-30; % degrees (negative)
theta_zero_degrees=25; % degrees
%
phi=phi_degrees*(pi/180); % converts to radians
theta_zero=theta_zero_degrees*(pi/180); % converts to radians
cto=cos(theta_zero);
tto=tan(theta_zero);
sto=sin(theta_zero);
%
h2=-yt;
h1=((x.^2)*tto^2)./(4*(x.*tto+h2));
EFH=h1+h2;
%
hold on
figure (1)
plot (x,EFH,'k+','linewidth' ,2.0)
axis([0 40 0 12]) ;
xlabel ('horizontal length of jump x (m)')
ylabel ('EFH (m)');
%
%
g=9.80665;
x=[0:1:40];
%
xt=10;
yt=-2; % 0, -1, -2, -3; % meters (negative)
phi_degrees=-30; % degrees (negative)
theta_zero_degrees=25; % degrees
%
```

```
%
phi=phi_degrees*(pi/180); % converts to radians
theta_zero=theta_zero_degrees*(pi/180); % converts to radians
cto=cos(theta_zero);
tto=tan(theta_zero);
sto=sin(theta_zero);
%
h2=-yt;
h1=((x.^2)*tto^2)./(4*(x.*tto+h2));
EFH=h1+h2;

hold on
figure (1)
plot (x,EFH,'k^','linewidth' ,2.0) ;% axis equal
axis([0 40 0 12]) ;
xlabel ('horizontal length of jump x (m)')
ylabel ('EFH (m)');

%
g=9.80665;
x=[0:1:40];
%
xt=10;
yt=-3; % 0, -1, -2, -3; % meters (negative)
phi_degrees=-30; % degrees (negative)
theta_zero_degrees=25; % degrees
%
%
phi=phi_degrees*(pi/180); % converts to radians
theta_zero=theta_zero_degrees*(pi/180); % converts to radians
cto=cos(theta_zero);
tto=tan(theta_zero);
sto=sin(theta_zero);
%
h2=-yt;
h1=((x.^2)*tto^2)./(4*(x.*tto+h2));
EFH=h1+h2;

hold on
figure (1)
plot (x,EFH,'ko','linewidth' ,2.0); %axis equal
axis([0 40 0 12]);
xlabel ('horizontal length of jump x (m)')
ylabel ('EFH (m)');

legend('yt=0 m ','yt=1 m','yt=2 m','yt=3 m');
```

2. Angled Linear Downslope Landing Code

```
% EFH for tabletop jump
% Andrew Swedberg
% NPS, April 2010
% yt=height above tabletop (m), written as negative value
% xt is length of tabletop (m)
```

```
% phi is angle of landing slope (radians), written as negative value
% theta_zero is angle of takeoff ramp (degrees)
% EFH is equivalent fall height
% x is range for length of jump, (m)
%
clear
format compact
g=9.80665;
x=[0:1:40];
grid on
%
xt=10;
yt=0; % meters (negative)
phi_degrees=-30; % degrees (negative)
theta_zero_degrees=25; % degrees
phi=phi_degrees*(pi/180); % converts to radians
theta_zero=theta_zero_degrees*(pi/180); % converts to radians
cto=cos(theta_zero);
tto=tan(theta_zero);
sto=sin(theta_zero);

[r1,c1,v1]=find(x<xt);
[r2,c2,v2]=find(x>=xt);

y1=v1*yt;
y2=yt+tan(phi)*(x(find(x>=xt))-xt);
y=[y1 y2];
%
phi1=v1*0;
phi2=v2*phi;
phi=[phi1 phi2];

vo=sqrt((x.^2)*g./(2*(x.*tto-y)*cto^2)); % init v to get to x & y
% velocity at x and y
v1=sqrt(vo.^2*cto^2+(vo.*sto-g*x./vo./cto).^2); %original way to find
velocity
v2=sqrt((vo.^2)-2*g*y); % impact velocity, same as v1
v3=sqrt(((x.^2)*g./(2*(x.*tto-y)*cto^2))-2*g*y);% alternate way; in my
thesis, in terms of x and y
%
theta=atan(tto-g*x./(vo.^2*cto^2)); %original way to find theta, impact
angle
theta2=atan(2*y./x-tto);  % alternate way--this matches the original
way
%
v_perp=v3.*sin(phi-theta); % perpendicular velocity
EFH1=(v_perp.^2)/(2*g);

figure (1)
hold on
plot (x,EFH1,'k.','linewidth' ,2.0)
xlabel ('horizontal length of jump x (m)')
ylabel ('EFH (m)');
axis([0 40 0 12]);
```

```
%%%%%%%%%%%%%%%%%%%%%%%%%%%%%%%%%%%%%%%%

g=9.80665;
x=[0:1:40];
%
xt=10;
yt=-1; % meters (negative)
phi_degrees=-30; % degrees (negative)
theta_zero_degrees=25; % degrees
phi=phi_degrees*(pi/180); % converts to radians
theta_zero=theta_zero_degrees*(pi/180); % converts to radians
cto=cos(theta_zero);
tto=tan(theta_zero);
sto=sin(theta_zero);

[r1,c1,v1]=find(x<xt);
[r2,c2,v2]=find(x>=xt);

y1=v1*yt;
y2=yt+tan(phi)*(x(find(x>=xt))-xt);
y=[y1 y2];
%
phi1=v1*0;
phi2=v2*phi;
phi=[phi1 phi2];

vo=sqrt((x.^2)*g./(2*(x.*tto-y)*cto^2)); % init v to get to x & y
% velocity at x and y
v1=sqrt(vo.^2*cto^2+(vo.*sto-g*x./vo./cto).^2); %original way to find
velocity
v2=sqrt((vo.^2)-2*g*y); % impact velocity, same as v1
v3=sqrt(((x.^2)*g./(2*(x.*tto-y)*cto^2))-2*g*y);% alternate way; in my
thesis, in terms of x and y
%
theta=atan(tto-g*x./(vo.^2*cto^2)); %original way to find theta, impact
angle
theta2=atan(2*y./x-tto);  % alternate way--this matches the original
way
%
v_perp=v3.*sin(phi-theta); % perpendicular velocity
EFH1=(v_perp.^2)/(2*g);

figure (1)
plot (x,EFH1,'k+','linewidth' ,2.0)
hold on
xlabel ('horizontal length of jump x (m)')
ylabel ('EFH (m)');
axis([0 40 0 12]);

%%%%%%%%%%%%%%%%%%%%%%%%%%%%%%%%%%%%%%%%
g=9.80665;
x=[0:1:40];
%
```

```
xt=10;
yt=-2; % meters (negative)
phi_degrees=-30; % degrees (negative)
theta_zero_degrees=25; % degrees
phi=phi_degrees*(pi/180); % converts to radians
theta_zero=theta_zero_degrees*(pi/180); % converts to radians
cto=cos(theta_zero);
tto=tan(theta_zero);
sto=sin(theta_zero);

[r1,c1,v1]=find(x<xt);
[r2,c2,v2]=find(x>=xt);

y1=v1*yt;
y2=yt+tan(phi)*(x(find(x>=xt))-xt);
y=[y1 y2];
%
phi1=v1*0;
phi2=v2*phi;
phi=[phi1 phi2];

vo=sqrt((x.^2)*g./(2*(x.*tto-y)*cto^2)); % init v to get to x & y
% velocity at x and y
v1=sqrt(vo.^2*cto^2+(vo.*sto-g*x./vo./cto).^2); %original way to find
velocity
v2=sqrt((vo.^2)-2*g*y); % impact velocity, same as v1
v3=sqrt(((x.^2)*g./(2*(x.*tto-y)*cto^2))-2*g*y);% alternate way; in my
thesis, in terms of x and y
%
theta=atan(tto-g*x./(vo.^2*cto^2)); %original way to find theta, impact
angle
theta2=atan(2*y./x-tto);  % alternate way--this matches the original
way
%
v_perp=v3.*sin(phi-theta); % perpendicular velocity
EFH1=(v_perp.^2)/(2*g);

figure (1)
plot (x,EFH1,'k^','linewidth' ,2.0)
hold on
xlabel ('horizontal length of jump x (m)')
ylabel ('EFH (m)');
axis([0 40 0 12]);

%%%%%%%%%%%%%%%%%%%%%%%%%%%%%%%%%%%%%%%%
g=9.80665;
x=[0:1:40];
%
xt=10;
yt=-3; % meters (negative)
phi_degrees=-30; % degrees (negative)
theta_zero_degrees=25; % degrees
phi=phi_degrees*(pi/180); % converts to radians
theta_zero=theta_zero_degrees*(pi/180); % converts to radians
```

```
cto=cos(theta_zero);
tto=tan(theta_zero);
sto=sin(theta_zero);

[r1,c1,v1]=find(x<xt);
[r2,c2,v2]=find(x>=xt);

y1=v1*yt;
y2=yt+tan(phi)*(x(find(x>=xt))-xt);
y=[y1 y2];
%
phi1=v1*0;
phi2=v2*phi;
phi=[phi1 phi2];

vo=sqrt((x.^2)*g./(2*(x.*tto-y)*cto^2)); % init v to get to x & y
% velocity at x and y
v1=sqrt(vo.^2*cto^2+(vo.*sto-g*x./vo./cto).^2); %original way to find
velocity
v2=sqrt((vo.^2)-2*g*y); % impact velocity, same as v1
v3=sqrt(((x.^2)*g./(2*(x.*tto-y)*cto^2))-2*g*y);% alternate way; in my
thesis, in terms of x and y
%
theta=atan(tto-g*x./(vo.^2*cto^2)); %original way to find theta, impact
angle
theta2=atan(2*y./x-tto);  % alternate way--this matches the original
way
%
v_perp=v3.*sin(phi-theta); % perpendicular velocity
EFH1=(v_perp.^2)/(2*g);

figure (1)
hold on
plot (x,EFH1,'ko','linewidth' ,2.0)
xlabel ('horizontal length of jump x (m)')
ylabel ('EFH (m)');
axis([0 40 0 12]);
legend('yt=0 m ','yt=1 m','yt=2 m','yt=3 m');
```

E. CIRCULAR TRANSITION CODES

1. Circular Transition Before Takeoff

```
function [T,Y]= before_takeoff
format compact
%clf
global g muu lambda beta gamma Z radius_min
lambda_degrees=35;
beta_degrees=10;
lambda=lambda_degrees*(pi/180); % radians
beta=beta_degrees*(pi/180); % radians
muu=0.05; % coefficient of friction of skis on snow
gamma=1.5; % This means 1.5 times the force of gravity
```

```
g=9.80665; % gravity
% Compute the initial velocity at the beginning of the transition
Z=10; % 10 meter in-run part

% Inputs:
% radius_min = minimum radius of circle in meters
% lambda = in degrees
% Returns:
% T      = Time vector
% Y      = Vector of Velocities and Epsilons
vti=sqrt(2*g*Z*(sin(lambda)-muu*cos(lambda)))
%vti=sqrt(2*g.*Z.*(cos(lambda)-muu.*sin(lambda)))
radius_min=(vti.^2)/(gamma*g)
% pause
% vo=velocity at the end of the in-run = beginning of the transition

% Set up the stopping criteria
options=odeset('Events', @circular_events);
% Set up the initial conditions
tspan=[0:.01:5];
IC=[vti;-lambda];
%initial conditions for the transition part
% velocity it at vo, angle (epsilon) begins at negative lambda
% Set up the time window to solve the ODE... may not take this long...
% better longer than shorter

% Make the ode45 solver call -- note that all parameters are passed.
% Stopping criteria is when epsilon reaches +beta
[T,Y]=ode45(@part1,tspan,IC,options);
Addl_Accel=(Y(:,1).^2)/radius_min;
%
time_at_beta=T(end); % Final time where epsilon reaches +beta
%beta-Y(end,2); % Value of epsilon - beta (should be zero)
%
figure(1)
plot(T,Y(:,1),'k','linewidth', 2.0) % Velocity
%title('velocity vs. time in a circular transition')
xlabel('time, (s)')
ylabel('velocity, (m/s)')
%
figure(2)
plot(T,(g*cos(Y(:,2))+Addl_Accel),'k', 'linewidth',2.0)
%title('Normal acceleration vs. time in a circular transition')
xlabel('time, (s)')
ylabel('Normal Force, (m/s^2)')
%
figure(3)
Y(:,2);
hold on
for i=[-2:0.01:0];
plot (i,cos(lambda),'k', 'linewidth',1.0)
end
%
partial_plot_vector=[T-1.9568];
plot(T,((g*cos(Y(:,2))+Addl_Accel)/g),'k.', 'linewidth',1.0)
```

```
%
for j=[T(end):0.01:3];
plot (j,cos(lambda), 'k', 'linewidth', 1.0)
end
%
axis ([-2 3 0 3])
%title('Ratio of normal accleration to g vs. time in a circular
transition')
xlabel('time, (s)')
ylabel('Ratio of Normal force to g')
%
function dvdt1=part1(t,v,muu,g,radius_min,lambda,beta)
global g muu lambda beta radius_min

    vv=v(1);
    epsilon=v(2);
    v_prime=-g*sin(epsilon)-muu*(((vv^2)/radius_min)+g*cos(epsilon));
    epsilon_prime=vv/radius_min;
    dvdt1=[v_prime; epsilon_prime];

    % Output (Y) is a matrix with two columns
    % Column 1 is the velocity during the transition part
    % Column 2 is the range of epsilon, that goes from -lambda to +beta
    % Need to use the last value of the velocity for the start of the
    % integration to get the value of vo.
```

2. Circular Transition Events

```
function[value, isterminal,direction]=events(T,Y)
    global lambda beta
    value(1)=Y(2)-beta;
    isterminal(1)=1;
    direction(1)=0;
    return
```

F. CLOTHOIDAL TRANSITION CODES

1. Radius Required for Given γ

```
clear

velocity=[5:1:15];
gamma=1.5;

g=9.80665;
radius=(velocity.^2)/(gamma*g);
plot (velocity,radius,'k+','linewidth',2.0); axis equal
title('plot of radius of transition with skier velocity')
xlabel('velocity (m/s) of skier at beginning of transition')
ylabel('radius required (m) for the given value of gamma')
hold on
velocity=[5:1:15];
gamma=1.75; %gamma=[1.2:0.2:2.0]
g=9.80665;
```

```
radius=(velocity.^2)/(gamma*g);
plot (velocity,radius,'k^','linewidth',2.0); axis equal
hold on
velocity=[5:1:15];
gamma=2.0; %gamma=[1.2:0.2:2.0]
g=9.80665;
radius=(velocity.^2)/(gamma*g);
plot (velocity,radius, 'ko','linewidth',2.0); axis equal

legend('gamma=1.5','gamma=1.75','gamma=2.0');%
,'gamma=1.8','gamma=2.0');
% % As the value of gamma varies from 1.2 to 2.0 (easier to harder on
the
% % human body), the radius required decreases.
%
% % For lower velocities, the value of gamma does not affect the radius
% % required as much as at high velocities.
```

2. Clothoid Transition Before Takeoff

```
function [T,Y] = clothoid_before_takeoff
global g A_squared muu lambda beta gamma Z L1 L2
%
format compact
%clf
lambda_degrees=35;
beta_degrees=10;
Z=10; % in meters: in-run portion
muu=0.05; % coefficient of friction
gamma=1.5; % This means 1.5 times the force of gravity
g=9.80665; % gravity
%
lambda=lambda_degrees*(pi/180); % radians
beta=beta_degrees*(pi/180); % radians
vti=sqrt(2*g*Z*(sin(lambda)-muu*cos(lambda)));
%vti2=sqrt(2*g*Z*(cos(lambda)-muu*sin(lambda)))
%
% This is the velocity at the beginning of the transition:  where the
% linear slope (infinite radius) meets the clothoidal shape
%
radius_min=(vti.^2)/(gamma*g);
%
% The radius_min is the shortest that the "circular" transition
% will be.  Every other radius length will be longer than that, as this
% will ensure the g-force felt by the skier is always less than a
% desired gamma value.
%
A_squared=(radius_min^2)*(lambda+beta);
A=sqrt(A_squared); % A is the flatness of the curve
L1=A_squared/radius_min;
L2=A_squared/radius_min;
clothoid_length=A*sqrt(lambda+beta);
total_transition_length=2*clothoid_length
constant1=(lambda+beta)/(2*L1^2);
```

```
constant2=(lambda+beta)/(2*L2^2);
%
options=odeset('Events',@clothoid_events2); % looks for this event
tspan1=[0:.05:4];
ic1=[vti 0];  % initial conditions for the first clothoid
[T,Y,TE,YE,IE]=ode45(@clothoid_ode1,tspan1,ic1,options);
TY=[T Y];
r1=A_squared./(Y(:,2));
size(r1);
%
% this is the radius--goes from infinity to radius_min
%Addl_accel_1=((Y(:,2).*(Y(:,1).^2))/A_squared)
Centrepital_accel_1=(Y(:,1).^2)./r1;
%
% time span is from 0 to 4 seconds; it really stops before this point
% initial velocity condition:  vti (velocity at transition)
% initial length of clothoid condition:  0
%
figure(1)
plot(T, Y(:,1),'k','linewidth', 2.0);
%title('velocity vs. time in a clothoid transition')
ylabel('velocity, (m/s)')
xlabel('time, (s)')

% The stopping criteria will be when the clothoid length = s.
% For the second clothoid, the initial conditions will be
% the velocity at the end of the first clothoid
%
options=odeset('Events',@second_clothoid_events2); % look for this
event
%[TT,YY,TTE,YYE,IIE] =
ode45(@clothoid_ode2,[T(end);6],[Y(end);L2],options)
tspan2=[T(end):.05:6];
ic2=[Y(end,1),L1]; % initial conditions for the second clothoid
%
[TT,YY,TTE,YYE,IIE] = ode45(@clothoid_ode2,tspan2,ic2,options);
TTYY=[TT YY];
%
r2=A_squared./(YY(:,2));
size(r2);
Centrepital_accel_2=(YY(:,1).^2)./r2;
%Addl_accel_22=((YY(:,2).*(YY(:,1).^2))/A_squared)
%Addl_accel_22-Addl_accel_2
%pause
%
% time span is from T(end) to 6 seconds (should stop before this point)
% initial velocity condition:  velocity at point of clothoid
intersection
% initial length of clothoid condition:  L1
%
hold on
plot(TT, YY(:,1),'k','linewidth', 2.0);
ylabel('velocity, (m/s)')
xlabel('time, (s)')
%
```

```
s1=Y(:,2);  % column of s, the position along the first clothoid
s2=YY(:,2); % column of s, the position along the second clothoid
% starts at end
size(s1);
size(s2);
%pause
zeta1=constant1*(s1.^2); % turning angle along first clothoid
zeta2=constant1*(s2.^2);
%zeta22=flipud(constant2*(s2.^2));
%pause
%zeta2=zeta1(end)+zeta22
%pause
theta1=-lambda+zeta1; % angle of path from horizontal on first clothoid
wuns=ones(size(s2));
zeta2=zeta2-wuns*zeta1(end);
%theta2=(theta1(end)*wuns+zeta2);
theta2=(theta1(end)*wuns-zeta2);% angle of path from horizontal:
second clothoid
zeta2=-zeta2;
zeta1;
zeta_degrees1=zeta1*180/pi
zeta_degrees2=zeta2*180/pi
% theta1
% zeta2
% theta2
%
figure(2)
hold on
%
normal_force_1=g*cos(theta1)+Centrepital_accel_1; % normalized force
(mass specific), divided by m.
normal_force_2=g*cos(theta2)+Centrepital_accel_2; % second term is
normal acceleration
plot(T,normal_force_1, 'k','linewidth', 2.0) ;
plot(TT,normal_force_2,'k','linewidth', 2.0) ;
%title('Normalized mass specific force vs. time in a clothoid
transition')
ylabel('Force, (m/s^2)')
xlabel('time, (s)')
%
%figure(3)
hold on
for i=[-2:0.01:0];
plot (i,cos(lambda),'k', 'linewidth',1.0)
end
for j=[TT(end):0.01:3];
plot (j,cos(lambda), 'k', 'linewidth', 1.0)
end
%
hold on
axis ([-2 3 0 3])
normal_force_in_g_1=(g*cos(theta1)+Centrepital_accel_1)/g; %normal
force in g's
normal_force_in_g_2=(g*cos(theta2)+Centrepital_accel_2)/g;
plot(T,normal_force_in_g_1,'k', 'linewidth',1.0)
```

```
plot(TT,normal_force_in_g_2,'k', 'linewidth',1.0)
%
%title('Normal force (g) vs. time in a clothoid transition')
xlabel('time, (s)')
ylabel('Ratio of Normalized mass specific force to g')

function dvdt1 = clothoid_ode1(t,v,lambda,A_squared,g,muu);
global g A_squared muu lambda beta gamma Z L1 constant
vv=v(1);
s=v(2);
v_prime=-g*sin((s.^2)/(2*A_squared)-lambda)-
muu*((s./A_squared)*(vv.^2)+g*cos((s.^2)/(2*A_squared)-lambda));
s_prime=vv;
dvdt1=[v_prime;s_prime];
%
% the first column of the dvdt1 vector is v_prime (s). The second
column is v.
%
function dvdt2 = clothoid_ode2(t,v,beta,A_squared,g,muu);
global g A_squared muu beta lambda gamma Z L1
vv=v(1);
s=v(2);
v_prime=g*sin((s.^2)/(2*A_squared)-beta)-
muu*((s./A_squared)*(vv.^2)+g*cos((s.^2)/(2*A_squared)-beta));
% originally had a "-g", and positive betas
% v_prime=-g*sin((s.^2)/(2*A_squared)+beta)-
muu*((s./A_squared)*(vv.^2)+g*cos((s.^2)/(2*A_squared)+beta));
s_prime=-vv;
dvdt2=[v_prime;s_prime];
```

3. Clothoid Plot

```
dt = .01 ;
t=(-2*pi):dt:(2*pi) ;
x = cumtrapz(sin(t.^2)) * dt ;
y = cumtrapz(cos(t.^2)) * dt ;
plot(x,y,'k', 'linewidth', 2.0) ; axis equal
axis([-1 2 -1 2])
```

4. Complete Clothoidal Transition Side View

```
% This program will find the shape of a clothoid transition
% for the in-run of a ski jump
clear
% Enter a lambda (existing slope) degree
% and a beta (desired take-off ramp/jump degree).

lambda_degrees=20;
beta_degrees=20;
%
% s1 = left side clothoid length at any point (downhill part)
% s2 = right side clothoid at any point length (uphill part)
% L1 = left side (longest) clothoid length (downhill part)
```

```
% L2 = right side (longest) clothoid length (uphill part)
%
% enter a value for the length of slope before entering the transition
%
Z=10; % in meters: in-run portion
mu=0.05; % coefficient of friction
gamma=1.5; % This means 1.5 times the force of gravity
g=9.80665; % gravity
%
lambda=lambda_degrees*(pi/180); % radians
beta=beta_degrees*(pi/180); % radians
% total_turn=(lambda+beta);
% lambda2=total_turn/2;
% beta2=total_turn/2;
rotation=(lambda-beta)/2;
%
vti=sqrt(2*g.*Z.*(cos(lambda)-mu.*sin(lambda)));
% This is the velocity at the beginning of the transition:  where the
% linear slope (infinite radius) meets the clothoidal shape
%
radius_min=(vti.^2)/(gamma*g)
%
% The radius_min is the shortest that the "circular" transition
% will be.  Every other radius length will be longer than that, as this
% will ensure the g-force felt by the skier is always less than a
% desired gamma value.
%
A_squared=(radius_min^2)*((lambda+beta)); % divide this by 2???
A=sqrt(A_squared);
clothoid_length=A*sqrt(lambda+beta)
total_transition_length=2*clothoid_length
%
s=[clothoid_length:-0.1:0];
%R=[radius_min:0.5:1000];
%
% varies the value of R from radius_min to a high value
% (infinite slope for a linear portion)
%
% clothoid: curve such that the reciprocal of the radius varies
linearly
%
%s=(A^2)./R; % relationship for a clothoid; used for the range of R
%
theta=(max(s))/(2*radius_min);
% since theta=L/(2*R)
%
L1=2*lambda*radius_min; % length of left clothoid
L2=2*beta*radius_min; % length of right clothoid
%
X1=s-(s.^5)./(40.*A.^4)+(s.^9)./(3456*A.^8);
% x coordinate for the clothoid shape
Y1=(s.^3)/(6*A.^2)-(s.^7)/(336*A.^6)+(s.^11)/(42240*A.^10);
% y coordinate for the clothoid shape
%
figure(1);
```

```
hold on
%plot of original clothoid (not rotated)
%plot(X1,Y1,'r','linewidth',3.0); axis equal; %X1 is black
%
%plot (0,radius_min, 'x'); % this 'x' marks the center of the circle
%
X2=X1-X1(1);
%X2=X1+X1(end)-X1(1);
Y2=Y1-Y1(1);
%plot(X2,Y2,'b','linewidth',3.0); axis equal; %X2 is blue
% this shifts the original clothoid so that the origin is correct
%
X3=(cos(theta)*X2)+(sin(theta)*Y2);
Y3=(-sin(theta)*X2)+(cos(theta)*Y2);
%plot(X3,Y3,'r','linewidth',2.0); axis equal; %X3 is red
% this rotates the clothoid to theta
%
X4=X3;
Y4=Y3-radius_min;
%plot(X4,Y4,'r','linewidth',2.0); axis equal; %X4 is thin red
% this shifts the y-axis so that it can be rotated about the new origin
%
X5=-X4+2*(X4(1));
Y5=Y4;
%plot(X5,Y5,'g','linewidth',2.0); axis equal; %X5 is thin green
%this does the same for the right side
%
X6=(cos(rotation)*X4)+(sin(rotation)*Y4);
Y6=(-sin(rotation)*X4)+(cos(rotation)*Y4);
%plot(X6,Y6,'c','linewidth',2.0); axis equal; %X6 is cyan
% this rotates the left side at the correct angle (lambda2)
%
X7=(cos(rotation)*X5)+(sin(rotation)*Y5);
Y7=(-sin(rotation)*X5)+(cos(rotation)*Y5);
%plot(X7,Y7,'y','linewidth',2.0); axis equal; %X7 is yellow
% this rotates the left side at the correct angle (lambda2)
%
X8=X6-X6(1);
Y8=Y6-Y6(1);
%plot(X8,Y8,colors(ii),'linewidth',2.0); axis equal; %X8 is black
plot(X8,Y8,'k','linewidth',2.0); axis equal; %X8 is black
% this is the plot of the left clothoid at the correct angle
%

X9=X7-X7(1);
Y9=Y7-Y7(1);
%plot(X9,Y9,colors(ii),'linewidth',2.0); axis equal;%X9 is black
plot(X9,Y9,'k','linewidth',2.0); axis equal;%X9 is black
%title('Plot of x and y coordinates of clothoid')
xlabel('x (m)')
ylabel('y (m)')
%legend('lambda=10','lambda=20','lambda=30');
%  this is the plot of the right clothoid at the correct angle
```

G. IN-RUN WITH AIR DRAG CODE

```
m=20; % kg
% rho_US is measured in lb/ft^3 ; see conversion
rho_US=0.0597;    % For 8000 feet at (0C, 32F) freezing
rho=rho_US*16.0185; % kg/m3 % conversion
A=0.5; % cross sectional area, m^2
Cd=0.42;% Drag coefficient, for a half sphere
g=9.80665;
lambda_degrees=25;
lambda=lambda_degrees*pi/180;
muu=0.05;
gg=g*sin(lambda)-muu*g*cos(lambda);
t=[0:0.1:2];
K=rho*A*Cd;
%
a=sqrt(2*m*gg/(rho*A*Cd));
%
distance=((a^2)/gg)*log(cosh(gg/a*t))
velocity=sqrt(2*m*gg/K)*tanh(t*sqrt(K*gg/2*m))
```

INITIAL DISTRIBUTION LIST

1. Defense Technical Information Center
   Ft. Belvoir, Virginia

2. Dudley Knox Library
   Naval Postgraduate School
   Monterey, California

3. Professor Mont Hubbard
   Mechanical Engineering Department
   University of California – Davis
   Davis, California

4. Professor Arthur Krener
   Department of Applied Mathematics
   Naval Postgraduate School
   Monterey, California

5. Professor Carlos Borges
   Department of Applied Mathematics
   Naval Postgraduate School
   Monterey, California

6. James A. McNeil
   Department of Physics
   Colorado School of Mines
   Golden, Colorado

7. COL Michael Phillips
   Department of Mathematical Sciences
   United States Military Academy
   West Point, New York

8. Lynn Harris
   Attorney at Law
   Provo, Utah

9. Victor Constant Ski Area
   United States Military Academy
   West Point, New York

10. Jasper Shealy
Rochester Institute of Technology
Rochester, New York

11. MAJ Andrew Swedberg
Department of Mathematical Sciences
United States Military Academy
West Point, New York